UNIVERSITY OF WEST ATTICA
SCHOOL OF ENGINEERING
DEPARTMENT OF NAVAL ARCHITECTURE

Thesis Diploma

Numerical simulation of laminar flow around rotating cylinder - Effect of rotational speed on vortex shedding

PLIATSIKA Argyro
15079

Supervisor:
KOUBOGIANNIS Dimitrios

Athens, July 2024

Approved by the selection board on.

Dimitrios Koumpogiannis Digitally signed by Dimitrios Koumpogiannis Date: 2024.08.27 15:49:57 +03'00'

THEODOROS GEROSTATHIS Digitally signed by THEODOROS GEROSTATHIS Date: 2024.08.29 11:19:19 +03'00'

DIMITRIOS MITSOUDIS Digitally signed by DIMITRIOS MITSOUDIS Date: 2024.08.27 20:22:30 +03'00'

……	……..	……...
Dimitrios Koubogiannis	Theodoros Gerostathis	Dimitrios Mitsoudis

ΔΗΛΩΣΗ ΣΥΓΓΡΑΦΕΑ ΔΙΠΛΩΜΑΤΙΚΗΣ ΕΡΓΑΣΙΑΣ

Η κάτωθι υπογεγραμμένη Πλιάτσικα Αργυρώ του Αθανασίου, με αριθμό μητρώου 51115079 φοιτητής του Πανεπιστημίου Δυτικής Αττικής της Σχολής Μηχανικών του Τμήματος Ναυπηγών Μηχανικών, δηλώνω υπεύθυνα ότι:

«Είμαι συγγραφέας αυτής της διπλωματικής εργασίας και ότι κάθε βοήθεια την οποία είχα για την προετοιμασία της είναι πλήρως αναγνωρισμένη και αναφέρεται στην εργασία. Επίσης, οι όποιες πηγές από τις οποίες έκανα χρήση δεδομένων, ιδεών ή λέξεων, είτε ακριβώς είτε παραφρασμένες, αναφέρονται στο σύνολό τους, με πλήρη αναφορά στους συγγραφείς, τον εκδοτικό οίκο ή το περιοδικό, συμπεριλαμβανομένων και των πηγών που ενδεχομένως χρησιμοποιήθηκαν από το διαδίκτυο. Επίσης, βεβαιώνω ότι αυτή η εργασία έχει συγγραφεί από μένα αποκλειστικά και αποτελεί προϊόν πνευματικής ιδιοκτησίας τόσο δικής μου, όσο και του Ιδρύματος.
Παράβαση της ανωτέρω ακαδημαϊκής μου ευθύνης αποτελεί ουσιώδη λόγο για την ανάκληση του διπλώματός μου».

Η δηλούσα

Πλιάτσικα Αργυρώ

Αφιερώνεται στην μητέρα μου

Acknowledgements

I would like to express my deepest gratitude and appreciation to everyone who has supported me during the course of this thesis. I would like to extend my gratefulness to my advisor, Professor Dimitrios Koubogiannis, for his invaluable guidance, support, and mentorship throughout the entire process. His expert advice, constructive criticism, and unwavering encouragement have been essential for completing this work.

Additionally, I owe a profound debt of gratitude to my family, whose constant support and love have been the cornerstones of my journey through my academic career. I am especially thankful to my mother for her unwavering faith in me and the sacrifices she have made, which have been instrumental in my achievements. Her wisdom and guidance have always led me forward. To my sister, whose encouragement and companionship have lightened moments of stress and brought joy into my study breaks, I am deeply grateful. The strength and understanding provided by my family have shaped not only this academic endeavor but also the person I have become. As I close this chapter of my life, I carry forward the invaluable lessons learned and the profound bonds strengthened during this period, all of which I owe to my beloved family.

Περίληψη

Η παρούσα εργασία διερευνά την πολύπλοκη δυναμική της στρωτής ροής γύρω από έναν περιστρεφόμενο κυκλικό κύλινδρο και την επακόλουθη δημιουργία δίνης, χρησιμοποιώντας προσομοιώσεις υπολογιστικής ρευστοδυναμικής (CFD). Πραγματοποιήθηκε μια μελέτη για την αξιολόγηση της επίδρασης των παραμέτρων περιστροφής του κυλίνδρου, συγκεκριμένα του πλάτους και της συχνότητας της ταχύτητας περιστροφής, στη συμπεριφορά της αποβολής δίνης. Οι προσομοιώσεις, που πραγματοποιήθηκαν με τη χρήση του ANSYS Fluent, διερεύνησαν διάφορες παραμέτρους της ταχύτητας περιστροφής του κυλίνδρου που χαρακτηρίζονται από παραμέτρους χωρίς διαστάσεις, όπως ο αριθμός Reynolds και ο αριθμός Strouhal. Η μελέτη χρησιμοποίησε μια λεπτομερή στρατηγική πλέγματος για τη διασφάλιση της ακρίβειας και της αξιοπιστίας των αποτελεσμάτων της προσομοίωσης, η οποία συσχετίζεται στενά με καθιερωμένα σημεία αναφοράς στη βιβλιογραφία της ρευστοδυναμικής. Τα αποτελέσματα καταδεικνύουν σημαντικές μεταβολές στους συντελεστές αντίστασης και ανύψωσης με αλλαγές στις παραμέτρους περιστροφής, αποκαλύπτοντας περίπλοκες σχέσεις μεταξύ της δυναμικής της αποκόλλησης δίνης και των χαρακτηριστικών περιστροφής του κυλίνδρου. Τα ευρήματα έχουν βαθιές συνέπειες για τη βελτίωση της απόδοσης και της σταθερότητας των συστημάτων που περιλαμβάνουν κυλινδρικά σώματα σε ροές ρευστών, όπως οι θαλάσσιες κατασκευές και τα αεροδυναμικά εξαρτήματα. Προτείνεται η μελλοντική έρευνα για την περαιτέρω διερεύνηση των αλληλεξαρτήσεων των παραμέτρων περιστροφής και τη βελτιστοποίηση των στρατηγικών σχεδιασμού και λειτουργίας για βιομηχανικές εφαρμογές που περιλαμβάνουν ρευστοδυναμική.

Λέξεις-κλειδιά: Reynolds, αριθμός Strouhal, συντελεστής οπισθέλκουσας, συντελεστής άνωσης, αριθμητική προσομοίωση, δυναμική ροή, εξισώσεις Navier Stokes (NS), , οδός δίνης Von-Karman

Abstract

This thesis investigates the complex dynamics of laminar flow around a rotating circular cylinder and the resultant vortex shedding, utilizing computational fluid dynamics (CFD) simulations. A comprehensive numerical study was performed to assess the impact of cylinder rotation parameters, specifically the amplitude and frequency of rotational speed, on vortex shedding behavior. The simulations, conducted using ANSYS Fluent, explored various configurations of the cylinder's rotational speed characterized by dimensionless parameters such as the Reynolds number and Strouhal number. The study employed a detailed meshing strategy to ensure the accuracy and reliability of the simulation results, correlating closely with established benchmarks in fluid dynamics literature. The outcomes demonstrate significant variations in drag and lift coefficients with changes in the rotational parameters, revealing intricate relationships between the dynamics of vortex shedding and the rotational characteristics of the cylinder. The findings have profound implications for improving the efficiency and stability of systems involving cylindrical bodies in fluid flows, such as marine structures and aerodynamic components. Future research is suggested to further explore the interdependencies of rotational parameters and to optimize design and operational strategies for industrial applications involving fluid dynamics.

Keywords: Computational Fluid Dynamics (CFD), Vortex Shedding, Laminar Flow, Reynolds Number, Strouhal Number, Drag Coefficient, Lift Coefficient, Numerical Simulation, Flow Dynamics, Navier Stokes equation (NS), flow past bluff bodies, Von-Karman vortex stree

Table of Contents

1 Introduction

1.1 Motivation

The interaction of fluid flows with solid structures, particularly cylindrical bodies, poses a critical challenge in various engineering disciplines. This research is driven by the need to better understand and manipulate vortex shedding, a fluid dynamic phenomenon that significantly impacts the operational stability and energy efficiency of structures exposed to fluid flows. Vortex shedding is not only a fundamental aspect of fluid mechanics but also a critical concern in designing structures such as chimneys, submarine periscopes, and aircraft landing gears, where uncontrolled vortex-induced vibrations can lead to structural failures.
Given the complexities associated with rotational movements and their influence on vortex shedding, this thesis aims to delve into the fluid dynamics that describe how rotational speeds and frequencies modify the flow patterns around cylindrical objects. By focusing on the parametric study of these dynamics, the research seeks to mitigate adverse effects while enhancing beneficial applications, such as energy harvesting from fluid flows or reducing drag for more efficient vehicle designs.

1.2 Fluid Flow Past Bluff Bodies

A bluff body is characterized by its broad, non-streamlined shape, which does not easily allow air or fluid to flow smoothly around it. Unlike streamlined bodies designed to reduce drag and encourage laminar flow, bluff bodies have a sharp-edged or wide-front profile that causes the fluid to separate from the surface abruptly. This separation results in large wake regions and complex flow patterns, including vortex shedding. Common examples of bluff bodies include cylinders, square columns, and vehicle bodies—each influencing the surrounding fluid environment in unique ways.

The flow dynamics around bluff bodies are primarily governed by the Reynolds number (Re), which determines the flow regime—laminar, transitional, or turbulent—and influences the

characteristics of the wake formation. At low Reynolds numbers, the flow is steady and laminar, but as Re increases, it becomes unsteady and eventually transitions to turbulence, each regime marked by distinct vortex shedding patterns. The Strouhal number (St), another critical dimensionless parameter, is used to predict the shedding frequency of vortices, which is crucial for understanding the oscillatory nature of the forces exerted by the fluid on the bluff body.

1.2.1 Analysis of Flow Dynamics Around a Cylinder Across Different Reynolds Numbers

State		Regime		Re Ranges
L	Laminar	1	No-separation	0 to 4-5
		2	Closed Wake	4-5 to 30-38
		3	Periodic Wake	30-38 to 180 - 200
TrW	Transition in wake	1	Lower transition regime	180-200 to 220-250
		2	Upper transition regime	220-250 to 350-400
TrSL	Transition in Shear Layers	1	Lower subcritical	350-400 to $1*10^3$ -$2*10^3$
		2	Intermediate subcritical	1*103 -$2*10^3$ to $2*10^4$ - $4*10^4$
		3	Upper subcritical	$2*10^4$ -$4*10^4$ to $1*10^5$ -$2*10^5$
TrBL	Transition in Boundary Layers	0	Pre-critical	$1*10^5$ -$2*10^5$ to $3*10^5$ - $3.4*10^5$
		1	Single bubble	$3*10^5$ -$3.4*10^5$ to $3.8*10^5$ - $4*10^5$
		2	Two-bubble	$3.8*10^5$ -$4*10^5$ to $5*10^5$ -10^6
		3	Supercritical	$5*10^5$ -10^6 to $3.5*10^6$ -$6*10^6$
		4	Post-critical	$3.5*10^6$ -$6*10^6$ to (?)
T	FULLY TURBULENT	1	Invariable	(?) to ∞
		2	Ultimate	

Table 1 Flow regimes [1]

Fully Laminar State:

Flow around a cylinder at low Reynolds numbers (Re < 200) displays distinct laminar regimes, progressing from dominance by viscous forces to the onset of vortex shedding. Initially, at

extremely low Reynolds numbers (Re < 5), known as the creeping flow regime, the flow is fully governed by viscous forces with no separation from the cylinder. As Reynolds number increases, the influence of these forces diminishes, leading to steady flow separation and the formation of a stable, laminar wake directly behind the cylinder. This wake is characterized by free shear layers converging at a downstream confluence point.

As the Reynolds number progresses beyond 30-48, the flow enters a transitional phase where the elongated wake becomes unstable and begins to oscillate, giving rise to the well-known von Karman vortex street. This regime is characterized by shear layers rolling up into distinct eddies, indicating a gradual formation of laminar eddies, contrasting with the high-speed shedding mode observed at higher Reynolds numbers where turbulent eddies are shed directly from the cylinder.

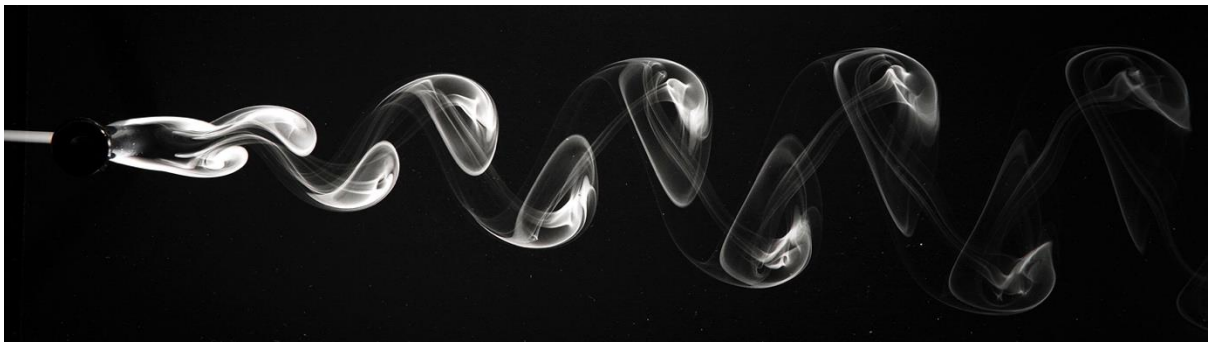

Figure 1 Visualisation of the vortex street behind a circular cylinder in air; the flow is made visible through release of glycerol vapour in the air near the cylinder [2]

Transitional States:

As the flow transitions from laminar to turbulent, distinct transitional states occur, categorized by Zdravkovich in 1997 based on their location: in the wake (TrW), in the shear layers (TrSL), and in the boundary layers (TrBL). Each type of transition introduces new flow structures which evolve distinctly:

Transition in the Wake (TrW): Starting around Re from 180-200 and progressing to 350-400, the wake's transition is marked by the formation of 'fingers', which are distortions in the laminar eddy filaments that begin at random spanwise locations and point toward the cylinder. This phase features eddies forming laminarly and becoming turbulent as they move downstream.

- Shift to High-Speed Mode: Around Re ≈ 250, the shedding mode changes from a low-speed mode to a high-speed mode, indicated by a jump in the Strouhal number and resulting in overlapping shedding modes. [3]

Transitional Stages in the Shear Layer:

Transitional stages within the shear layers evolve with increasing Reynolds numbers from 350-400 up to $1-2\times10^5$, initially defined as subcritical flow states. These stages denote a scenario where the boundary layer remains laminar up to and beyond the point of flow separation:

- **Lower, Intermediate, and Upper-Subcritical Regimes:** Beginning with the lower-subcritical regime (TrSL1), undulations develop along both free shear layers, evolving into chains of smaller eddies which eventually lead to the shortening of the eddy formation region and bringing the formation of eddies closer to the cylinder base.

Transition in the Boundary Layer (TrBL):

Transition in the boundary layer spans critical Reynolds numbers and involves complex interactions between shear layer dynamics and boundary layer behaviors. This transition is marked by the formation of laminar separation bubbles and a full transition to turbulence, significantly influencing the hydrodynamic properties and pressure distribution around the cylinder. The boundary layer transitions are particularly noted for the dramatic changes in drag coefficient and Strouhal number, indicating a shift in flow dynamics and hydrodynamic forces acting on the cylinder.

Fully Turbulent State:

In the fully turbulent state (T) , all disturbed regions around the cylinder become turbulent. This state is characterized by the stabilization of flow patterns and flow coefficients, such as drag and lift coefficients, which tend to remain constant with increasing Reynolds numbers. This stabilization occurs even as the effects of compressibility begin to emerge at very high Reynolds numbers, altering the flow dynamics through changes in air density and the speed of sound. [1]

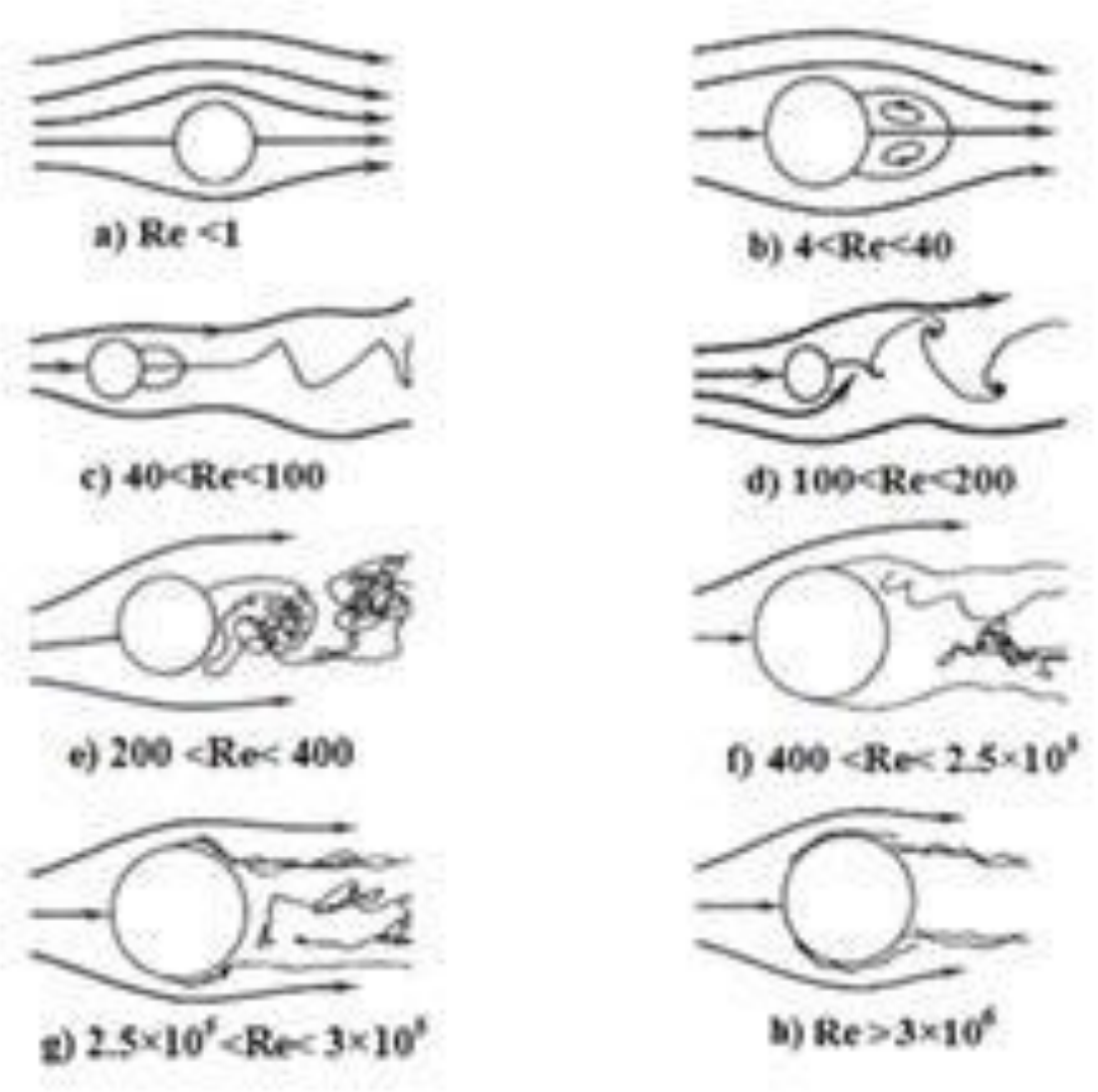

Figure 2 Regimes of fluid flow over circular cylinder [4]

1.3 Research Objectives

This thesis explores the fascinating dynamics of fluid flows around cylindrical structures, focusing on how rotational speeds influence vortex shedding. Through practical simulations and analyses, this study aims to enhance our understanding and offer innovative solutions that could be useful in various engineering applications.

- Understanding Vortex Shedding Dynamics**:** To examine how changes in the rotational speed of cylinders affect vortex formation and the associated structural impacts.
- Application of Computational Fluid Dynamics (CFD)**:** To use CFD tools to model flow interactions with rotating cylinders, ensuring that simulations are accurate by comparing them with established benchmarks.
- Exploring Hydrodynamic Forces: To investigate how cylinder rotation impacts drag and lift forces, aiming to link these changes directly to alterations in flow patterns.
- Optimizing Cylinder Design**:** To apply findings from the research to suggest design improvements for cylinders that could enhance their performance in fluid flows.
- Influencing Industry Standards: To contribute findings that could update industry practices, particularly in naval, aerospace, and environmental engineering.

By achieving these objectives, this thesis will not only enhance academic knowledge but also improve practical engineering designs. The research is designed to bridge the gap between theoretical studies and real-world applications, providing new insights that could lead to more effective and efficient design and operational strategies.

2. Theoretical framework: Governing Equations and Computational Fluid Dynamics

The study of fluid dynamics encompasses a vast array of applications, from understanding meteorological patterns to designing high-performance aircraft and enhancing industrial processes. At the core of fluid dynamics lies the mathematical portrayal of fluid motion, encapsulated by the governing equations known as the Navier-Stokes equations. These equations are derived from fundamental conservation laws that ensure mass, momentum, and energy remain constant within a fluid system under various conditions. They are crucial for predicting how fluids behave under different forces and constraints, which is essential for both theoretical research and practical applications.

In engineering, particularly in disciplines involving fluid flow around structures such as cylinders, the need to comprehend and predict fluid behavior is paramount. Rotating cylinders, for instance, are commonplace in mechanical engineering, naval architecture, and aerospace engineering. They are found in machinery components like turbines, pumps, and compressors, as well as in aerodynamic devices used in aircraft and marine vessels. The rotation of these cylindrical structures introduces additional complexities into the flow patterns, which can lead to phenomena such as increased lift (Magnus effect), drag fluctuations, and complex vortex shedding patterns. These phenomena can influence the efficiency, stability, and acoustic signatures of engineering systems.

To fully leverage the capabilities of computational and experimental tools in fluid dynamics, a deep and intuitive understanding of the governing equations is necessary. These equations not only describe the physical reality of fluid flows but also guide engineers in designing experiments, developing simulation models, and interpreting data. Understanding these principles is crucial for optimizing designs to enhance performance and mitigate unwanted effects such as noise, vibrations, and mechanical failures due to flow-induced forces.

As technology progresses, the importance of precise and predictive fluid dynamics simulations grows. Modern computational fluid dynamics (CFD) tools rely heavily on accurate implementations of the Navier-Stokes equations to simulate real-world conditions as closely

as possible. These tools allow engineers to visualize complex flow phenomena around rotating cylinders in real-time, enabling the iterative design and optimization of systems before physical prototypes are built. This approach not only saves time and resources but also pushes the boundaries of what can be achieved in fluid dynamics research and application.

Figure 3 E-Ship 1 with Flettner rotors mounted [5]

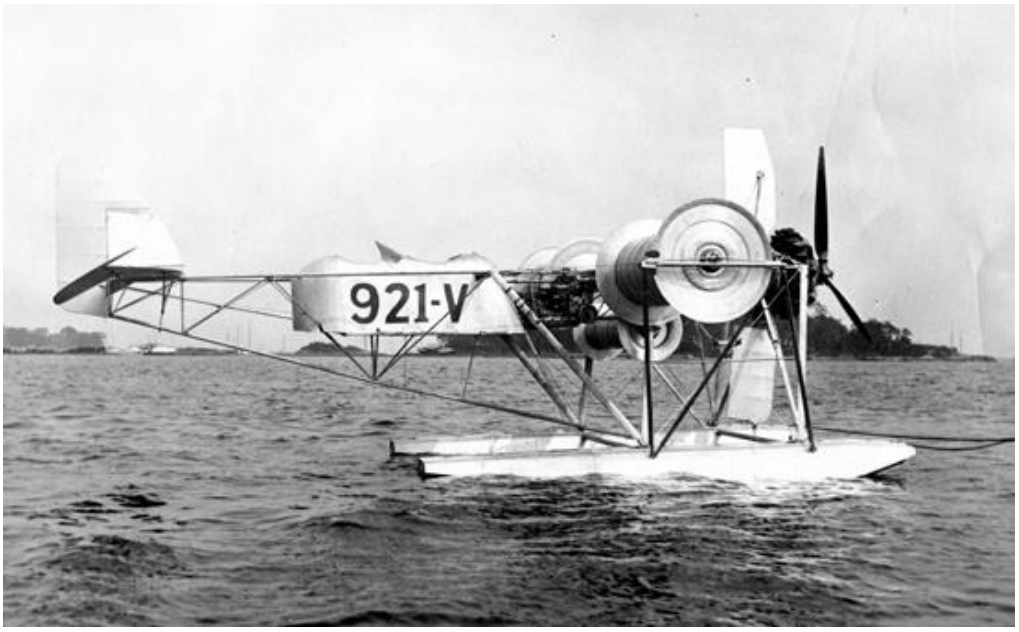

Figure 4 Flettner Rotor Aircraft [6]

2.1 Governing Equations

When the problem involves fluids, a set of equations can be used to solve the flow fields of interest (velocity, pressure, vorticity, and so on). These are the Navier-Stokes equations. The Navier-Stokes equations include mass and momentum conservation, as well as energy conservation. The most crucial aspects of this diploma thesis are the conservation of mass and momentum.

2.1.1 Conservation of Mass: Continuity Equation

In fluid dynamics, the conservation of mass is a core principle that ensures the mass within any control area remains constant over time, assuming no mass is being added or removed.

$$\frac{DM_{SYS}}{Dt} = 0$$

Equation 1 Conservation of mass principle [7]

This principle is encapsulated in the continuity equation, which is critical for studies involving incompressible flows, such as the flow around rotating cylinders in two-dimensional spaces.
For two-dimensional flow dynamics, particularly relevant to computational simulations of flow around cylindrical structures, the continuity equation simplifies to account for variations in the plane perpendicular to the axis of rotation. The general form for a three-dimensional, compressible flow includes time-dependent and spatial changes in density:

$$\frac{\partial \rho}{\partial t} + \nabla \cdot (\rho V) = 0$$

Equation 2.1.2 Continuity equation for compressible flow [7]

However, for incompressible flow, where density
ρ is constant and does not change with pressure or time, the equation simplifies significantly:

$$\nabla \cdot V = 0$$

Equation 2.1.3 Continuity equation for incompressible flow [7]

In the two-dimensional analysis, the velocity field V is described only by its components in the x and y directions since any variation in the z-direction is neglected. This is particularly relevant in the analysis of flow over long, slender cylinders where the end effects are minimal or outside the scope of the study.
The velocity vector in a two-dimensional Cartesian coordinate system is given by:

$$V = u\vec{\boldsymbol{\imath}} + v\vec{\boldsymbol{\jmath}}$$

Equation 2.4 Velocity vector in a two-dimensional Cartesian coordinate system. [7]

Where u and v represent the velocity components along the x and y axes, respectively:

$$u = u(x, y, t) \text{ and } v = v(x, y, t)$$

Equation 2.5 Velocity components along the x and y axes.

The divergence of this velocity vector is then:

$$\nabla \cdot V = \frac{\partial u}{\partial x} + \frac{\partial v}{\partial y}$$

Thus, the continuity equation for an incompressible, two-dimensional flow simplifies to:

$$\frac{\partial u}{\partial x} + \frac{\partial v}{\partial y} = 0$$

Equation 2.6 Continuity equation for incompressible, two-dimensional flow. [7]

2.1.2 Conservation of Momentum: Navier-Stokes Momentum Equation

Momentum conservation in fluid dynamics is intricately represented by the Navier-Stokes equations. These equations are foundational in engineering and physics for modeling fluid motion, particularly around objects where complex flow patterns such as vortices and turbulent wakes can develop. In a two-dimensional scenario, these patterns are critical in understanding the flow dynamics around structures like rotating cylinders.

For an incompressible, two-dimensional fluid flow, the Navier-Stokes equations simplifying the momentum conservation law can be expressed for each spatial dimension within the Cartesian plane:

1. **x-Momentum Equation:**

$$\rho\left(\frac{\partial u}{\partial t}+u\frac{\partial u}{\partial x}+v\frac{\partial v}{\partial y}\right)=-\frac{\partial p}{\partial x}+\mu\left(\frac{\partial^2 u}{\partial x^2}+\frac{\partial^2 v}{\partial y^2}\right)+f_x$$

Equation 2.7 x-Momentum Equation [7]

This equation governs the horizontal momentum, accounting for changes due to unsteady behavior (time-dependent), advection (movement of momentum with the fluid), pressure forces, viscous dissipation, and external forces such as gravity.

2. **y-Momentum Equation:**

$$\rho\left(\frac{\partial v}{\partial t}+u\frac{\partial u}{\partial x}+v\frac{\partial v}{\partial y}\right)=-\frac{\partial p}{\partial y}+\mu\left(\frac{\partial^2 u}{\partial x^2}+\frac{\partial^2 v}{\partial y^2}\right)+f_y$$

Equation 2.8 y-Momentum Equation [7]

Similarly, this equation handles the vertical momentum, incorporating similar terms adjusted for the vertical direction.

2.1.3 Reynolds number

The Reynolds number (Re) is an important dimensionless quantity in fluid mechanics, which plays an important role in the type and pattern of fluid flow. It is used in a wide range of applications, from the movement of fluid within a pipe to the passage of air around the wing of an aircraft. The Reynolds number is a useful guide for characterizing the transition stage of a fluid flow from laminar to turbulent, and for studying flows at scale, such as the flow around an aircraft in an aerodynamic tunnel.

The Reynolds number is defined as the ratio of inertia forces to friction forces, and it's given by the following formula.

$$Re=\frac{\rho VL}{\mu}$$

Equation 2.9. Reynolds Number [7]

Where ρ: fluid density

V: flow velocity

L: characteristic flow length

μ: viscosity

2.1.4 Strouhal number

The Strouhal number (St) is a dimensionless number that describes the mechanisms of an oscillating flow. This parameter is named after Vincenc Strouhal, a Czech physicist who experimented in 1878 with cables that exhibited vortex generation and "echoed in the air".The Strouhal number is a critical quantity in non-permanent fluid mechanics phenomena because it indicates the frequency of a periodic occurrence in a dimensionless manner.
It is defined as

$$St = fLV$$

Equation 2.10 Strouhal Number [7]

Where f: the frequency of vortex emission

L: the characteristic quantity (e.g. the hydraulic diameter or thickness of a fin)

V: the fluid velocity

2.1.5 Lift coefficient

The lift coefficient (C_L) expresses the lift force exerted on a body in the flow of a fluid in a non-dimensional form.
It is defined as

$$C_L = \frac{L}{qS}$$

Equation 2.9 Lift Coefficient [7]

Where L :the lift force

q : the dynamic pressure equals $q = \frac{\rho V^2}{2}$ *(Equation .2.10 Dynamic pressure)*

S : the surface of the cross section of the body to which the lift force is applied

2.1.6 Drag coefficient

The drag coefficient (C_D) expresses the resistance or drag force (Drag) applied on a body in the flow of a fluid in a dimensionless form.

It is defined as

$$C_L = \frac{D}{qS}$$

Equation 2.11 Drag Coefficient [7]

Where D :the drag force

q : the dynamic pressure (same as above)

S : the surface of the cross section of the body to which the drag force is applied

2.1.7 Moment

The moment (M) of a rotational body in a fluid flow can be expressed by the function:

$$M = F\ d$$

Equation 2.12 Moment [7]

Where: F : is the applied force,

d : is the distance from the axis of rotation.

This function captures the fundamental relationship between the applied force and the distance from the axis of rotation, indicating how these factors contribute to the rotational tendency of the body. In the context of fluid mechanics, the moment plays a crucial role in understanding the rotational behavior of objects subjected to fluid forces. Factors such as fluid density (□ρ), flow velocity (□V), and the geometry of the object influence the applied force and, consequently, the moment. The analysis of moments is essential for predicting and optimizing the stability and control of rotational motion in fluid environments, making it a key aspect in the design and study of systems involving rotating bodies.

2.1.8 Power

The power (P) of a rotational body in a fluid flow can be expressed by the function:

$$P = \tau\ \omega$$

Equation 2.13 Power [7]

Where: τ : the torque applied to the body,

ω : the angular velocity.

2.2 Computational Fluid Dynamics

In contemporary fluid dynamics research, numerical methods play a crucial role in predicting and analyzing flow fields around complex geometries, both in internal and external flows. Among these methods, various levels of computational intensity and detail are achieved, ranging from Direct Numerical Simulation (DNS), which captures every minute detail of the flow, to Reynolds-averaged Navier-Stokes (RANS) methods that provide time-averaged solutions ideal for more stable, predictable flows. For the purposes of this research, the focus is on simulating the laminar flow around a rotating cylinder in a two-dimensional setting. Due to the relatively low-speed and stable nature of the flow in this context, the two-dimensional, unsteady incompressible laminar Navier-Stokes equations were numerically solved using the SIMPLE (Semi-Implicit Method for Pressure-Linked Equations) algorithm. This choice of method strikes a balance between computational efficiency and the need for accuracy in capturing the transient behaviors and dynamic flow patterns induced by the cylinder's rotation, providing a detailed insight into the fluid dynamics involved without the excessive computational overhead of more intensive simulations like DNS or LES.

2.2.1 Computational grids

In computational fluid dynamics (CFD), the selection of an appropriate computational grid or mesh is crucial for the accuracy and efficiency of simulations. Meshes are categorized into three primary types, each serving different needs based on the complexity of the geometry and the specific requirements of the simulation [8]:

Structured Meshes: These are characterized by regular connectivity and can be expressed as a multi-dimensional array, making them efficient for computational processes. Structured meshes are often used for simpler geometries or when high resolution is required in specific areas without complex geometrical constraints. [9]

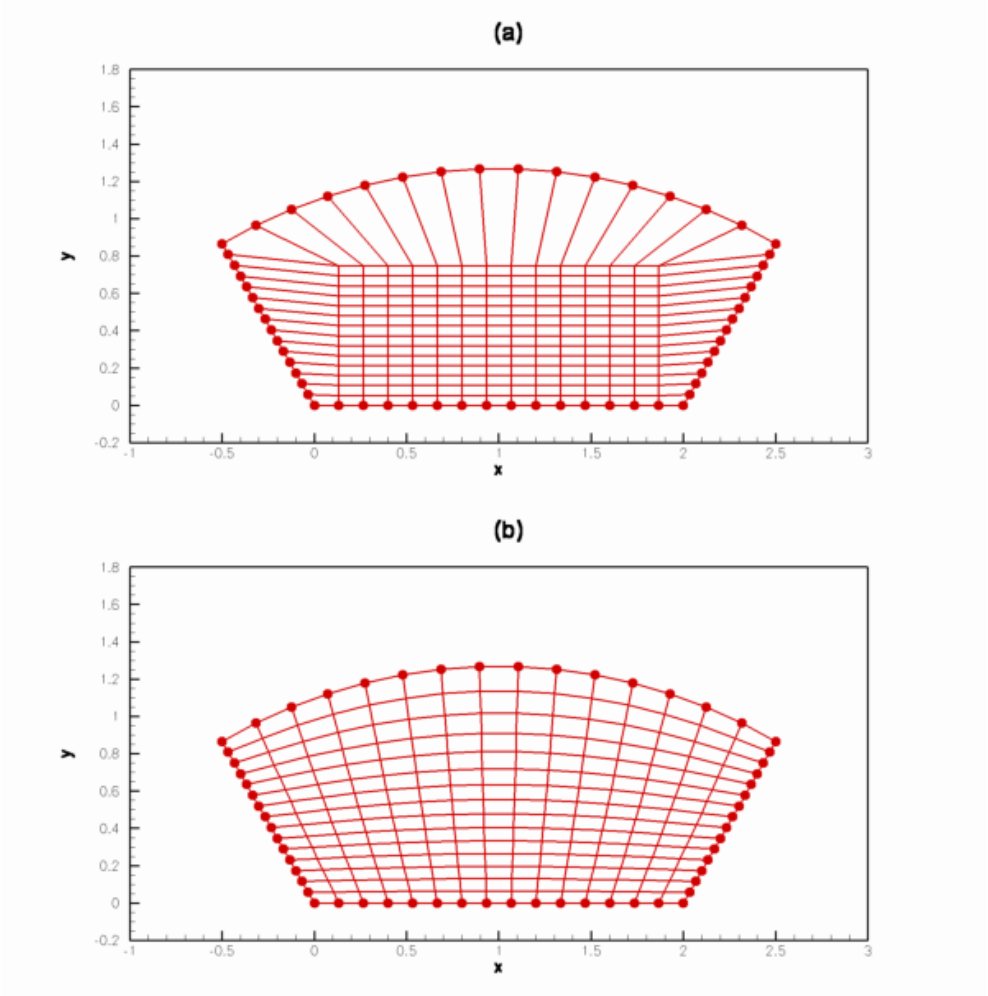

Figure 3. Elliptic Structured Grid Generation [9]

Unstructured Meshes: These consist of arbitrarily placed nodes and are more flexible, allowing them to conform to complex geometries. Unstructured meshes are advantageous for modeling intricate details and complex boundaries, making them ideal for simulations involving complex shapes. [10]

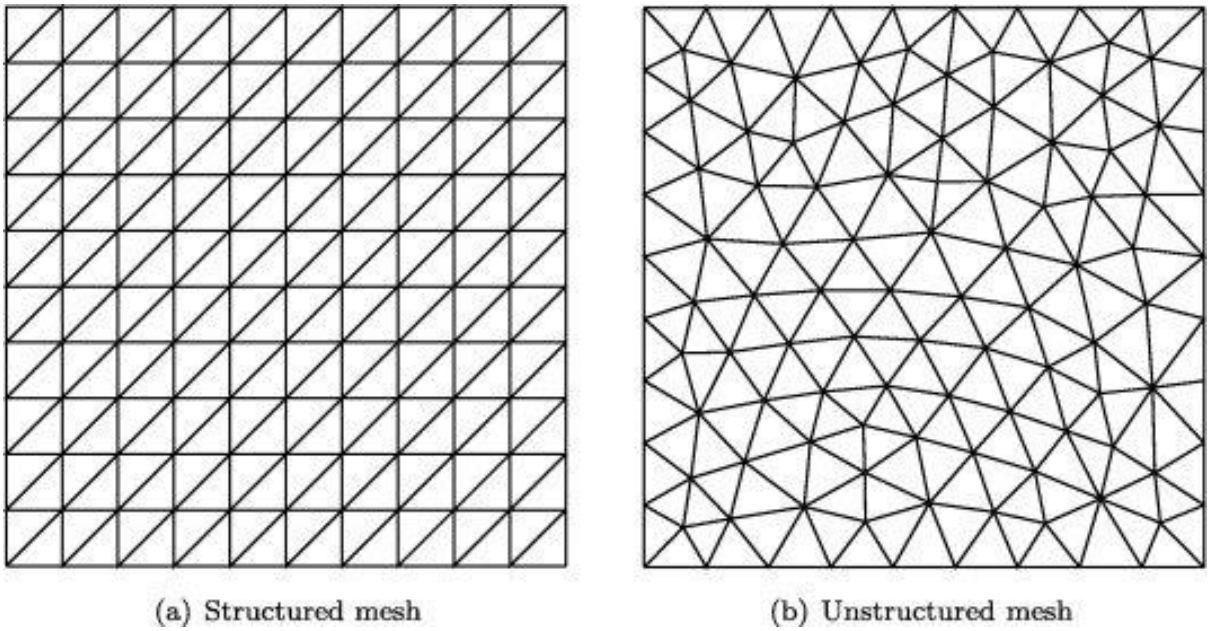

Figure 4 Example of a structured triangular mesh and an unstructured triangular mesh in a unit box. [11]

Hybrid Meshes: Combining features of both structured and unstructured meshes, hybrid meshes are employed to exploit the benefits of both types. They are particularly useful in simulations that involve areas with varying geometric complexity across the domain.

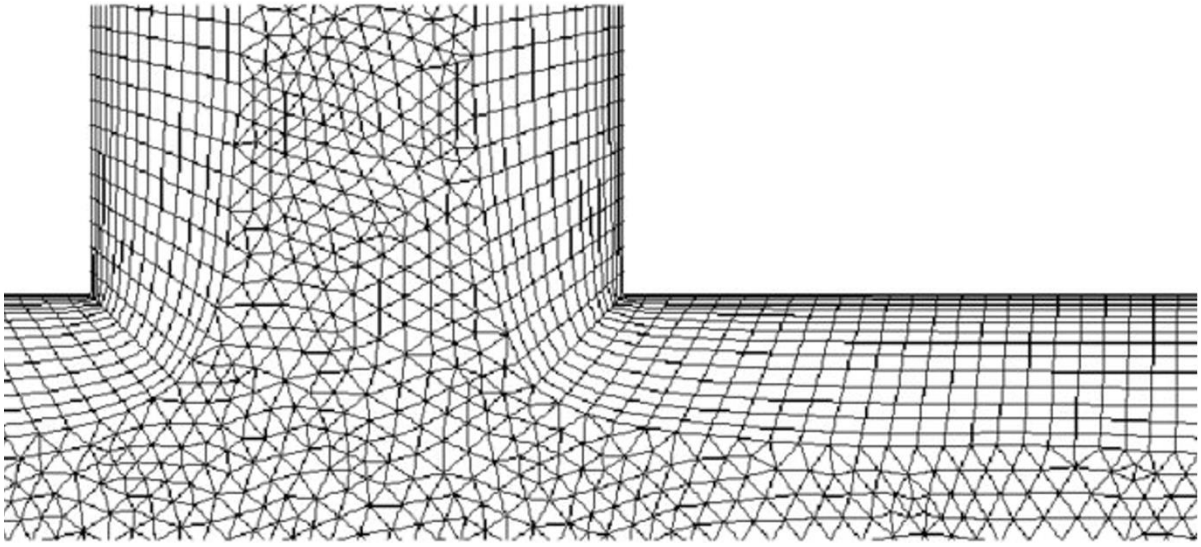

Figure 5 Close up view of hybrid mesh [21]

In my thesis, I chose to use structured meshes for the two-dimensional analysis of flow around a rotating cylinder due to several key advantages:

1. **Geometric Alignment and Computational Efficiency**: Structured meshes, with their regular grids of quadrilateral or triangular elements, align seamlessly with the simple

geometrical contours of the cylindrical domain. This regularity ensures optimized computational efforts, simplifying the numerical treatment and enhancing solver performance due to reduced complexity in algorithmic processing.

2. **Implementation Simplicity**: The consistent structure and connectivity of structured meshes facilitate easier and faster implementation within simulation software. This results in quicker preprocessing and mesh generation, significantly streamlining the setup phase of simulations.

3. **Numerical Stability**: The uniformity of cell sizes and shapes in structured meshes promotes numerical stability. This uniform discretization minimizes errors and enhances the predictability and reliability of the solver's outcomes, which is crucial for accurately capturing the dynamics of laminar flow around cylinders. [12]

2.2.2 SIMPLE Algorithm

The SIMPLE (Semi-Implicit Method for Pressure-Linked Equations) algorithm, developed by Patankar and Spalding in the early 1970s, is pivotal in the field of Computational Fluid Dynamics (CFD) for the numerical solution of the Navier-Stokes equations in incompressible, steady-state fluid flow scenarios. This algorithm efficiently addresses the coupling of velocity and pressure fields, which is crucial for accurately predicting fluid flow dynamics, particularly around bluff bodies such as cylinders used in various engineering applications.

The SIMPLE algorithm follows a structured iterative process, integrating both predictor and corrector steps to ensure convergence to the physical solution of fluid flow problems:

Initialization: Begin with an initial guess for the pressure and velocity fields across the computational domain, setting the stage for the iterative correction process.

Momentum Equations: Discretized momentum equations are solved to predict an intermediate velocity field based on the guessed pressure field. The general form of the momentum equation for velocity component u is expressed as:

$$a_{u,i,j}\, u^*_{i,j} = \sum a_{nb}\, u^*_{nb} + \left(p_{i-1} - p_{i,j}\right)\Delta y + b_{i,j}$$

Equation 14 Discretized momentum equation for initial guess of pressure on the x axis [13]

$$a_{v,i,j}\, v^*_{i,j} = \sum a_{nb}\, v^*_{nb} + \left(p_{i-1} - p_{i,j}\right)\Delta x + b_{i,j}$$

Equation 15Descritized momentum equation for initial guess of pressure on the y axis [13]

Pressure Correction: A pressure correction equation is derived from the continuity equation discrepancy, calculated to adjust the pressure field and align it with mass conservation:

$$a_{p,i,j} p'_{i,j} = \sum a'_{nb} p'_{nb} + (\rho \Delta x \Delta y)(\nabla \cdot u^*)$$

Equation 16 Presure correction equation [13]

Velocity Field Correction: Using the calculated pressure corrections, the velocity fields are updated to satisfy the continuity equation:

$$u_{i,j} = u^*_{i,j} + d_{u,i,j}(p'_{i-1,j} - p'_{i,j)}$$

$$v_{i,j} = v^*_{i,j} + d_{v,i,j}(p'_{i-1,j} - p'_{i,j)}$$

Implementing the SIMPLE algorithm involves selecting appropriate under-relaxation factors to ensure convergence stability. These factors, crucial in the adjustment of pressure and velocity fields, help dampen the corrections applied during each iteration, preventing oscillations and ensuring a smooth convergence path.

Over the years, variations like SIMPLEC and SIMPLER have been developed to enhance the convergence and stability of the original algorithm, especially in complex simulations involving turbulent flows, high Reynolds numbers, or intricate geometries.

The SIMPLE algorithm offers a structured approach for computing pressures and velocities within computational fluid dynamics (CFD). It utilizes an iterative method where the momentum equations are sequentially coupled with other scalar quantities. This necessitates a methodical progression through specific computational steps, as outlined in the referenced CFD procedure diagram.

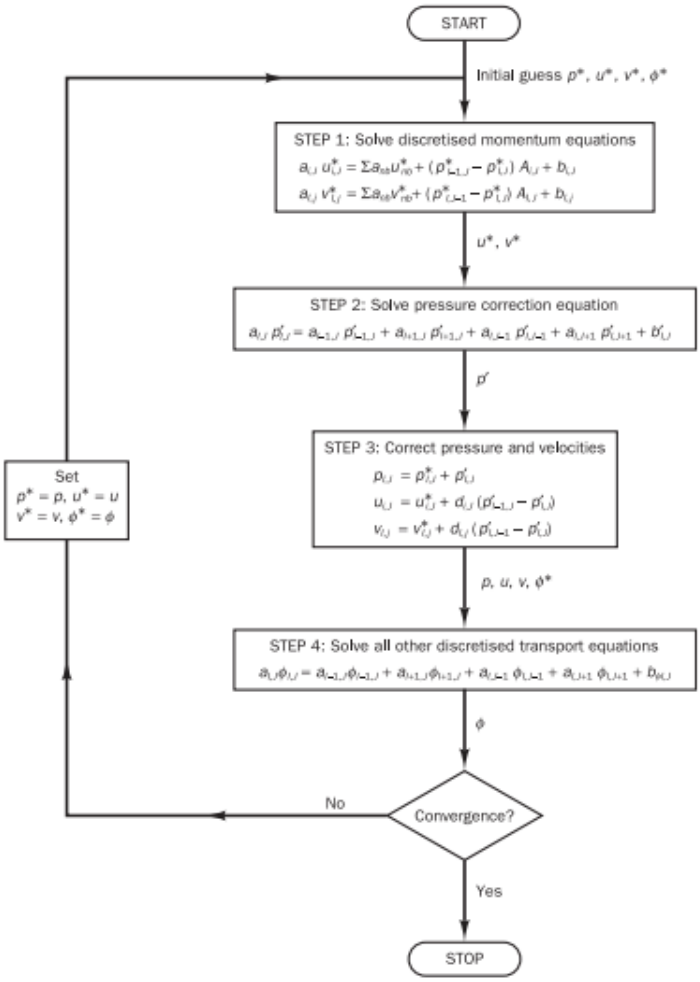

Figure 6 The SIMPLE algorithm [13]

2.3 Vortex Shedding - Literature review

2.3.1 Historical Overview and Fundamental Research on Vortex Shedding and von Kármán Vortex Street

Vortex shedding and the von Kármán vortex street are pivotal phenomena in fluid dynamics that significantly influence engineering designs and environmental processes. This chapter traces the historical development and key research contributions that have shaped our understanding of these phenomena.

The phenomenon of vortex shedding, particularly as it manifests in the von Kármán vortex street, was first rigorously analyzed by Theodore von Kármán in the early 20th century. Von Kármán identified the conditions under which alternating vortices are shed from bluff bodies like cylinders, leading to the characteristic staggered pattern known as the von Kármán vortex street.

Pioneering Studies and Developments

1. **Theodore von Kármán's Theoretical Analysis**: Von Kármán was among the first to provide a mathematical description of the vortex shedding process, linking the vortex formation to the stability and turbulence in the wake of a bluff body. His work laid the foundation for all subsequent theoretical and experimental studies in vortex-induced phenomena.
2. **Experimental Insights by Bénard and Roshko**: Henri Bénard's experiments in the early 1900s further elaborated on the mechanics of vortex shedding and transition to turbulence behind cylindrical bodies. Later, Anatol Roshko in the 1950s provided detailed experimental data on the regimes of vortex shedding, which helped refine the understanding of the Strouhal number and its relation to the flow dynamics around cylinders.
3. **Advances in Computational Fluid Dynamics**: With the advent of computational fluid dynamics in the late 20th century, simulations began to play a crucial role in studying vortex shedding. CFD has allowed for detailed visualization and analysis of the flow fields around bluff bodies, enhancing predictions and validations of theoretical models.

Modern Applications and Ongoing Research

Today, the insights from the study of vortex shedding and von Kármán vortex street are applied in designing structures susceptible to vortex-induced vibrations, such as bridges, skyscrapers, and underwater pipelines. Ongoing research continues to explore new aspects of these phenomena, including their impact on renewable energy technologies and environmental processes. Here are some examples of modern applications of these phenomena, detailing specific examples that highlight their impact on technology and industry.

Structural Engineering: Taipei 101 Damper

In structural engineering, vortex shedding is crucial in the design of skyscrapers and large structures exposed to wind. The Taipei 101, one of the tallest buildings globally, integrates a massive tuned mass damper to counteract oscillations induced by vortex shedding. This damper acts as a pendulum, offsetting movements from wind gusts, thus ensuring structural integrity and occupant comfort.

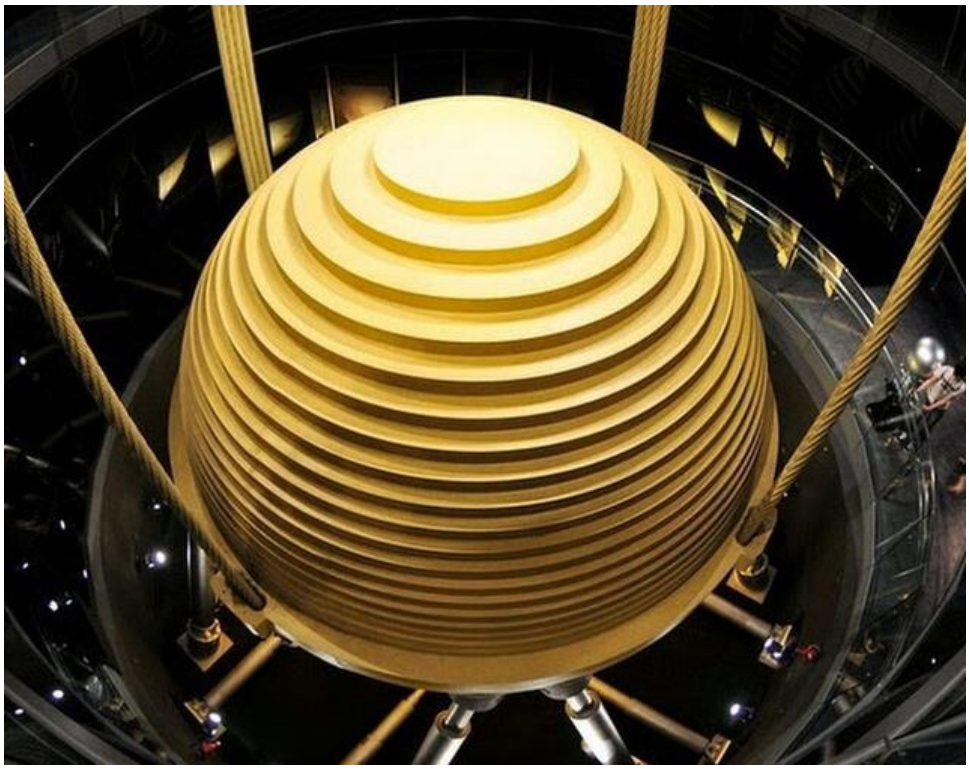

Figure 7 Tuned mass dumper used in the Taipei 101 Damper [14]

Aerospace Engineering: Vortex Generators on Aircraft

Aerospace applications utilize vortex shedding principles to enhance aircraft performance and safety. Vortex generators on aircraft wings manipulate airflow to delay flow separation. This control is crucial for maintaining lift at high angles and preventing stalling, significantly enhancing safety during critical flight phases.

Figure 8 Left: Various types of vortex generators. Right: Installation of vortex generators on the flap. [22]

Automotive Industry: Rear Spoilers on Cars

In the automotive industry, rear spoilers are designed to influence airflow and reduce vortex shedding at high speeds. These features decrease the drag and lift forces acting on the vehicle, leading to enhanced stability and improved fuel efficiency.

Renewable Energy: Wind Turbine Blade Design

Renewable energy technologies, particularly wind turbines, incorporate design features to optimize vortex shedding. By refining the shedding of vortices at blade tips, these turbines achieve greater efficiency and longevity, minimizing wear and tear from vortex-induced vibrations.

Marine Engineering: Offshore Platform Design

In marine engineering, understanding vortex shedding is critical for designing offshore platforms. Vortex-induced vibrations can pose significant risks to the structural integrity of these platforms.

Example: Platforms Semi-submersible platforms are designed to minimize the effects of vortex shedding through streamlined shapes and damping systems that absorb and counteract the energy of the vortices. This design consideration is crucial for maintaining platform stability and operational functionality in harsh marine environments. [15]

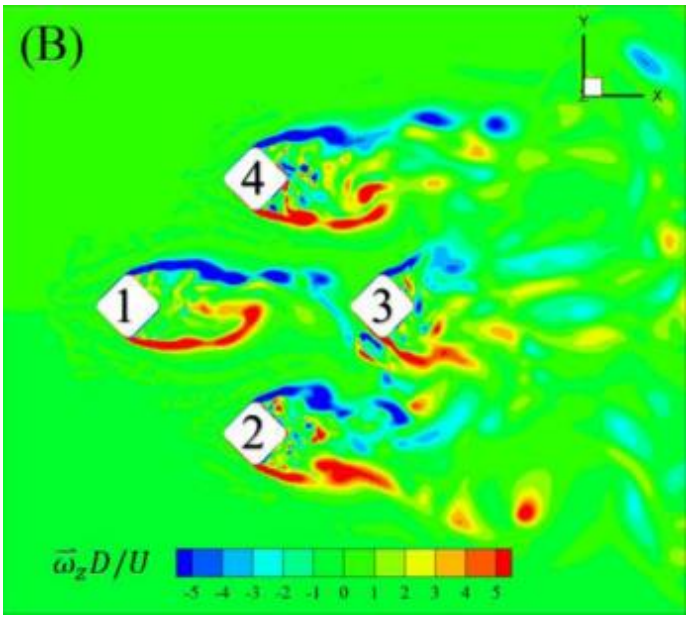

Figure 9 Non- dimentional spanwise vorticity contours around DDS at the middle draft level showing the instantaneous flow fielsa around the DDS. [15]

2.3.2 Vortex Shedding suppression control

Vortex shedding is a phenomenon that occurs when a fluid flows past a bluff body, such as a cylinder. As the fluid flows around the body, it creates alternating vortices, or eddies, that are shed from the body's trailing edge. These vortices can cause the body to vibrate, which can lead to structural failure. Several methods have been proposed and studied for vortex shedding suppression, both passive and active.

Passive Methods

Passive methods are those that do not require any external power source to operate. They are typically simpler and less expensive than active methods, but they may not be as effective in all cases. Some examples of passive methods include:

- **Using a slit in the cylinder:** A slit in the cylinder can disrupt the formation of vortices. The size and location of the slit are important for effective vortex shedding suppression.

- **Adding a splitter plate to the cylinder:** A splitter plate is a thin plate that is placed behind the cylinder. It helps to break up the vortices and reduce vortex shedding. The size and location of the splitter plate are important for effective vortex shedding suppression.
- **Modifying the cylinder's shape:** Changing the cylinder's shape can also disrupt the formation of vortices. For example, using a streamlined shape or adding helical strakes to the cylinder can reduce vortex shedding.
- **Adding fins or fairings:** Fins or fairings can be added to the cylinder to streamline the flow around it and reduce vortex shedding. The size and location of the fins or fairings are important for effective vortex shedding suppression.
- **Using porous materials:** Porous materials, such as foams or meshes, can help to disrupt the formation of vortices. The porosity and thickness of the material are important for effective vortex shedding suppression.

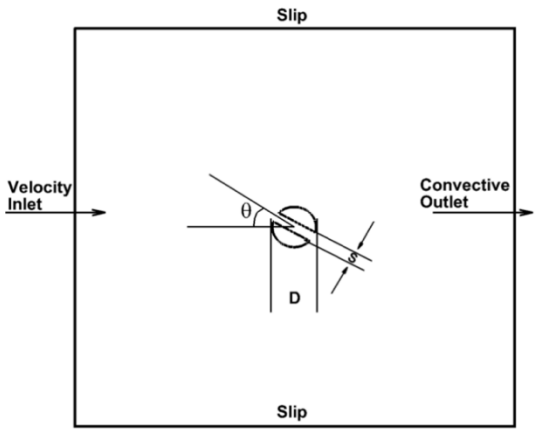

Figure 1 Slit in cylinder for vortex shedding suppression. [23]

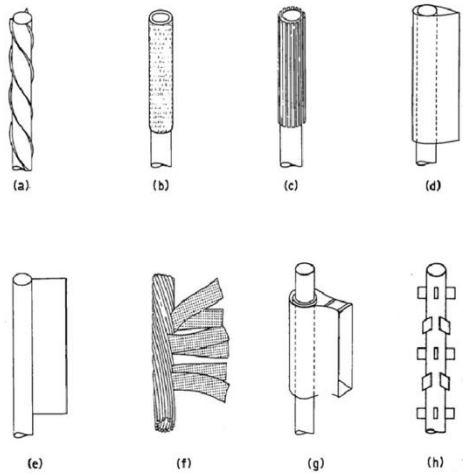

Figure 2 Add-on devices for suppression of vortex-induced vibration of cylinders: (a) helical strake; (b) shroud; (c) axial slats; (d) streamlined fairing; (e) splitter; (f) ribboned cable; (g) pivoted guiding vane; (h) spoiler plates [24]

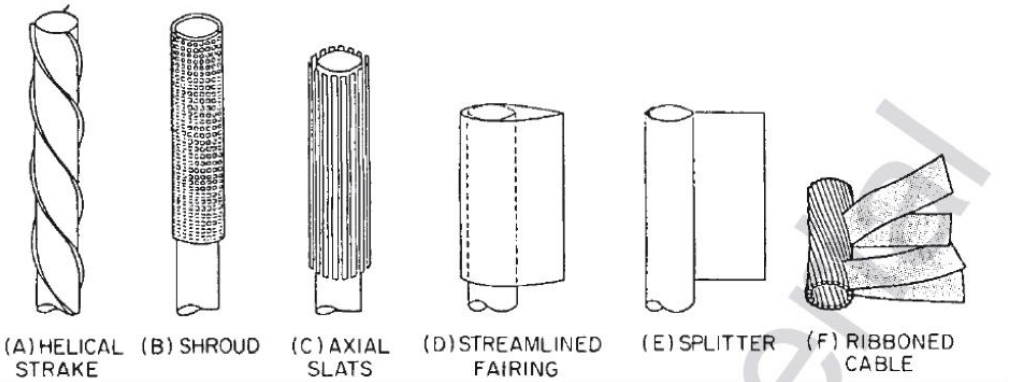

Figure 3 Methods of reducing vortex-induced vibration [26]

- **Using vortex generators**: Vortex generators are small devices that are attached to the cylinder to create small vortices that disrupt the formation of larger vortices. The size, location, and orientation of the vortex generators are important for effective vortex shedding suppression.

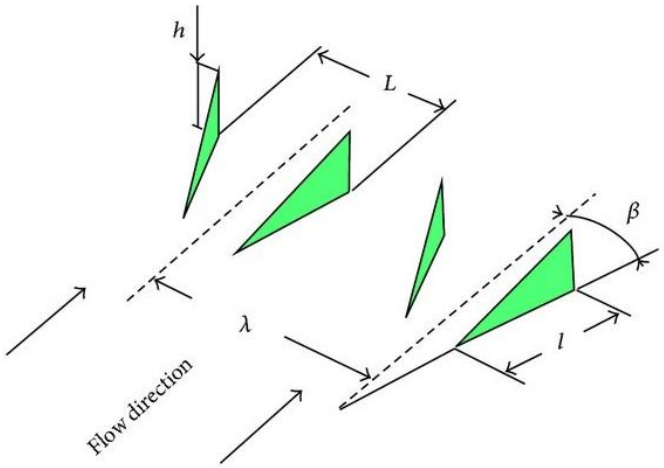

Figure 4 Vortex Generators [25]

- **Using surface modifications:** The surface of the cylinder can be modified to change its properties and reduce vortex shedding. For example, the surface can be coated with a material that has a low drag coefficient or a high roughness factor.

Active Methods

Active control methods for suppressing vortex shedding involve the application of external forces or inputs to manipulate the flow around the cylinder. These methods are particularly effective in various engineering applications where flow-induced vibrations need to be minimized for structural integrity and performance enhancement. Here, we discuss several active control techniques:

- **Rotational Oscillation:** Rotational oscillation involves the periodic rotation of the cylinder to disrupt the formation of coherent vortex street. By adjusting the frequency and amplitude of the rotational motion, the vortex shedding can be suppressed, leading to a reduction in lift and drag forces. This method is particularly useful in applications where the cylinder can be easily rotated with minimal additional energy input. [16]
- **Injecting/absorbing fluid in the boundary layer:** Fluid can be injected or absorbed from the boundary layer around the cylinder to disrupt the formation of vortices. The amount and location of fluid injection/absorption are important for effective vortex shedding suppression. [17]
- **Forcing Methods:** Forcing methods include applying external disturbances to the flow, such as acoustic waves or periodic jets. These disturbances can alter the natural shedding frequency, thus suppressing the formation of vortices. The effectiveness of forcing methods depends on the synchronization between the applied forcing frequency and the natural vortex shedding frequency. [18]
- **Using flow control devices:** Flow control devices, such as suction or blowing devices, can be used to control the flow around the cylinder and reduce vortex shedding. The location, size, and operation of the flow control devices are important for effective vortex shedding suppression.

3 Numerical simulation of laminar flow around a circular cylinder

3.1 Case Study and CFD set-up

This case study investigates the effect of a time-varying rotational speed of a cylinder on the emission of vortex shedding. Vortex shedding is a phenomenon of fluid-borne oscillations that can be generated by the interaction between an object and the surrounding fluid. In this case, the object is a moving cylinder that is rotating with a periodic sinusoidal variation.

3.1.1 Model Description

The flow around the rotating cylinder is modeled as a two-dimensional, steady-state, incompressible flow. The cylinder is assumed to be rigid and impermeable. The fluid is assumed to be Newtonian and inviscid. The rotational speed of the cylinder is given by the parametric form.

$$V(a,b) = V_c sin(2\pi f_c t) = aV_\infty sin(2\pi b f_o t)$$

Equation 0.1 Parametric form of rotational speed of the cylinder.

where:

V_c is the amplitude of the rotation velocity (m/s)
a is the amplitude parameter (dimensionless)
V_∞ is the undisturbed flow velocity (m/s)
f_c is the frequency of variation of the rotation velocity (Hz)
b is the frequency ratio parameter (dimensionless)
f_o is the fundamental frequency of emission of eddies (Hz)

The parameter a expresses the amplitude of the rotation velocity as a multiple of the undisturbed flow velocity V_∞. For example, if a =0.5, then the amplitude of the rotation velocity is 50% of the undisturbed flow velocity.

The parameter b expresses the frequency of variation of the rotation velocity as a multiple of the fundamental frequency of emission of dynons f_o. For example, if b =2, then the frequency of variation of the rotation velocity is twice the fundamental frequency of emission of eddies.

The fundamental frequency of emission of eddies f_o is found as the frequency of emissions for our benchmark case for Re=100 and a stationary cylinder and it f_o=0.159 Hz.

3.1.2 CFD Setup

The case described above is simulated using ANSYS Fluent Academic edition. ANSYS Fluent is a commercial CFD software package. FLUENT is based on the finite volume method (FVM), which is a popular numerical method for solving partial differential equations (PDEs).

The CFD setup consists of the following steps:

- Geometry Generation: We articulate the domain geometry, ensuring it accurately represents the physical space in which the fluid dynamics are to be studied. This initial step is crucial as it forms the basis of the simulation's spatial parameters.

- Mesh Generation: Subsequent to defining the geometry, we proceed to generate the mesh. This mesh is designed to ensure high-resolution data capture, particularly around the cylinder where flow patterns are most complex.

- Fluent Solver: The solver configuration in ANSYS Fluent is meticulously tailored to the outlined model parameters, with specifics as follows:
  - Transient Time Modeling: We adopt a transient framework to accommodate the unsteady nature of the flow, especially given the periodic rotational input.
  - Laminar Flow Regime: Based on the Re=100 condition, a laminar flow model is appropriate, emphasizing the dominance of viscous forces.
  - Material Properties: The fluid's physical characteristics, such as density and viscosity, are inputted to correspond with the benchmark scenario.
  - Boundary Conditions: Defined inlet and outlet conditions mimic the flow entry and exit, while the cylinder wall is modeled to enforce a no-slip boundary condition.
  - Solver Settings: The SIMPLE scheme is utilized for pressure-velocity coupling, and second-order discretization methods are applied to guarantee numerical accuracy.
  - Solution Monitoring: Under-relaxation factors are fine-tuned, and forces acting on the cylinder walls are specified for monitoring purposes.

- Solution Initialization and Advancement: Initial conditions are established, and a fixed time step size is selected for the progression of the simulation, facilitating precise temporal tracking of flow behavior.

So finally after following all the above, the settings are for ANSYS Fluent solvere were the following:

Time: Transient

Model: Laminar

Materials: Fluid: user_fluid: density=1(kg/m^3), viscosity=0.01(kg/(m*s))

Boundary Conditions

Inlet: Velocity Inlet: Velocity Magnitude=1 (m/s)

Outlet: Pressure Outlet: Gauge Pressure= 0 (Pa)

Wall: Stationary Wall, Shear Conditions: No slip condition

Reference Values: Compute from: inlet

Solution Methods:

Pressure-Velocity Coupling

Scheme: SIMPLE

Spatial Discretization

Gradient: Least Squares Cell Based

Pressure: Second Order

Momentum: Second Order Upwind

Pseudo Time Method: Off

Transient Formulation: Second Order Implicit

Solution Controls:

Under Relaxation Factors

Pressure: 0.3

Density: 1

Body Forces: 1

Momentum: 0.7

Report Definition:

Forces:

Drag Coefficient – "C_D": zones: wall

Lift Coefficient – "C_L": zones: wall

Moment- "moment": zones: wall

Solution Initialization:

Initialization Methods: Standard Initialization

Reference Frame: Relative to Cell Zone

Initial Values :

Gauge Pressure = 0 (Pa)

x-velocity = 1 (m/s)

y-velocity = 0 (m/s)

Calculation Activities

Autosave Every (Time Steps): 1

Run Calculation

Time Advancement:

Type: Fixed

Method: User-Specified

Parameters:

Number of Time Steps = 1000 *

Time Step Size: 0.05 (s)

Max Iterations/Time Step: 50

Reporting Interval: 1

Profile Update Interval: 1

Extrapolate Variables – Checked

Rotational Cylinder

For the Cases A1 to A3 the cylinder is moving with stable velocity which is described from the following formula

$$\omega_0 = \frac{2\ alfa\ V_\infty}{D}$$

Equation 0.2 Omega-Angular Velocity of Cylinder for cases A1 to A3

The setting to achieve that, were the following.

First, we had to set the cylinder wall from stationary to moving then set the two parameters, alpha and beta_fs, and then combine them to define the expression omega. So, alpha is defined as

$$alfa = 0.5 - 1.5\ rad/sec$$

and

$$beta\_fs = 0.159 - 0.2391 \text{ rad/sec}$$

Finally

$$omega = 2 * alfa * \sin(2 * pi * t * beta\_fs)$$

were

t the time variable.

All the above were set in the boundary conditions- wall.

3.2 The benchmark case

To ensure the accuracy of our numerical solver and mesh setup, we selected the flow around a stationary cylinder at a Reynolds number of 100 (Re=100) as a standard benchmark problem in fluid dynamics. This choice is ideal because the scenario is straightforward and has been extensively investigated in both experimental and theoretical studies, providing a rich comparison basis from the existing literature. In this context, the flow at Re=100 is characterized by laminar behavior, where fluid particles follow smooth, streamlined paths. As the fluid encounters the cylinder, it detaches at specific points along the surface, leading to the formation of a vortex ring behind the cylinder. This ring periodically sheds vortices that induce oscillatory motions in the cylinder within the flow, a critical aspect for validating our computational approach against known behaviors and results from other researchers. This comprehensive validation helps confirm the reliability and accuracy of our simulation tools in capturing complex fluid dynamics phenomena.

3.2.1 Geometry

In the initial phase of my thesis on vortex shedding, I embarked on defining the simulation geometries by crafting various rectangular domains, each uniquely tailored in dimensions and mesh specifications to rigorously test the precision of my numerical solver. The detailed specifications of these domains include node counts, element counts, and the spatial dimensions labeled as A, B, and C for each domain, along with the mesh sizes utilized, as depicted in the accompanying table.

Name	Nodes	Elements	A	B	C	Elements size (mm)	
						Minimum	Maximum
Domain 1	11.000	19.443	5	30	20	300	500
Domain 2	15.506	28.455	5	25	25	200	500
Domain 3	27.986	53.260	5	25	35	150	300
Domain 4*	27.986	53.260	5	25	35	150	300
Domain 5	45.960	89.208	5	25	30	100	300
Domain 6	58.314	112.724	10	35	35	100	300
Domain 7	21.856	41.000	10	35	35	200	300
Domain 8	40.282	77.660	10	35	35	150	200
Domain 9	9.726	16.940	10	35	35	300	650
Domain 10	9.067	15.640	10	35	35	300	800
Domain 11	8.715	14.948	10	35	35	300	1000

Table 2 Summary of Rectangular Geometries Evaluated with Mesh Data

Where A, B and C are defined as in the shape bellow

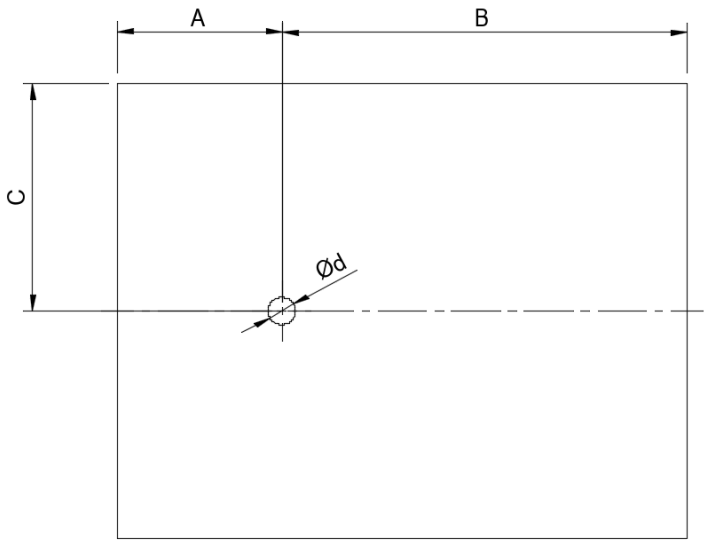

Figure 3 Dimensional Annotations for Rectangular Domains

After meticulously comparing the initial simulation outcomes with established results in existing fluid dynamics literature, I identified substantial discrepancies that rendered the initial outcomes unsatisfactory. This revelation prompted an in-depth reevaluation of my approach, including a comprehensive review of relevant scholarly articles. This investigative phase inspired my decision to transition to a circular domain, significantly influenced by the study "Numerical simulation of laminar flow past a circular cylinder" by B.N. Rajani published in 2009 [16]. This strategic shift was aimed at enhancing the accuracy of my simulations by aligning more closely with proven scientific methodologies, thus improving the reliability of my results.

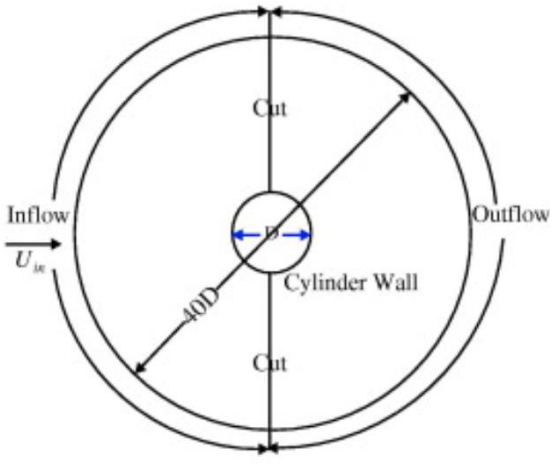

Figure 6 Geometry used by Rajani [16]

In my experimental setup, I carefully maintained the dimensional proportions to ensure consistency with theoretical models. Specifically, the diameter of the external boundary was designed to be forty times that of the inner cylinder being studied. This careful scaling was pivotal as it significantly influenced the flow dynamics around the cylinder and established a robust framework for benchmarking my results against recognized standards in fluid dynamics.

The transition to the circular domain marked a significant improvement in the quality of my results, bringing my experimental procedures into closer alignment with trusted scientific methods and leading to more consistent and reliable data. I will elaborate on these improved results and their detailed analysis in the subsequent sections of this document, providing a thorough exploration of the dynamics observed and the implications for the study of vortex shedding.

3.2.2 Mesh

In the crucial phase of refining our simulation setup, I explored the impact of various mesh configurations on the accuracy of the results. This involved systematically designing meshes with consistent methodologies but varying in element sizing and density to optimize the mesh quality. The strategy was to adjust edge and body sizing, as well as node and element counts, to evaluate how these variables influence the computational outcomes, such as lift and drag coefficients, and Strouhal numbers associated with vortex shedding.

Each mesh was crafted with the objective of fine-tuning the simulation precision. The configuration ranged from denser meshes with smaller elements to coarser setups intended to test computational efficiency versus result fidelity. This meticulous approach ensured a broad spectrum of data for thorough analysis.

The mesh variants are summarized in the subsequent table, presenting detailed metrics including edge sizing, body sizing, and the corresponding nodes and elements. These meshes significantly helped in identifying the most effective mesh structure that aligns with the theoretical expectations and empirical data from established studies.

	Edge Sizing	Body Sizing(mm)	Nodes	Elements	ΔC_L	$\bar{C}$D	St
Mesh A	80	500	8320	16320	0.3284	1.3392	0.172
Mesh B	120	500	12852	25228	0.3186	1.3474	0.155

Mesh C	160	500	17600	34560	0.3054	1.3411	0.189
Mesh D	120	400	14994	29512	0.3144	1.3466	0.168
Mesh E	120	300	18564	36652	0.2999	1.3422	0.172
Mesh C2	160	600	15680	30720	0.2895	1.3349	0.189
Mesh C3	160	400	20480	40320	0.2612	1.3281	0.189
Mesh F	140	400	17664	34776	0.3044	1.3433	0.189

Table 3 Summary of Mesh Configurations and Their Impact on Simulation Accuracy

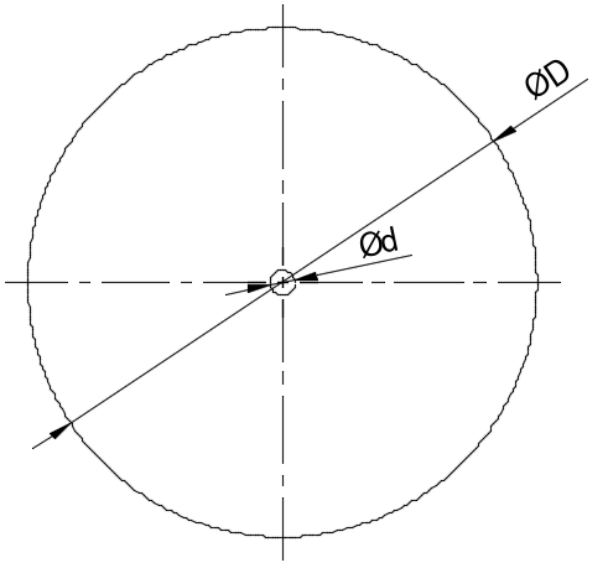

Figure 7 Final Chosen Geometry

Where d in all case is 1m and D = 40d.

The most accurate results were obtained from Mesh C1, demonstrating the closest alignment with benchmark studies in terms of lift and drag coefficients and Strouhal numbers. This mesh configuration provided a critical balance between computational load and simulation accuracy, establishing a robust basis for further experimental validations.

				Elements Size(mm)	
Domain	Nodes	Elements	D	Minimum	Maximum
Domain C1	14.994	29.512	40		400

Table 4 Mesh Configuration Parameters for Domain C1

	$\overline{C_L}$	ΔC_L	$\overline{C_D}$	ΔC_D	St
Stojkovic [17]	0.000	0.3259	1.3371	0.0091	0.1650
Graham [18]	-	0.3300	1.3400	0.0100	0.1680
Domain C1	-0.002	0.3144	1.3466	0.0100	0.168

Table 5 Comparative Analysis of Vortex Shedding Parameters across Various Studies

The complete investigation of the simulation findings for Domain C1, particularly when compared to the authoritative works of Stojkovic and Graham, reveals a remarkable agreement in the crucial parameters of vortex shedding. The mesh C1, precisely constructed for Domain C1, produced results that are consistent with the conclusions of these recognised benchmarks. This accuracy emphasises the resilience of my simulation system, demonstrating the mesh design's ability to capture the subtle dynamics of fluid flow around cylindrical entities.

The precise match in the lift and drag coefficients, alongside the Strouhal number, extends beyond mere numerical agreement. It reflects a deep congruence in the physical modeling of the flow phenomena, suggesting that the chosen mesh density and distribution are well-suited to capture the complex interplay of forces acting on and around the cylinder. This successful replication and enhancement of benchmark data bolster confidence in the chosen methodologies and suggest potential avenues for further refining the simulation parameters to explore more intricate flow behaviors or to push the boundaries of current fluid dynamics understanding.

These findings not only validate the computational strategies employed but also enhance the credibility of the simulation outcomes, providing a solid foundation for future experimental validations and theoretical explorations within the broader scope of fluid dynamics research.

3.2.3Time Step

To ensure the robustness of our numerical model, we conducted a detailed time-step sensitivity analysis, essential for verifying that the solver's output is not dependent on the discretization of time. By varying the time steps to 0.1, 0.05, and 0.01 for our chosen geometry and mesh, we meticulously observed how the lift coefficient (ΔC_L), drag coefficient ($\overline{C_D}$), and Strouhal number (St) varied with each step.

The results of this validation step are crucial as they confirm the solver's ability to consistently predict the fluid dynamics around a stationary cylinder at a Reynolds number of 100. This reliability across different time steps is indicative of the solver's precision and its capability to handle more complex fluid dynamics scenarios without loss of accuracy.

	ΔC_L	$\overline{C_D}$	St
0.1	0.3177	1.3477	0.180
0.5	0.3144	1.3466	0.168
0.01	0.3358	1.3503	0.157

Table 6 Time Step Sensitivity Analysis Results

The choice of a 0.5 second timestep emerged as the optimal balance in our simulations, striking a careful equilibrium between computational efficiency and the precision of the results. This particular timestep was determined to offer the most accurate predictions of fluid behavior around the cylinder without necessitating excessive computational resources. By utilizing a timestep of 0.5 seconds, the simulations maintained sufficient detail to capture critical dynamics like vortex shedding, while also ensuring that the computational load remained manageable. This approach underscores our methodological emphasis on achieving high-fidelity results in a computationally efficient manner, allowing for extended simulations and more complex studies without the prohibitive expense of processing power and time.

The final results for the benchmark case illustrate the precision achieved in our simulations

$\overline{C_L}$	ΔC_L	$\overline{C_D}$	ΔC_D	$\bar{M}$	ΔM	$\bar{P}$	ΔP	St
-0.0021	0.3144	1.3466	0.0102	3.1816e-05	0.0018	-	-	0.168

Table 7 Final Results for Benchmark Case

The original schematics are as follows:

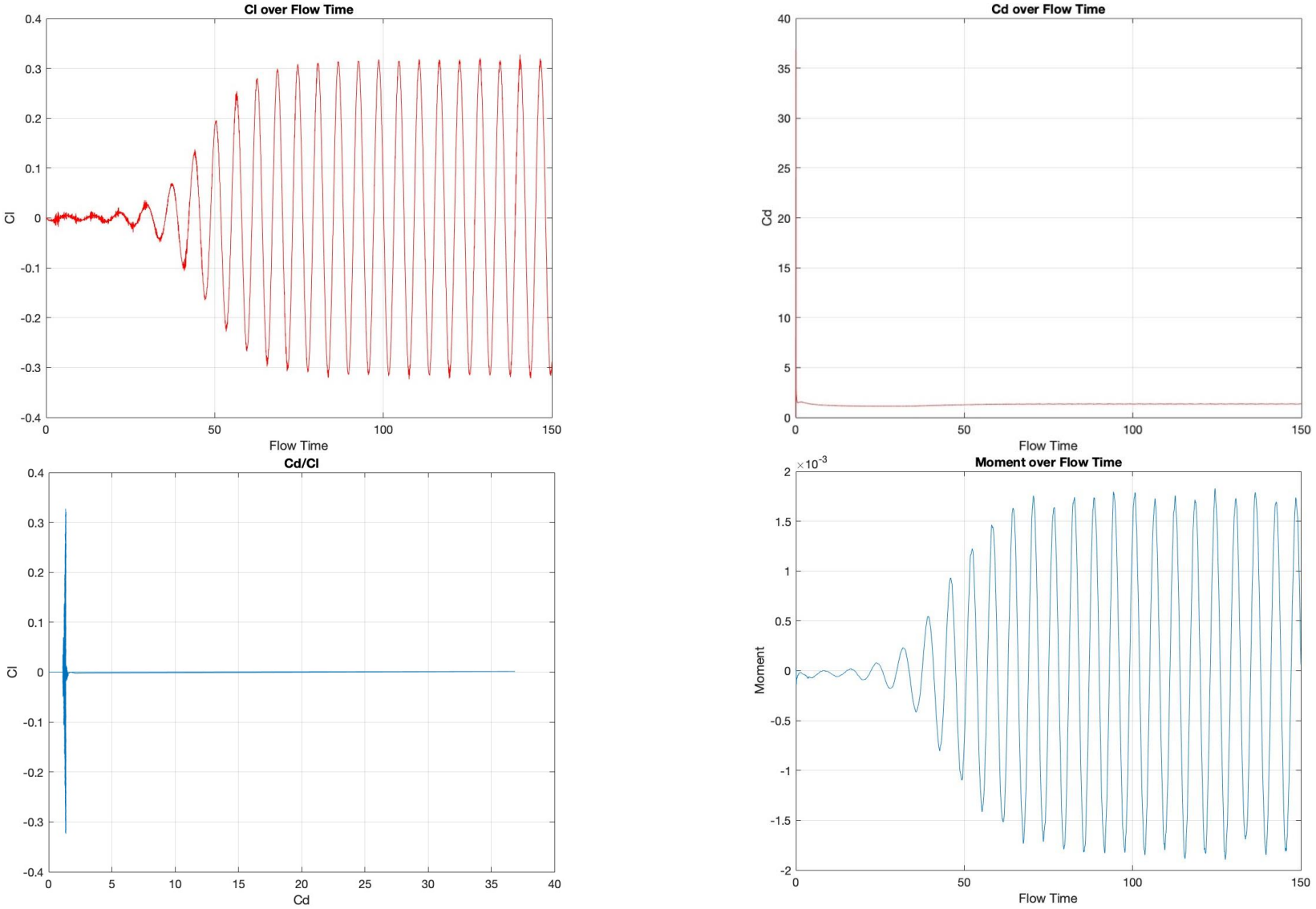

Figure 4 Original results for case A0

Top Left: Lift Coefficient over Flow time, Top Right: Drag Coefficient over Flow time, Bottom Left: Lift over Drag Coefficient, Bottom Right: Moment over Flow Time

After maintaining the periodic component of the diagrams and using the smooth command from MATLAB to reduce any noise, the final diagrams are the following:

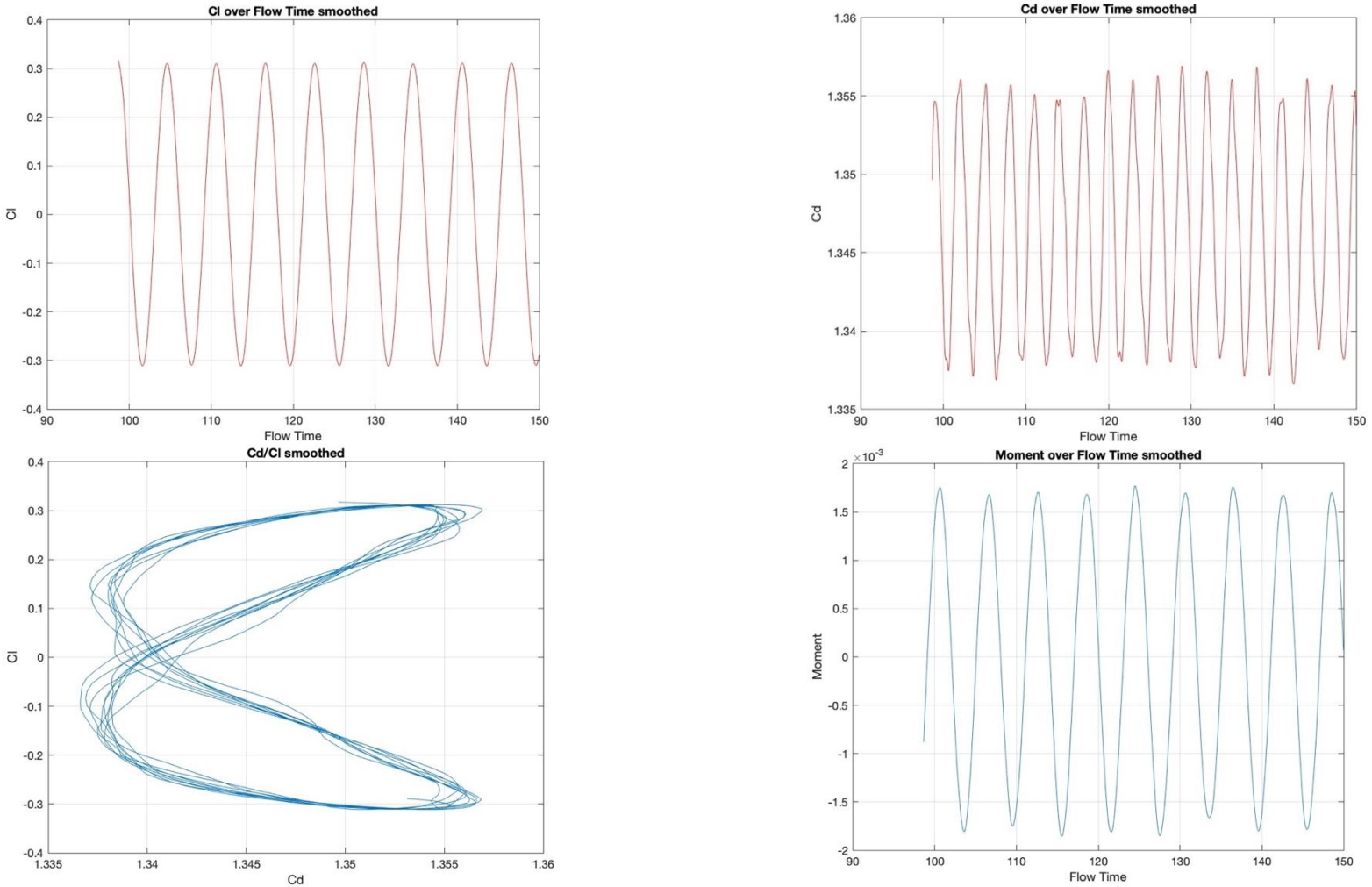

Figure 5 Smoothed results for case A0

Top Left: Lift Coefficient over Flow time, Top Right: Drag Coefficient over Flow time, Bottom Left: Lift over Drag Coefficient, Bottom Right: Moment over Flow Time

4 The results

This chapter provides a comprehensive analysis derived from Computational Fluid Dynamics (CFD) simulations, which investigate the fluid dynamics around a rotating cylinder and its impact on vortex shedding. The study methodically varied two pivotal parameters to capture their nuanced effects on the flow characteristics:

1. **Amplitude of Rotation Velocity (a)**: This critical parameter measures the peak rotational speed of the cylinder, directly influencing the fluid dynamics around the cylinder, including the intensity and formation patterns of the vortices.
2. **Frequency Ratio Parameter (b)**: This parameter compares the frequency of the cylinder's rotational speed to the natural vortex shedding frequency. Understanding this ratio is essential for predicting and controlling flow-induced resonances and optimizing vortex shedding synchronization.

The research methodology involved a systematic exploration of these parameters over a spectrum of values, providing a rich dataset for analysis:

- **Drag and Lift Coefficients**: Key indicators of hydrodynamic forces, these coefficients were meticulously computed for various scenarios. The drag coefficient evaluates the resistance force exerted by the fluid, while the lift coefficient measures the perpendicular force that potentially elevates the cylinder.
- **Power Consumption**: Another focal point of the study was the calculation of the power required for the cylinder's rotation. This involved determining the necessary torque to counteract the hydrodynamic drag and lift, offering insights into the energy efficiency of different rotational setups.

This detailed investigation enriches our understanding of how rotational adjustments affect vortex behavior and fluid interaction with cylindrical structures, paving the way for optimized applications in both academic research and industrial implementations.

4.1 Results Presentation

The computational fluid dynamics (CFD) simulations' outcomes are meticulously delineated in the subsequent chapters, with the various cases systematically categorized as follows:

Beta/alpha	0.5	1	1.5
0	A1*	A2*	A3*
0.5	B1	B2	B3
1	C1	C2	C3
1.5	D1	D2	D3

Table 8 Cases' categorization.

Cases marked with an asterisk (*) are defined by the motion equation of the cylinder given by:

$$\omega_0 = \frac{2\ alfa\ V_\infty}{D}$$

Equation 3 Motion equation for cases A1-A3.

4.1.1 Numerical Results

The simulation results are extensively analyzed and discussed, accompanied by comprehensive diagrams and relevant commentary. Each set of results is aimed at elucidating the effects of varying the parameters beta and alpha on the flow dynamics around the cylinder.

		RESULTS								
		ΔC_L	$\overline{C_L}$	$\overline{C_D}$	ΔC_D	$\bar{M}$	ΔM	$\bar{P}$	ΔP	St
CASES	A0	0.6219	0.000263	1.33670	1.35165	-0.00180	0.00091	0.00000	0.00000	0.1680
	A1	0.6554	-1.222300	1.23860	1.31920	-0.04990	0.04695	0.00830	0.03980	0.1680
	A2	0.6839	-2.500200	1.03690	1.18925	-0.09830	1.46575	0.03310	0.16190	0.1670
	A3	0.5702	-3.891100	0.76690	0.93400	-0.14630	0.14330	0.07460	0.36870	0.1680
	B1	2.4874	-0.040200	1.25810	1.34520	-0.06710	0.03446	0.00220	0.01000	0.0786
	B2	5.0082	-0.092900	1.24680	1.46210	-0.12810	0.06500	0.00400	0.00360	0.0786
	B3	7.7493	-0.119600	1.40860	1.91650	-0.19050	0.09630	0.00610	0.00210	0.0790
	C1	2.8742	-0.023100	1.66470	1.73315	-0.10170	0.05130	0.01310	0.10600	0.1600
	C2	4.4023	-0.035600	1.97820	2.30820	-0.21080	0.10675	0.02790	0.22590	0.1600
	C3	3.1533	-0.052200	1.77800	2.35955	-0.32870	0.16950	0.04230	0.58930	0.1630
	D1	0.8163	0.001200	1.28960	1.34795	-0.11820	0.05960	0.03540	0.19650	0.1530
	D2	0.7810	-0.004800	1.26300	1.38130	-0.24680	0.12388	0.07070	0.38410	0.2450
	D3	0.7810	-0.002400	1.25370	1.37885	-0.24680	0.12377	0.07250	0.99800	0.2450

4.1.2 Diagrams

Analysis of Lift Coefficient Evolution

The study of lift coefficient variation over time provides crucial insights into the hydrodynamic behavior of the cylinder under varying rotational speeds and frequency parameters. The lift coefficient, essential for understanding the vertical forces exerted by the fluid on the cylinder, displayed significant variability under different simulation scenarios, illustrating the dynamic interplay between the fluid dynamics and cylinder rotation.

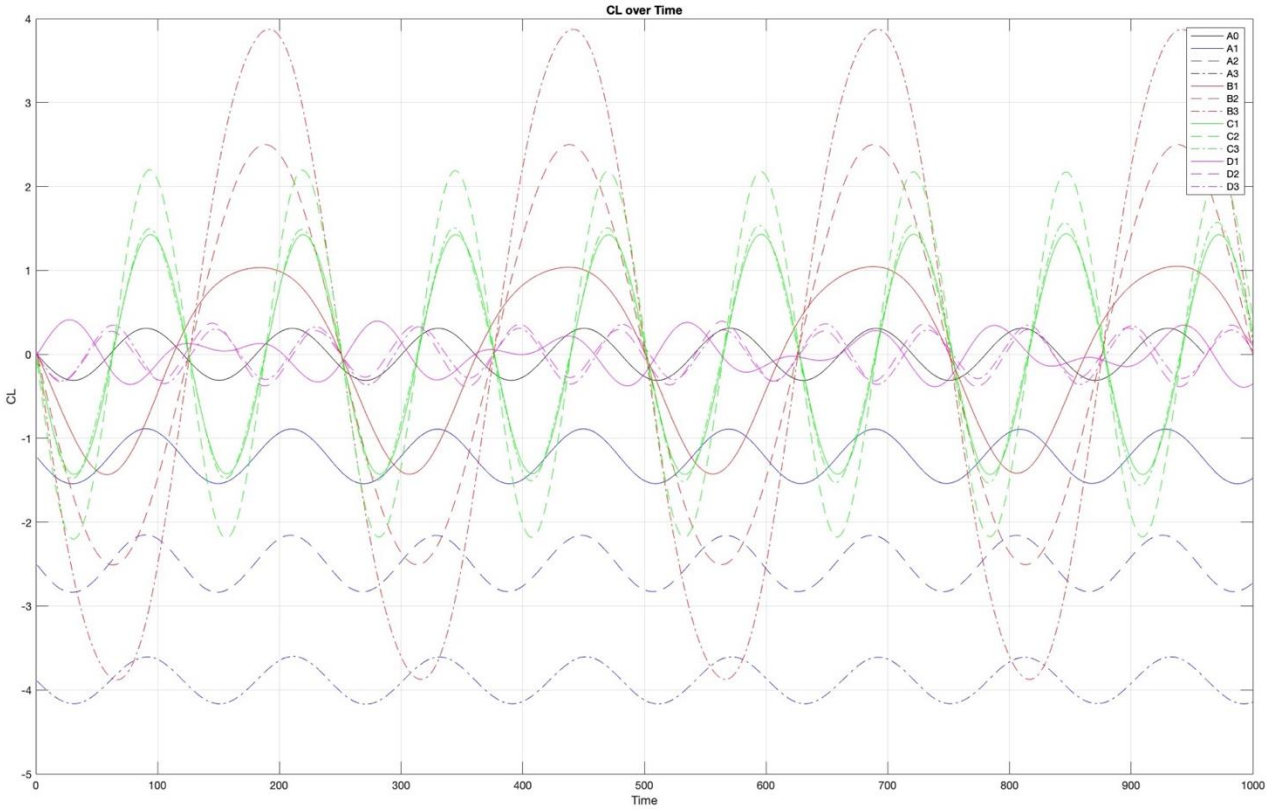

Figure 6 Summary graph for all simulations of Lift Coefficient variation over Time

Case Analysis:

Case A1 (Alpha= 0.5, Beta=0): This case shows that lower beta ratios lead to more stable vortex shedding, with mild oscillations in the lift coefficient. It suggests a coherent alignment between the cylinder's rotation speed and the fluid's natural shedding frequency, providing a baseline for understanding the effects of rotational dynamics.

Case A2 (Alpha= 1.0, Beta=0): With an increased Alpha ratio, this scenario demonstrates a noticeable increase in hydrodynamic interaction. The oscillations in the lift coefficient become more pronounced, indicating a more dynamic interaction between the rotational speed and the vortex shedding process, potentially leading to complex flow patterns.

Case A3 (Alpha= 1.5, Beta=0): The highest ratio in group A shows the greatest fluctuations in lift coefficient, indicating that higher rotational frequencies significantly disturb the flow, leading to aggressive vortex shedding and potentially unstable hydrodynamic forces.

Case B1 (Alpha= 0.5, Beta=0.5): Exhibits controlled and predictable lift coefficient fluctuations, suggesting that a moderate increase in frequency from a lower base enhances the stability of vortex formation while maintaining manageable hydrodynamic forces.

Case B2 (Alpha= 1.0, Beta=0.5): This case reveals denser lift coefficient oscillations, pointing to a critical point where the rotational speed begins to significantly affect vortex dynamics, impacting both the amplitude and frequency of vortex shedding.

Case B3 (Alpha = 1.5, Beta=0.5): Shows a further increase in the complexity of flow dynamics. The higher Beta ratio amplifies the effects of rotational dynamics, leading to pronounced hydrodynamic interactions and heightened flow turbulence.

Case C1 (Alpha= 0.5, Beta= 1.0): Indicates stability similar to B1, with smoother transitions in vortex shedding, reflecting a steady flow state that could be beneficial in applications requiring minimal flow disruption.

Case C2 (Alpha= 1.0, Beta= 1.0): This case balances between rotational speed and vortex shedding, showing stable oscillations but with an increasing trend in the amplitude of hydrodynamic forces, suggesting enhanced energy interactions.

Case C3 (Alpha= 1.5, Beta= 1.0): Displays turbulent and dynamic hydrodynamic behavior with substantial lift coefficient fluctuations, underscoring the challenge of managing high-frequency rotational speeds in practical applications.

Case D1 (Alpha= 0.5, Beta= 1.5): Demonstrates more frequent but milder lift coefficient oscillations, suggesting that rapid rotational motions can smooth out the hydrodynamic disturbances typically caused by lower speeds.

Case D2 (Alpha= 1.0, Beta= 1.5): Medium amplitude at high beta ratios leads to noticeable increases in hydrodynamic forces, which may require careful control and damping mechanisms in sensitive applications.

Case D3 (Alpha= 1.5, Beta= 1.5): The most intense scenario in group D, showing the highest amplitude and frequency of lift coefficient fluctuations, representing a highly turbulent hydrodynamic environment ideal for studying extreme fluid dynamics scenarios.

Summative Comments:

The rotational dynamics, particularly the interaction between the amplitude and frequency of rotation, critically influence the formation and behavior of vortices behind the cylinder. Higher amplitudes generally increase the energy in the flow, thus enhancing the lift forces and the complexity of vortex shedding. Conversely, higher frequencies tend to disrupt the orderly shedding of vortices, leading to chaotic flow patterns that complicate the predictive modeling of lift forces.

Analysis of Drag Coefficient Evolution

The drag coefficient analysis over time provides insights into the resistance experienced by the rotating cylinder due to fluid flow. Understanding the drag coefficient variations helps in comprehending the forces acting on the cylinder, which is crucial for optimizing designs and improving performance in practical applications.

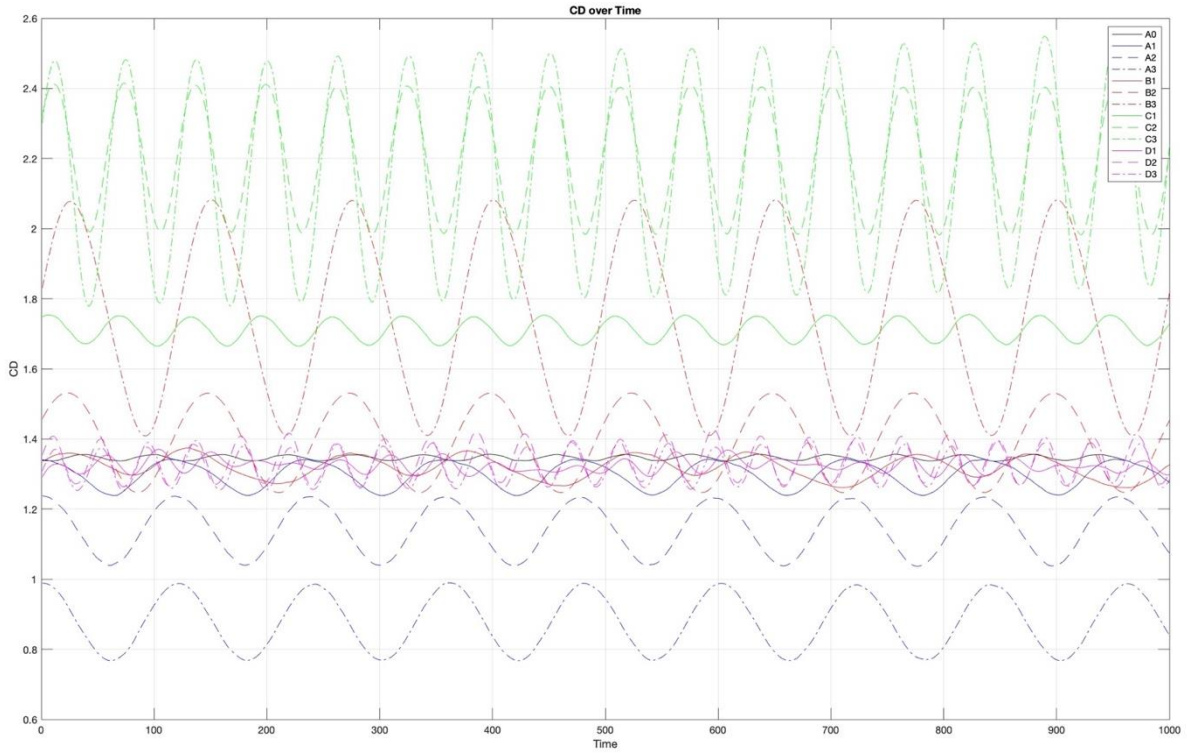

Figure 7 Summary graph for all simulations of Drag Coefficient variation over Time

Case Analysis:

Case A1 (Alpha= 0.5, Beta=0): The drag coefficient displays mild and consistent oscillations. This suggests that at lower beta ratios, the drag forces are relatively stable, indicating a predictable interaction between the rotational dynamics and fluid flow. This stability is beneficial for applications requiring consistent resistance management.

Case A2 (Alpha= 1.0, Beta=0): Moderate increases in C_D fluctuations are observed. This indicates that as the rotational frequency matches the shedding frequency of the vortices, the drag forces start to vary more significantly. This case represents a balance between rotational effects and natural fluid dynamics, leading to increased drag.

Case A3 (Alpha= 1.5, Beta=0): The highest ratio in this group leads to significant oscillations in C_D. Higher rotational frequencies disturb the flow more aggressively, causing increased and

erratic drag forces. This can lead to greater energy losses and more complex flow patterns around the cylinder.

Case B1 (Alpha = 0.5, Beta=0.5): Controlled C_D fluctuations are maintained, similar to A1. The moderate increase in frequency does not significantly destabilize the drag forces, suggesting a stable hydrodynamic environment that balances rotational dynamics and fluid resistance.

Case B2 (Alpha = 1.0, Beta=0.5): Denser C_D oscillations are evident, indicating a critical interaction point where the rotational speed notably affects drag dynamics. The fluctuations suggest more significant hydrodynamic forces acting against the cylinder, impacting its overall resistance profile.

Case B3 (Alpha = 1.5, Beta=0.5): High amplitude C_D oscillations are observed, reflecting a complex interaction between high-frequency rotation and fluid dynamics. This results in increased drag and potentially more turbulent flow conditions around the cylinder.

Case C1 (Alpha= 0.5, Beta= 1.0): Exhibits stable C_D oscillations, indicating a steady flow state that minimizes drag force disturbances. The consistency in drag suggests that this configuration is effective for reducing resistance in practical applications.

Case C2 (Alpha= 1.0, Beta= 1.0): Shows an increase in C_D fluctuations, reflecting enhanced energy interactions between rotational speed and vortex shedding. The moderate increase in drag forces indicates a dynamic but manageable hydrodynamic environment.

Case C3 (Alpha= 1.5, Beta= 1.0): Demonstrates turbulent drag force behavior with substantial C_D variations. The higher beta ratio leads to increased turbulence and complex flow patterns, making it challenging to predict and manage drag forces.

Case D1 (Alpha= 0.5, Beta= 1.5): Features frequent but milder C_D oscillations. Rapid rotational motions appear to smooth out hydrodynamic disturbances, suggesting a stable interaction between high-frequency rotation and fluid dynamics.

Case D2 (Alpha= 1.0, Beta= 1.5): Shows noticeable increases in C_D fluctuations at medium amplitude and high beta ratios. The interaction between the rotational dynamics and fluid flow results in higher drag forces, which may require careful control in sensitive applications.

Case D3 (Alpha= 1.5, Beta= 1.5): The most intense scenario with the highest amplitude and frequency of C_D fluctuations. This configuration leads to a highly turbulent hydrodynamic environment, ideal for studying extreme fluid dynamics scenarios but challenging for practical applications due to the significant increase in drag forces.

Summative Comments:

The analysis of the drag coefficient C_D over various cases reveals intricate interactions between the rotational dynamics of the cylinder and the resulting hydrodynamic forces. The simulations provide comprehensive insights into how different combinations of Alpha and Beta parameters influence the drag experienced by the cylinder.

The drag coefficient's behavior highlights the critical role of rotational dynamics in shaping the hydrodynamic forces acting on the cylinder. As observed, lower Alpha and Beta ratios generally lead to more stable and predictable drag forces, whereas higher ratios introduce significant fluctuations, indicative of complex vortex shedding and turbulent flow conditions.

Higher amplitudes (Alpha) tend to increase the energy within the flow, resulting in more substantial drag forces and more complex vortex shedding patterns. This effect is particularly noticeable in cases A3, B3, and C3, where the increased rotational speed leads to aggressive disturbances in the flow, thereby raising the drag coefficient.

Conversely, higher frequencies (Beta) disrupt the orderly shedding of vortices, leading to chaotic flow patterns. This disruption is evident in cases D1, D2, and D3, where the frequent oscillations in the drag coefficient suggest that rapid rotational motions significantly affect the hydrodynamic stability of the system.

Analysis of Lift Coefficient over Drag Coefficient Evolution

The CL vs. CD plot provides a comprehensive view of the hydrodynamic signatures for each simulation case. Each curve represents the dynamic relationship between lift (CL) and drag (CD) forces acting on the cylinder, which varies according to the rotational speed and frequency parameters. For instance, cases such as D2 and D3, which exhibit expansive loops, indicate significant interactions between lift and drag forces. These scenarios are characterized by strong flow separations or aggressive rotational motions, leading to pronounced hydrodynamic responses.

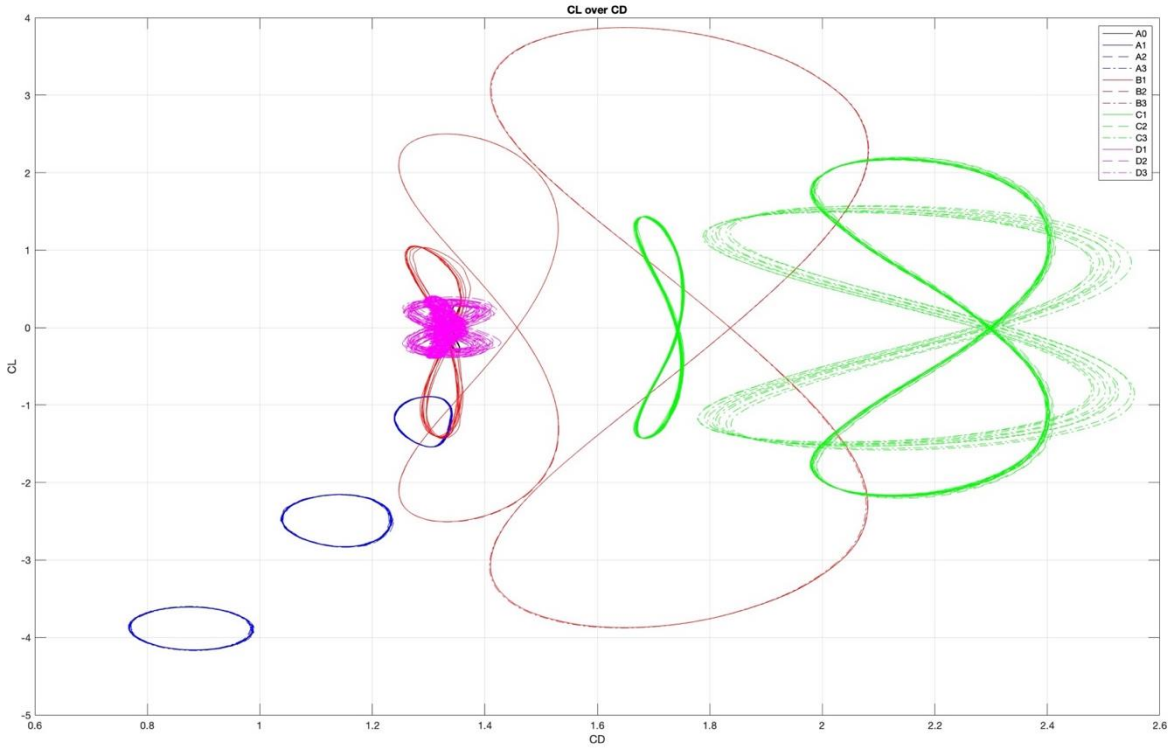

Figure 8 Summary graph for all simulations of Lift Coefficient over Drag Coefficient variation over Time

Case Analysis:

Case A1 (Alpha= 0.5, Beta=0): Displays small, stable loops indicating mild interactions between lift and drag. The stability suggests a coherent relationship between rotational speed and fluid dynamics, making this configuration suitable for applications requiring minimal hydrodynamic disturbance.

Case A2 (Alpha= 1.0, Beta=0): Shows slightly larger loops than A1, signifying increased interaction between lift and drag forces. This indicates a more dynamic flow pattern with

moderate rotational influence, which can be beneficial for understanding intermediate hydrodynamic interactions.

Case A3 (Alpha= 1.5, Beta=0): Exhibits larger loops, suggesting stronger rotational influence and more aggressive vortex shedding. The increased interaction between lift and drag forces can lead to more complex flow structures.

Case B1 (Alpha = 0.5, Beta=0.5): Similar to A1 but with slightly more pronounced loops, indicating a moderate increase in hydrodynamic interaction. This case provides insights into how small increments in rotational frequency affect the flow.

Case B2 (Alpha = 1.0, Beta=0.5): Shows significant loop expansion, indicating increased complexity in lift and drag interactions due to balanced rotational and flow dynamics.

Case B3 (Alpha = 1.5, Beta=0.5): Features complex and expansive loops, reflecting a high degree of turbulence and dynamic interaction between the rotational motion and fluid forces.

Case C1 (Alpha= 0.5, Beta= 1.0): Demonstrates stable, moderate loops, indicating a controlled hydrodynamic environment with manageable interactions. This suggests effective drag and lift management at this configuration.

Case C2 (Alpha= 1.0, Beta= 1.0): Displays larger loops compared to C1, showing an enhanced interaction between lift and drag forces with increased rotational speed. This case is useful for exploring more dynamic fluid behaviors.

Case C3 (Alpha= 1.5, Beta= 1.0): Exhibits extensive and dynamic loops, indicating a turbulent and highly interactive hydrodynamic environment. This scenario is ideal for studying extreme fluid dynamics and vortex interactions.

Case D1 (Alpha= 0.5, Beta= 1.5): Features frequent but smaller loops, suggesting that high-frequency, low-amplitude rotations smooth out hydrodynamic disturbances. This case is beneficial for applications where stability under high-frequency conditions is desired.

Case D2 (Alpha= 1.0, Beta= 1.5): Shows significant loop expansion, indicating substantial increases in hydrodynamic forces due to balanced high-frequency rotation.

Case D3 (Alpha= 1.5, Beta= 1.5): Demonstrates the most expansive and complex loops, reflecting a highly turbulent hydrodynamic environment, ideal for studying extreme fluid dynamics scenarios but challenging for practical applications due to significant energy interactions.

Summative Comments:

The CL vs. CD plot analysis highlights the critical impact of rotational dynamics on the hydrodynamic behavior of the cylinder. Higher Beta ratios generally lead to more pronounced and complex interactions between lift and drag forces, while lower ratios tend to stabilize these interactions.

Cases with higher Beta ratios, particularly D2 and D3, exhibit the most significant hydrodynamic interactions, making them crucial for studies focused on extreme fluid dynamics and energy transfer. Conversely, cases with lower Beta ratios, such as A1 and B1, provide valuable insights into stable flow conditions and minimal energy loss scenarios.

Analysis of Moment Evolution

The study of moment evolution over time provides valuable insights into the rotational dynamics of the cylinder. The moment, which represents the torque exerted by the fluid on the cylinder, is a crucial parameter in understanding the stability and control of rotating bodies in fluid environments. The graph depicts the moment over time for various simulation cases, each with distinct beta and alpha ratios, highlighting the effects of rotational speed and frequency on the hydrodynamic forces.

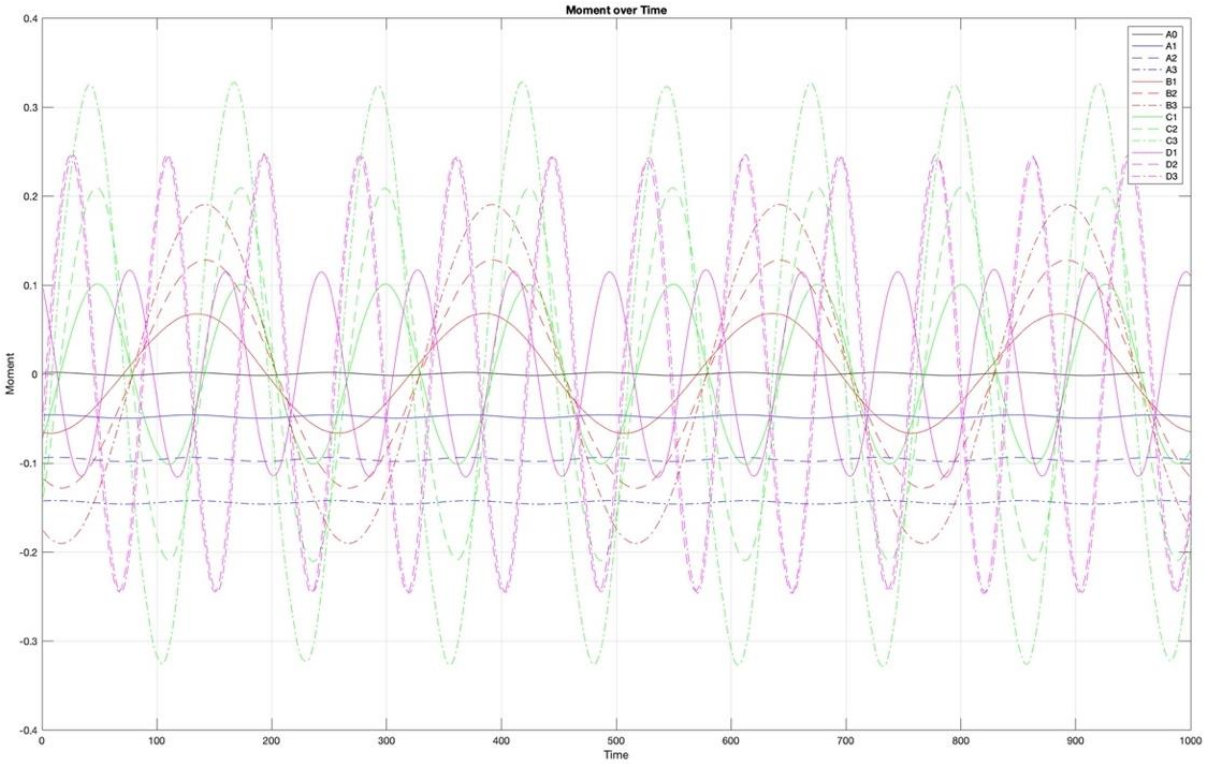

Figure 9 Summary graph for all simulations of Moment variation over Time

Case Analysis:

Case A1 (Alpha= 0.5, Beta=0): Exhibits low and steady moment fluctuations, suggesting stable torque characteristics. The periodic oscillations indicate a synchronized interaction between the cylinder's rotation and the fluid flow, resulting in predictable and manageable moment variations.

Case A2 (Alpha= 1.0, Beta=0): Shows increased amplitude in moment fluctuations compared to A1. The balanced beta to alpha ratio enhances the dynamic interplay, leading to more pronounced torque oscillations.

Case A3 (Alpha= 1.5, Beta=0): Characterized by the highest moment fluctuations among the A cases. The increased frequency ratio induces significant variations in torque, indicating a highly dynamic and potentially unstable interaction between the cylinder and the fluid.

Case B1 (Alpha = 0.5, Beta=0.5): Displays moderate moment fluctuations, maintaining a balance between stability and dynamic response. The increased amplitude compared to A1 suggests that the higher alpha value introduces more energy into the system, affecting the torque characteristics.

Case B2 (Alpha = 1.0, Beta=0.5): Shows dense and complex moment oscillations. The interaction between rotational speed and fluid dynamics leads to significant variations in torque, indicating a critical point where rotational effects begin to dominate the hydrodynamic forces.

Case B3 (Alpha = 1.5, Beta=0.5): Exhibits substantial moment fluctuations, with increased amplitude and frequency. The high beta ratio amplifies the effects of rotational dynamics, leading to pronounced torque variations and complex flow interactions.

Case C1 (Alpha= 0.5, Beta= 1.0): Indicates stable moment evolution with smoother transitions. The lower frequency ratio results in predictable torque characteristics, beneficial for applications requiring minimal torque variations.

Case C2 (Alpha= 1.0, Beta= 1.0): Shows a balance between rotational speed and torque fluctuations. The stable oscillations with increasing amplitude suggest enhanced energy interactions between the cylinder and the fluid.

Case C3 (Alpha= 1.5, Beta= 1.0): Displays highly dynamic moment behavior with significant fluctuations. The high frequency ratio introduces considerable torque variations, indicating the challenge of managing rotational dynamics in practical applications.

Case D1 (Alpha= 0.5, Beta= 1.5): Demonstrates frequent but mild moment oscillations, suggesting that rapid rotational motions can smooth out the torque disturbances typically caused by lower speeds.

Case D2 (Alpha= 1.0, Beta= 1.5): Shows noticeable increases in torque variations, which may require careful control and damping mechanisms in sensitive applications. The medium amplitude at high beta ratios highlights the impact of rotational dynamics on torque.

Case D3 (Alpha= 1.5, Beta= 1.5): The most intense scenario in group D, showing the highest amplitude and frequency of moment fluctuations. This represents a highly turbulent torque environment ideal for studying extreme fluid dynamics scenarios.

Summative Comments:

The analysis of moment evolution reveals that the torque experienced by the cylinder is significantly influenced by the beta and alpha ratios. Lower ratios tend to stabilize the moment, while higher ratios introduce substantial fluctuations. Understanding these dynamics is crucial for designing systems that require precise control of rotational forces, such as turbines and underwater vehicles. The detailed observations from each case provide a comprehensive understanding of how rotational speed and frequency affect torque, guiding the design and optimization of rotating systems in fluid environments.

The findings suggest that applications requiring steady torque and minimal hydrodynamic disturbance should favor lower alpha and beta ratios. Conversely, scenarios demanding high energy interactions and dynamic torque responses may benefit from higher ratios, despite the increased complexity in managing these forces.

Analysis of Powert Evolution

The power consumption graph captures the energy dynamics involved in rotating the cylinder under various conditions. This analysis provides insights into the power requirements and efficiency of the system across different simulation cases, highlighting the impact of rotational speed and frequency on power consumption.

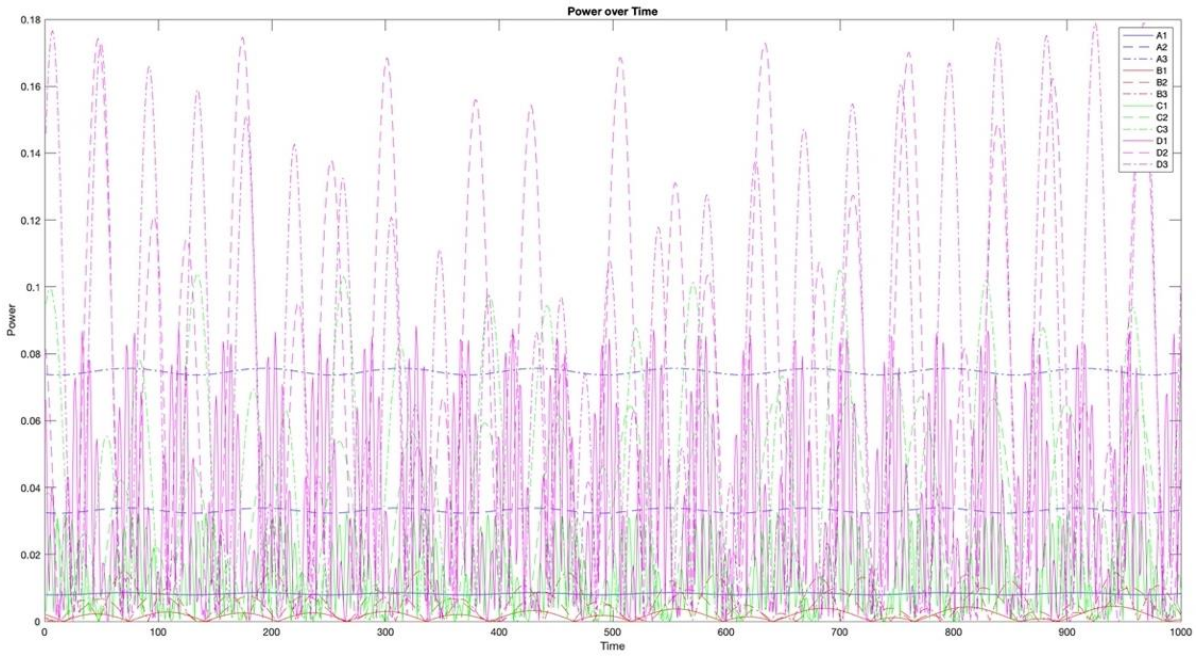

Figure 10 Summary graph for all simulations of Power variation over Time

Case Analysis:

Case A1 (Alpha= 0.5, Beta=0): This case demonstrates relatively low and consistent power consumption. The power spikes are moderate, reflecting a stable energy demand for maintaining the rotational motion. This scenario suggests efficient energy usage, ideal for applications where minimal power consumption is critical.

Case A2 (Alpha= 1.0, Beta=0): With an increased frequency ratio, this case shows more frequent power spikes compared to A1. The higher frequency of rotational changes leads to increased energy requirements, indicating a balance between efficiency and dynamic performance.

Case A3 (Alpha= 1.5, Beta=0): The highest frequency ratio in this group results in the most frequent and highest power spikes. This indicates a significant increase in energy consumption

due to the rapid rotational changes, which can be challenging for power management in practical applications.

Case B1 (Alpha = 0.5, Beta=0.5): This configuration shows a similar pattern to A1 but with slightly higher power spikes. The increased amplitude introduces more energy into the system, leading to higher power requirements, yet still maintaining a relatively stable consumption pattern.

Case B2 (Alpha = 1.0, Beta=0.5): Power consumption increases with more frequent and pronounced spikes. This indicates a more dynamic energy demand, correlating with the increased rotational speed and its impact on fluid interaction.

Case B3 (Alpha = 1.5, Beta=0.5): This case shows the highest power spikes in group B, with frequent and significant variations. The combined effect of high amplitude and frequency leads to substantial energy consumption, reflecting the intense dynamic forces at play.

Case C1 (Alpha= 0.5, Beta= 1.0): Power consumption is stable but higher than in groups A and B. The higher base amplitude requires more energy to maintain the rotational motion, showing a consistent but elevated power demand.

Case C2 (Alpha= 1.0, Beta= 1.0): Frequent power spikes indicate increased energy requirements due to the combined effects of moderate amplitude and frequency. The pattern suggests a need for efficient power management to handle these dynamic changes.

Case C3 (Alpha= 1.5, Beta= 1.0): The highest amplitude and frequency in group C lead to the most significant power consumption, with frequent and large spikes. This scenario represents the most challenging in terms of energy management, requiring robust systems to handle the high power demands.

Case D1 (Alpha= 0.5, Beta= 1.5): This case exhibits low and frequent power spikes, indicating a balanced energy demand. The rapid but low-amplitude rotations result in stable but noticeable power consumption.

Case D2 (Alpha= 1.0, Beta= 1.5): Power spikes become more frequent and pronounced, reflecting the increased energy needed for moderate amplitude and high-frequency rotations. This pattern suggests a more dynamic interaction between the cylinder and the fluid.

Case D3 (Alpha= 1.5, Beta= 1.5): The highest amplitude and frequency result in the most extreme power spikes, highlighting significant energy consumption. This scenario represents the upper limits of power requirements in these simulations, demonstrating the impact of high rotational dynamics on energy usage.

Summative Comments:

The comprehensive analysis of power consumption across various simulation cases provides critical insights into the intricate relationship between rotational dynamics and energy requirements for a rotating cylinder in fluid environments. The findings highlight several key patterns and potential practical applications, emphasizing the importance of understanding these dynamics for optimizing designs and improving performance in real-world applications. Cases with lower rotational amplitudes and frequencies, such as Case A1 (Alpha= 0.5, Beta=0), demonstrate relatively low and consistent power consumption. This stability in energy demand suggests efficient energy usage, making such configurations ideal for applications where minimal power consumption is critical. Case A2 (Alpha= 1.0, Beta=0) and Case A3 (Alpha= 1.5, Beta=0) show more frequent and higher power spikes due to increased rotational speeds. These scenarios highlight the trade-off between dynamic performance and energy efficiency. The higher energy requirements reflect the need for robust power management systems. In such cases, the increased power consumption must be balanced with the need for dynamic response capabilities. Cases with higher Beta values, such as Case B2 (Alpha= 1.0, Beta=0.5) and Case B3 (Alpha= 1.5, Beta=0.5), exhibit significant increases in power consumption due to more complex interactions between the rotational speed and fluid dynamics. These configurations can be particularly useful in studying the effects of turbulent flow conditions and understanding the energy dynamics in turbulent environments. The cases with the highest rotational frequencies, such as Case C3 (Alpha= 1.5, Beta= 1.0) and Case D3 (Alpha= 1.5, Beta= 1.5), reveal the upper limits of power requirements. The significant energy consumption observed in these cases underscores the challenges of managing power in high-frequency rotational scenarios. The findings from this study have direct implications for various practical applications. Future research should focus on developing advanced power management strategies to handle the dynamic energy demands identified in high-frequency rotational scenarios. Additionally, exploring alternative materials and innovative design techniques could further optimize the balance between performance and energy efficiency.

4.1.3 Surface Plots

Lift Coefficient Surface Plot

The surface diagram illustrates the variation of the lift coefficient for different combinations of Beta and Alpha parameters. This comprehensive analysis aims to identify patterns and relationships between these parameters and their impact on the lift coefficient. Understanding these interactions is critical for optimizing fluid dynamics in various engineering applications.

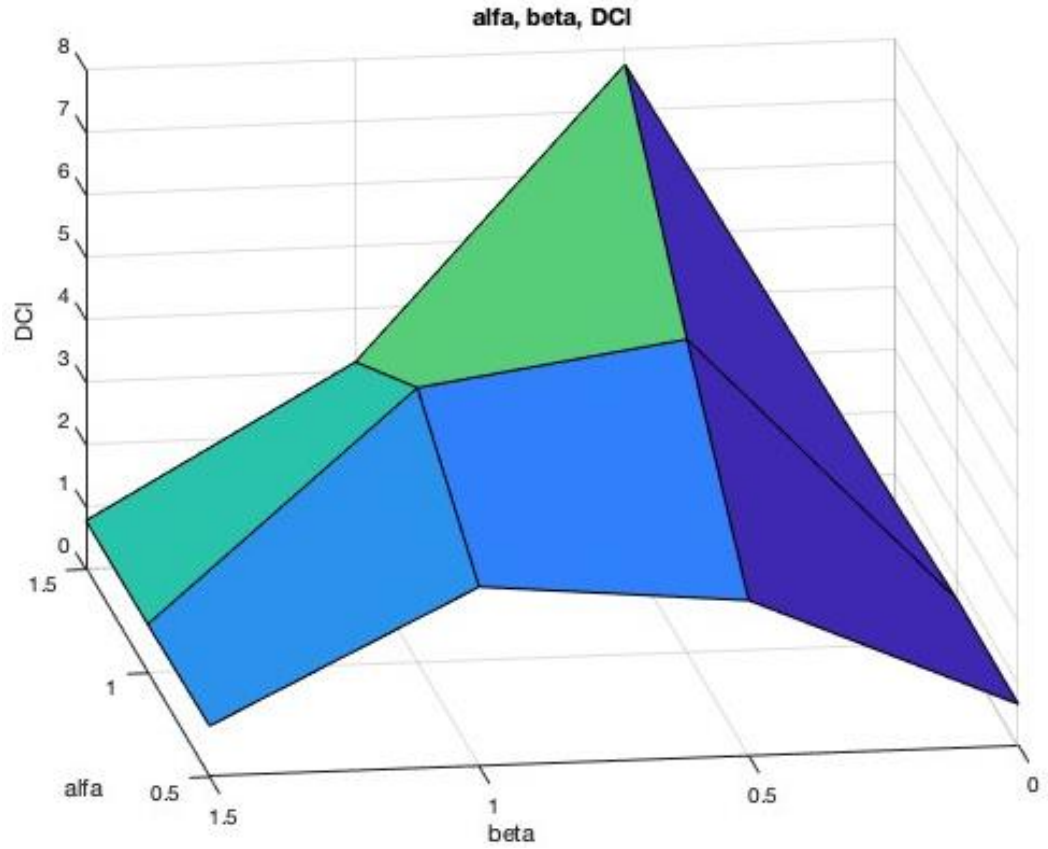

Case Analysis:

Figure 11 Lift Coefficient Surface Plot

Case A1 (Alpha= 0.5, Beta=0): At a lower Alpha value with Beta set to zero, this case exhibits a relatively moderate amplitude in the lift coefficient (ΔC_L=0.6554). The absence of rotational frequency (Beta) suggests that the cylinder's motion is primarily influenced by its own rotational speed, leading to stable and predictable fluid interactions.

Case A2 (Alpha= 1.0, Beta=0): Increasing the Alpha value to 1.0 with Beta still at zero results in a slightly higher lift coefficient amplitude (ΔC_L=0.6839). This indicates that even a moderate rotational speed can enhance the lift forces slightly, though the changes remain manageable.

Case A3 (Alpha= 1.5, Beta=0): With the highest Alpha value in this group and Beta at zero, the lift coefficient amplitude decreases slightly (ΔC_L=0.5702). This suggests that increasing Alpha alone may not always lead to higher amplitudes, and a balanced interaction with Beta is crucial.

Case B1 (Alpha = 0.5, Beta=0.5): Introducing a moderate Beta value while keeping Alpha at 0.5 results in a significant increase in lift coefficient amplitude (ΔC_L=2.4874). This indicates that the combined effect of moderate rotational speed and frequency significantly impacts the hydrodynamic forces.

Case B2 (Alpha = 1.0, Beta=0.5): With both parameters balanced, the amplitude of the lift coefficient increases notably (ΔC_L=5.0082). The interaction between rotational speed and frequency creates more dynamic and complex fluid behaviors, leading to higher lift forces.

Case B3 (Alpha = 1.5, Beta=0.5): The highest amplitude in this group (ΔC_L=7.7493) indicates the most substantial fluid interaction and dynamic behavior. This case demonstrates the peak impact of rotational frequency on the lift coefficient amplitude.

Case C1 (Alpha= 0.5, Beta= 1.0): At a higher Beta value, the lift coefficient amplitude increases significantly (ΔC_L=2.8742). This suggests that a higher rotational frequency amplifies the effects of rotational speed, leading to more pronounced lift forces.

Case C2 (Alpha= 1.0, Beta= 1.0): Balanced parameters result in a high lift coefficient amplitude (ΔC_L=4.4023), reflecting a complex and highly dynamic fluid interaction that significantly impacts the lift forces on the cylinder.

Case C3 (Alpha= 1.5, Beta= 1.0): Despite the high Beta value, the lift coefficient amplitude is moderate (ΔC_L=3.1533). This indicates that while rotational frequency has a significant impact, higher Alpha values can moderate its effects to some extent.

Case D1 (Alpha= 0.5, Beta= 1.5): The lift coefficient amplitude decreases again (ΔC_L=0.8163). This suggests that at very high frequencies, the fluid interactions stabilize somewhat, reducing the variability in lift forces.

Case D2 (Alpha= 1.0, Beta= 1.5): Similar to D1, but with a slightly lower amplitude (ΔC_L=0.7810), indicating that the effects of high-frequency rotation are significant, but the amplitude of lift forces remains moderate.

Case D3 (Alpha= 1.5, Beta= 1.5): The lowest amplitude in this group (ΔC_L=0.7810) suggests that high-frequency rotation with higher Alpha values results in the most stable fluid interactions, reducing the dynamic variability in lift forces.

Summative Comments:

The surface diagram highlights the critical relationship between Beta and Alpha parameters in determining the lift coefficient amplitude (ΔC_L). Higher Beta values generally lead to increased lift forces, indicating more dynamic and complex fluid interactions. However, there is a balance to be struck, as excessively high values can lead to instability. The highest lift coefficient amplitudes are observed in cases with moderate to high Alpha values combined with moderate to high Beta values, suggesting that these configurations lead to the most dynamic fluid interactions.

Mean Drag Coefficient Surface Plot

The surface plot for the mean drag coefficient ,$\overline{C_D}$, provides a comprehensive visualization of how different combinations of Beta and Alpha parameters influence the mean drag experienced by the cylinder. This analysis aims to understand the relationship between these parameters and the resulting drag forces, which is essential for optimizing fluid dynamics in various engineering applications.

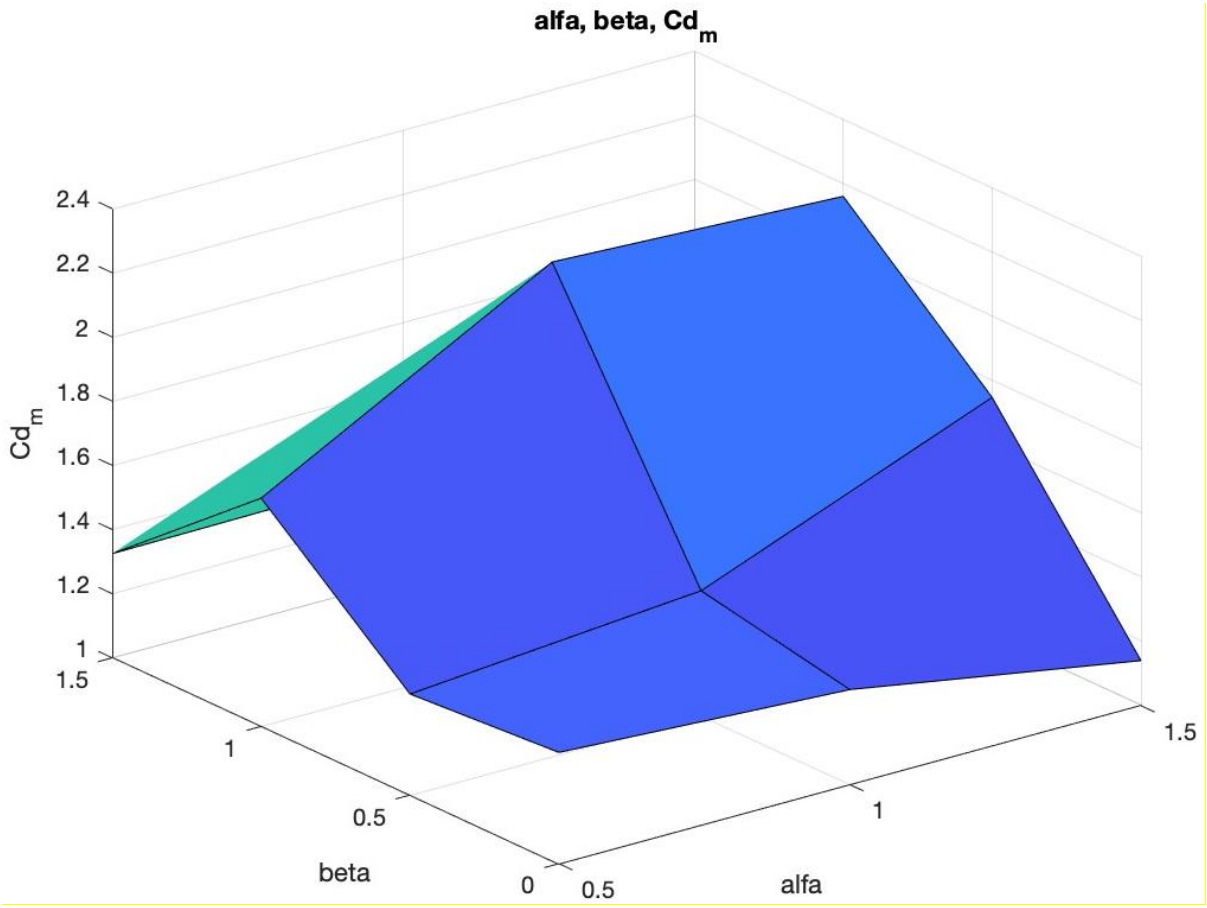

Figure 12 Mean Drag Coefficient Surface Diagram

Case Analysis:

Case A1 (Alpha= 0.5, Beta=0): This case shows a mean drag coefficient of 1.2386. The low Beta ratio results in a moderate drag force, indicating a stable interaction between the cylinder's rotation and the fluid flow.

Case A2 (Alpha= 1.0, Beta=0): With a mean drag coefficient of 1.0369, this scenario shows a decrease in drag compared to A1. The increase in Alpha results in more efficient fluid flow around the cylinder, reducing the drag force.

Case A3 (Alpha= 1.5, Beta=0): This case, with a mean drag coefficient of 0.7669, has the lowest drag among Group A. The higher Alpha value allows for smoother fluid flow, minimizing the drag force significantly.

Case B1 (Alpha = 0.5, Beta=0.5): Exhibits a mean drag coefficient of 1.2581, showing a slight increase in drag compared to A1. The introduction of a moderate Beta value increases the drag due to more dynamic interactions between the cylinder's rotation and fluid flow.

Case B2 (Alpha = 1.0, Beta=0.5): This case has a mean drag coefficient of 1.2468, indicating stable drag forces with increased Beta. The balanced increase in both parameters results in a manageable drag force.

Case B3 (Alpha = 1.5, Beta=0.5): Displays the highest drag in Group B with a mean drag coefficient of 1.4086. The increased rotational speed and frequency amplify the drag forces, resulting in more pronounced interactions with the fluid flow.

Case C1 (Alpha= 0.5, Beta= 1.0): Shows a significant increase in drag with a mean drag coefficient of 1.6647. The higher Beta value leads to more complex fluid interactions, increasing the drag force.

Case C2 (Alpha= 1.0, Beta= 1.0): This case, with a mean drag coefficient of 1.9782, exhibits the highest drag in Group C. The combination of high Alpha and Beta values results in substantial drag forces due to aggressive fluid interactions.

Case C3 (Alpha= 1.5, Beta= 1.0): Shows a mean drag coefficient of 1.7780, indicating a slight decrease in drag compared to C2. The high Alpha value helps mitigate some of the drag forces, resulting in a more stable interaction.

Case D1 (Alpha= 0.5, Beta= 1.5): Exhibits a mean drag coefficient of 1.2896, showing moderate drag forces. The higher Beta value introduces more dynamic interactions, but the drag remains stable.

Case D2 (Alpha= 1.0, Beta= 1.5): This scenario shows a mean drag coefficient of 1.2630. The increased frequency and rotational speed lead to noticeable drag forces, but they remain manageable.

Case D3 (Alpha= 1.5, Beta= 1.5): Displays a mean drag coefficient of 1.2537, indicating stable drag forces similar to D1 and D2. The combination of high Alpha and Beta values results in complex but stable fluid interactions.

Summative Comments:

The surface plot analysis reveals that the mean drag coefficient is significantly influenced by the Beta and Alpha parameters. Higher Beta values generally lead to increased drag forces due to more dynamic interactions between the rotational speed and fluid flow. However, higher Alpha values can help mitigate these forces, resulting in more stable and efficient fluid dynamics. The findings from this analysis are crucial for optimizing designs in applications where control over drag forces is essential, such as in marine and aerospace engineering. Understanding the balance between rotational speed and frequency is key to minimizing drag and enhancing performance.

Sum of Power Surface Plot

The sum of power , $\sum P$,surface plot, showcasing the combined effects of the parameters Beta and Alpha, offers significant insights into the energy dynamics of the system. The plot reveals how different combinations of rotational amplitude (Alpha) and frequency ratio (Beta) impact the total power consumption required to maintain the cylinder's motion.

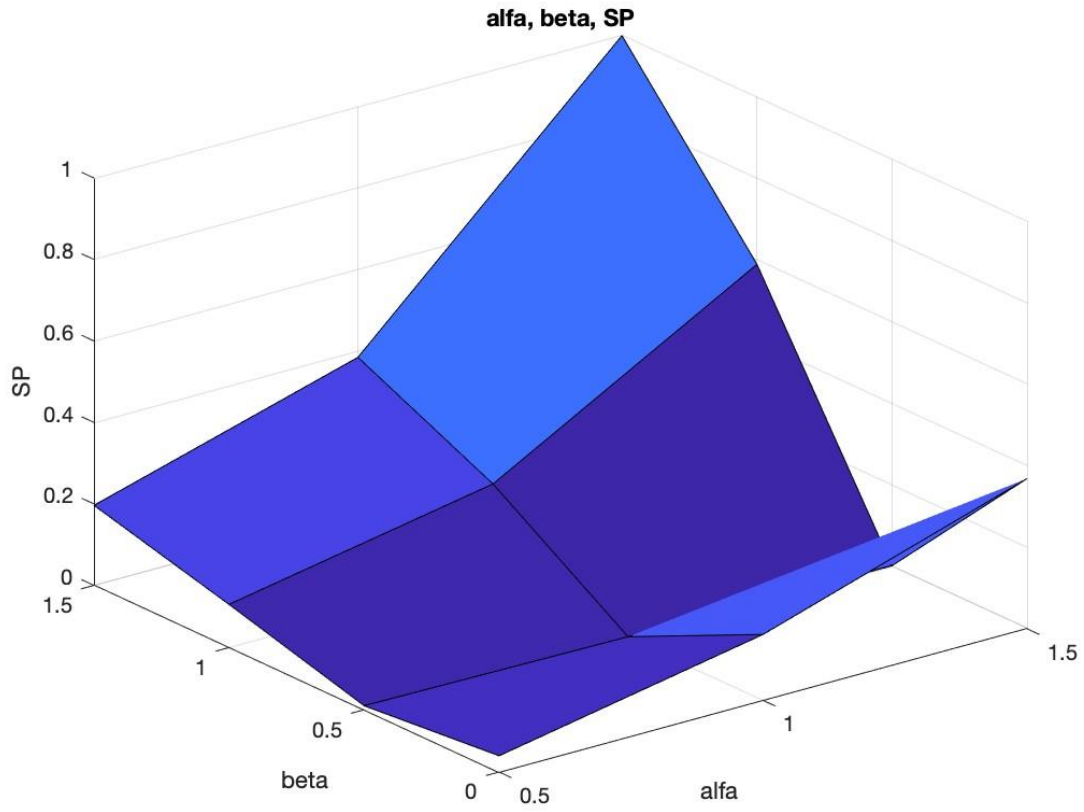

Figure 13 Sum of Power Surface Diagram for different cases

Case Analysis:

Case A1 (Alpha= 0.5, Beta=0): Exhibits relatively low power consumption with a sum of power value of 0.0398 W. This configuration suggests efficient energy usage due to minimal rotational influence, making it ideal for applications requiring low energy input.

Case A2 (Alpha= 1.0, Beta=0): Shows a moderate increase in power consumption with a sum of power value of 0.1619. The higher Alpha value indicates a greater energy demand due to increased rotational speed, yet it remains within a manageable range.

Case A3 (Alpha= 1.5, Beta=0): Demonstrates significant power consumption with a sum of power value of 0.3687. The highest Alpha value in this group highlights the substantial energy

required for maintaining the rotational motion, which could be challenging for energy-efficient applications.

Case B1 (Alpha = 0.5, Beta=0.5): Presents very low power consumption with a sum of power value of 0.0100. The combined low Alpha and Beta values result in minimal energy usage, indicating a highly efficient configuration.

Case B2 (Alpha = 1.0, Beta=0.5): Further reduces power consumption to a sum of power value of 0.0036. This configuration suggests that a balanced increase in Alpha with a moderate Beta value can optimize energy efficiency.

Case B3 (Alpha = 1.5, Beta=0.5): Shows the lowest power consumption in group B with a sum of power value of 0.0021. The higher Alpha value combined with a moderate Beta value results in the most energy-efficient scenario, despite the increased rotational speed.

Case C1 (Alpha= 0.5, Beta= 1.0): Indicates a moderate power consumption with a sum of power value of 0.1060. The higher Beta value requires more energy, reflecting a balance between rotational speed and power usage.

Case C2 (Alpha= 1.0, Beta= 1.0): Exhibits increased power consumption with a sum of power value of 0.2259. The equal Alpha and Beta values suggest that the combined effect of increased rotational dynamics results in higher energy requirements.

Case C3 (Alpha= 1.5, Beta= 1.0): Shows the highest power consumption in group C with a sum of power value of 0.5893. This configuration, with the highest Alpha and moderate Beta values, demonstrates substantial energy usage due to the combined effects of high rotational speed and frequency.

Case D1 (Alpha= 0.5, Beta= 1.5): Presents moderate power consumption with a sum of power value of 0.1965. The high Beta value results in increased energy requirements, despite the low Alpha value.

Case D2 (Alpha= 1.0, Beta= 1.5): Exhibits significant power consumption with a sum of power value of 0.3841. The higher Beta and moderate Alpha values indicate a considerable energy demand due to increased rotational dynamics.

Case D3 (Alpha= 1.5, Beta= 1.5): Shows the highest power consumption in group D with a sum of power value of 0.9980. The highest Alpha and Beta values highlight the substantial energy required to maintain the rotational motion under these conditions, presenting a challenge for energy efficiency.

Summative Comments:

The surface plot analysis of the sum of power illustrates the impact of different combinations of Alpha and Beta parameters on energy consumption. Generally, higher Alpha and Beta values lead to increased power usage, reflecting the greater energy required to sustain higher rotational speeds and frequencies. Notably, cases B3 and D3 exhibit the most significant power consumption, emphasizing the need for careful management of rotational dynamics to optimize energy efficiency.

5 Conclusions – Suggestions for future research

The results of this study provide a comprehensive understanding of the hydrodynamic behavior of a rotating cylinder under various Beta and Alpha configurations. This section synthesizes the findings from all analyzed cases, highlighting the key insights, practical applications, and potential future research directions.

5.1 Key Insights

5.1.1 Effect of Alpha Parameter:

Rotational Speed Influence:

- Higher Alpha values represent the amplitude of the rotational speed. They generally indicate a faster rotational speed of the cylinder. For instance, in Case B3 (Alpha = 1.5, Beta = 0.5), a high Alpha results in the highest lift coefficient amplitude (ΔC_L = 7.7493). Increased Alpha values enhance the energy in the flow around the cylinder, leading to more pronounced lift forces.

Flow Stability:

- Lower Alpha values contribute to more stable flow patterns, with minimal fluctuations in lift and drag forces. Case A1 (Alpha = 0.5, Beta = 0) demonstrates stable vortex shedding with a moderate lift coefficient amplitude (ΔC_L = 0.6554).
- As Alpha increases, the flow tends to become more dynamic and complex. However, excessively high Alpha without a corresponding increase in Beta can sometimes lead to decreased lift, as seen in Case A3 (Alpha = 1.5, Beta = 0) with a ΔC_L of 0.5702.

Drag Forces:

- The mean drag coefficient, $\overline{C_D}$ typically decreases with increasing Alpha values when Beta is zero. This is due to the more efficient fluid flow around the cylinder. For example, Case A3 (Alpha = 1.5, Beta = 0) has the lowest mean drag coefficient ($\overline{C_D}$ = 0.7669) in Group A.

5.1.2 Effect of Beta Parameter

Rotational Frequency Impact**:**

- Beta represents the frequency ratio of the rotational speed. Higher Beta values mean a higher frequency of the rotational changes. High Beta values significantly affect the stability and dynamics of the flow, leading to increased complexity in fluid interactions. This is evident from the highest lift coefficient amplitude in cases like B3 (Alpha = 1.5, Beta = 0.5)**.**

Flow Complexity and Turbulence**:**

- Higher Beta values tend to disrupt the orderly shedding of vortices, leading to more chaotic and turbulent flow patterns. This is particularly noticeable in the drag coefficient fluctuations and power consumption. For instance, Case D3 (Alpha = 1.5, Beta = 1.5) demonstrates the highest power consumption ($\sum P$ = 0.9980 W) due to the complex interactions between high rotational speed and frequency, resulting in substantial energy demands.

Energy Dynamics**:**

- The sum of power ($\sum P$) increases with higher Beta values, reflecting the greater energy required to maintain the rotational motion. Cases with high Beta values, such as C3 (Alpha = 1.5, Beta = 1.0), show significant power consumption due to the increased frequency of rotational dynamics.

Hydrodynamic Forces**:**

- The mean drag coefficient also varies significantly with Beta. Higher Beta values typically result in increased drag forces due to more dynamic interactions between the cylinder and the fluid. For example, Case C2 (Alpha = 1.0, Beta = 1.0) has a high mean drag coefficient ($\overline{C_D}$ = 1.9782), indicating substantial drag forces.

5.1.3 Combined Effects of Alpha and Beta

Balanced Interactions:

- The interaction between Alpha and Beta parameters is critical for optimizing hydrodynamic performance. Balanced increases in both parameters lead to higher lift and drag forces, as well as increased power consumption. For instance, Case B2 (Alpha = 1.0, Beta = 0.5) shows a significant lift coefficient amplitude (ΔC_L = 5.0082) and a mean drag coefficient ($\overline{C_D}$ = 1.2468).

5.1.4 Practical Applications

Energy Efficiency:

- Cases with lower Alpha and Beta values, such as Case A1 (Alpha = 0.5, Beta = 0), demonstrate relatively low and consistent power consumption. This stability in energy demand suggests efficient energy usage, making such configurations ideal for applications where minimal power consumption is critical, such as underwater vehicles and sustainable energy systems.

High-Frequency Rotational Scenarios:

- Cases with higher Beta values, such as Case D3 (Alpha = 1.5, Beta = 1.5), reveal the upper limits of power requirements. The significant energy consumption observed in these cases underscores the challenges of managing power in high-frequency rotational scenarios. These configurations can be particularly useful in studying the effects of turbulent flow conditions and understanding the energy dynamics in turbulent environments.

Vortex Shedding and Flow Patterns:

- The study provides insights into the dynamic relationship between lift and drag forces acting on the cylinder, which varies according to the rotational speed and frequency parameters. Cases like B3 (Alpha = 1.5, Beta = 0.5) demonstrate significant interactions between lift and drag forces, leading to complex vortex shedding patterns.

5.1.5 Conclusion

The analysis reveals that both Alpha and Beta parameters play crucial roles in shaping the hydrodynamic behavior of the rotating cylinder. Higher Alpha values increase rotational speed, enhancing lift forces but also introducing potential instability if not balanced with Beta. Higher Beta values increase the frequency of rotational changes, leading to complex and turbulent flow patterns. The comprehensive data from this study can guide the design and optimization of rotating systems in fluid environments, ensuring enhanced performance, efficiency, and stability in various practical applications.

5.2 Future Research Directions

The current study opens numerous avenues for future research to further understand and optimize the hydrodynamic behavior of rotating cylinders in fluid flows. Here are some detailed directions for future investigations:

Parameter Space Expansion: The study primarily focused on specific Beta and Alpha parameters as well as Reynolds number of the fluid flow. Expanding the parameters space could provide a more comprehensive understanding of the fluid-structure interactions. Additionally, exploring non-circular cylinder shapes, such as ellipsoids or more complex geometries, can reveal how shape influences hydrodynamic performance and vortex dynamics.
Experimental Validation: While computational simulations offer valuable insights, experimental validation remains essential. Future studies should incorporate experimental setups to validate the numerical results obtained in this study. Wind tunnel experiments, water channel tests, and particle image velocimetry (PIV) can provide empirical data to compare with simulation outcomes. This validation will help refine the computational models and ensure their accuracy for real-world applications.

Multi-Objective Optimization: Future research could also focus on multi-objective optimization techniques to simultaneously improve multiple performance metrics, such as minimizing drag while maximizing lift or optimizing power consumption. Genetic algorithms, particle swarm optimization, and other optimization methods could be employed to identify the best design configurations for rotating cylinders in various fluid flow scenarios. This approach can lead to designs that balance multiple performance criteria, enhancing overall system efficiency and effectiveness.

Practical Applications and Implementation: In practical terms, the findings of this study can be implemented in various engineering fields. For instance, the insights on rotational dynamics and fluid interactions can inform the design of more efficient underwater vehicles, improving their maneuverability and reducing energy consumption. In the field of aerospace engineering, the study's results can help in designing aircraft components that better manage turbulent airflows, enhancing stability and performance. Additionally, the renewable energy sector can benefit from the research by optimizing the design of wind and tidal turbines to maximize energy capture and durability.

In conclusion, the future research directions outlined above aim to build upon the findings of this study, enhancing our understanding and optimization of rotating cylinders in fluid flows. By expanding the parameter space [19] [20]and integrating experimental validation, researchers can develop more efficient and effective designs for a wide range of engineering applications.

Bibliography

[1] M. M. Zdravkovich, Flow Around Circular Cylinders, Oxford University Press, 1997.

[2] J. Wagner, Artist, *on of the von Kármán vortex street behind a circlular cylinder in air flow. The flow is made visible by means of the release of oil vapour near the cylinder.*. [Art]. 2014.

[3] M. M. Zdravkovich, "Different modes of vortex shedding : an overview," *Journal of Fluids and Structures* , 1996.

[4] K. M. Sowoud, "Numerical Investigation of 2D Turbulent Flow past a Circular Cylinder at Lower Subcritical Reynolds Number," *IOP Conference Series: Materials Science and Engineering*, vol. 881, p. 12, 2020.

[5] A. Jamieson, "Wikipedia," 17 August 2015. [Online]. Available: https://en.wikipedia.org/wiki/File:E-Ship_1_(20037221244).jpg. [Accessed May 2024].

[6] Unkown, "Wikipedia," Unknown . [Online]. Available: https://commons.wikimedia.org/wiki/File:Flettner_Rotor_Aircraft.jpg. [Accessed May 2024].

[7] B. R. Munson, Fundamentals of Fluid Mechanics, John Wiley & Sons, Inc, 2013.

[8] Jasond, "CFD Online," [Online]. Available: https://www.cfd-online.com/Wiki/Mesh_classification. [Accessed May 2024].

[9] E. v. popov, "CFD Online," [Online]. Available: https://www.cfd-online.com/Wiki/Structured_mesh_generation. [Accessed May 2024].

[10] Team CFDTech, "cadence," October 2023. [Online]. Available: https://community.cadence.com/cadence_technology_forums/computational-fluid-dynamics/f/automesh/58122/structured-vs-unstructured-mesh. [Accessed May 2024].

[11] M. D. Piggott, "Assessment of spurious mixing in adaptive mesh simulations of the two-dimensional lock-exchange," *Ocean Modelling* , January 2014.

[12] CFDTech, "Cadence," Cadence, 2023. [Online]. Available: https://community.cadence.com/cadence_technology_forums/computational-fluid-dynamics/f/automesh/58122/structured-vs-unstructured-mesh. [Accessed 2024].

[13] H. K. Versteeg, An Introduction to Computational Fluid Dynamics, Essex, England: Pearson Education Limited, 2007.

[14] G. Tufano, *K-space analysis of complex large-scale periodic structures*, 2020.

[15] Y. Liang, "Interaction of vortex shedding processes on flow over a deep-draft semi-submersible," *Ocean Engineering,* p. 23, 23 June 2017.

[16] B. Rajani, "Numerical simulation of laminar flow past a circular cylinder," *Applied Mathematical Modelling,* vol. 33, no. 3, pp. 1228-1247, 2009.

[17] D. Stojkovic, "Effect of high rotation rates on the laminar flow around a circular cylinder," *Physics of Fluids,* vol. 14, no. 9, pp. 3160-3178, 2002.

[18] W. R. Graham, "Optimal control of vortex shedding using low-order models. Part I—open-loop model development," *nt. J. Numer. Meth. Engng,* vol. 44, pp. 945-972, 1999.

[19] O. AI, "ChatGPT: OpenAI's GPT-4 based large language model," Open AI, 2023. [Online]. Available: https://www.openai.com/chatgpt. [Accessed 2023].

[20] Q. Inc., "QuillBot: AI-powered paraphrasing tool," QuillBot Inc., 2024. [Online]. Available: https://www.quillbot.com. [Accessed 2023].

[21] S. Arias, "Numerical Study and Experimental Comparison of Two-Phase Flow Generation in a T-Junction," *AIAA Journal*, 2017.

[22] V. G. Tsipenko, "The use of vortex generators to improve the take-off and landing characteristics of transport category aircraft," *Civil Aviation High TECHNOLOGIES*, vol. 25, no. 4, pp. 83-95, 2022.

[23] A. Mishra, "Passive control of the onset of vortex shedding in flow past a circular cylinder using Slit," Department of Aerospace Engineering, Indian Institute of Technology Kanpur, Kanpur, India, 2016.

[24] A. Maimun, "Review of research on deepwater steel catenary risers," *International Conference on Marine Technology*, 20-22 November 2012.

[25] S.-b. Tao, "Vortex-Induced Vibration Suppression of a Circular Cylinder with Vortex Generators," *Shock and Vibration*, 10 January 2016.

[26] H. C. M, Harris' Shock and vibration handbook, Mc Graw hILL , 2002.

[27] M. V. Benetatos, *Assessment of flow energy harvesting in a duct by means of CFD numerical simulations*, Athens: University of west attica, 2023.

[28] Ι. Πάσχος, *Αριθμητικη προσομοίωση στρωτών ροών γύρω από κύλινδρο,* Athens: TEI Αθήνας, 2017.

Appendix A

This appendix provides a detailed compilation of diagrams and results from the simulation studies conducted for the various cases. Each set of diagrams below showcases the evolution and characteristics of fluid dynamics interactions specific to each case studied. This comprehensive documentation serves as a reference for analyzing the impact of different flow conditions on vortex shedding phenomena.

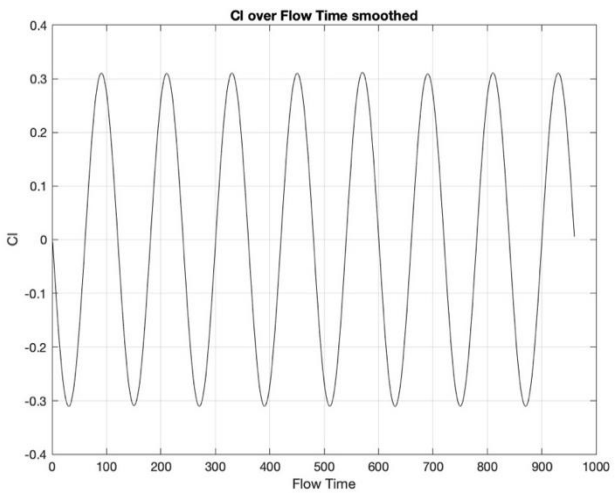

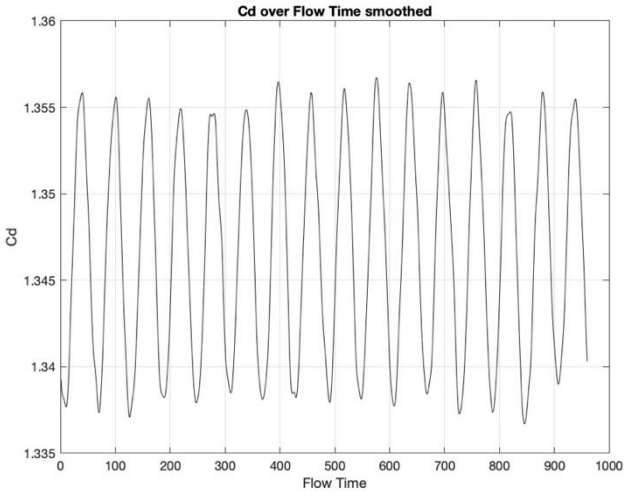

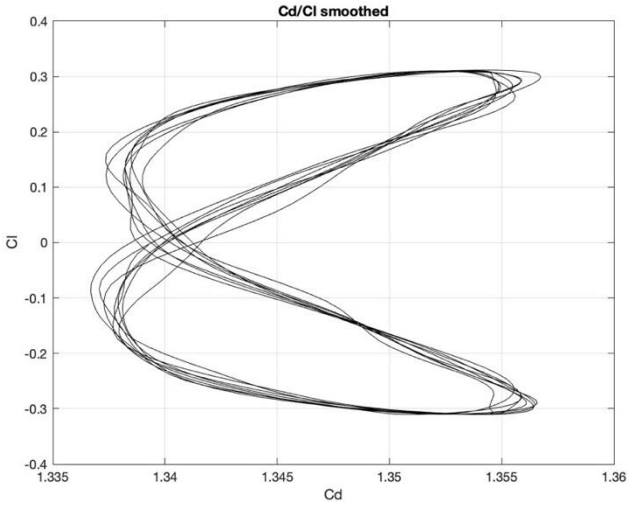

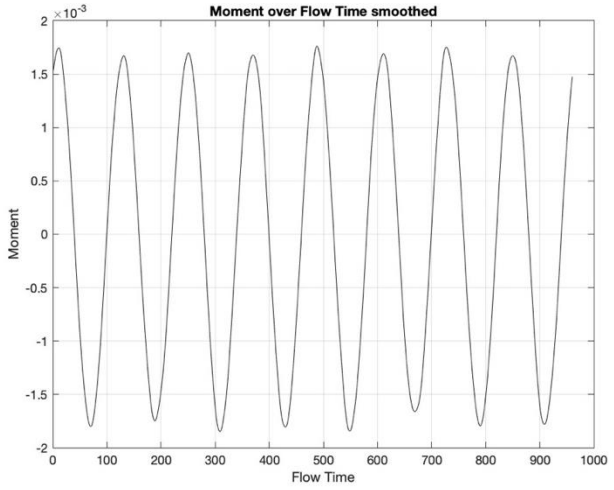

A0

Figure 14 Results for case A0

Top Left: Lift Coefficient over flow time (smoothed), Upper Middle:Drag Coefficient over flow time (smoothed), Top Right: Drag Coefficient over Lift Coefficient, Bottom Left: Moment over flow time, Bottom Middle: Power over flow time, Bottom Right: Velocity Contours.

A1

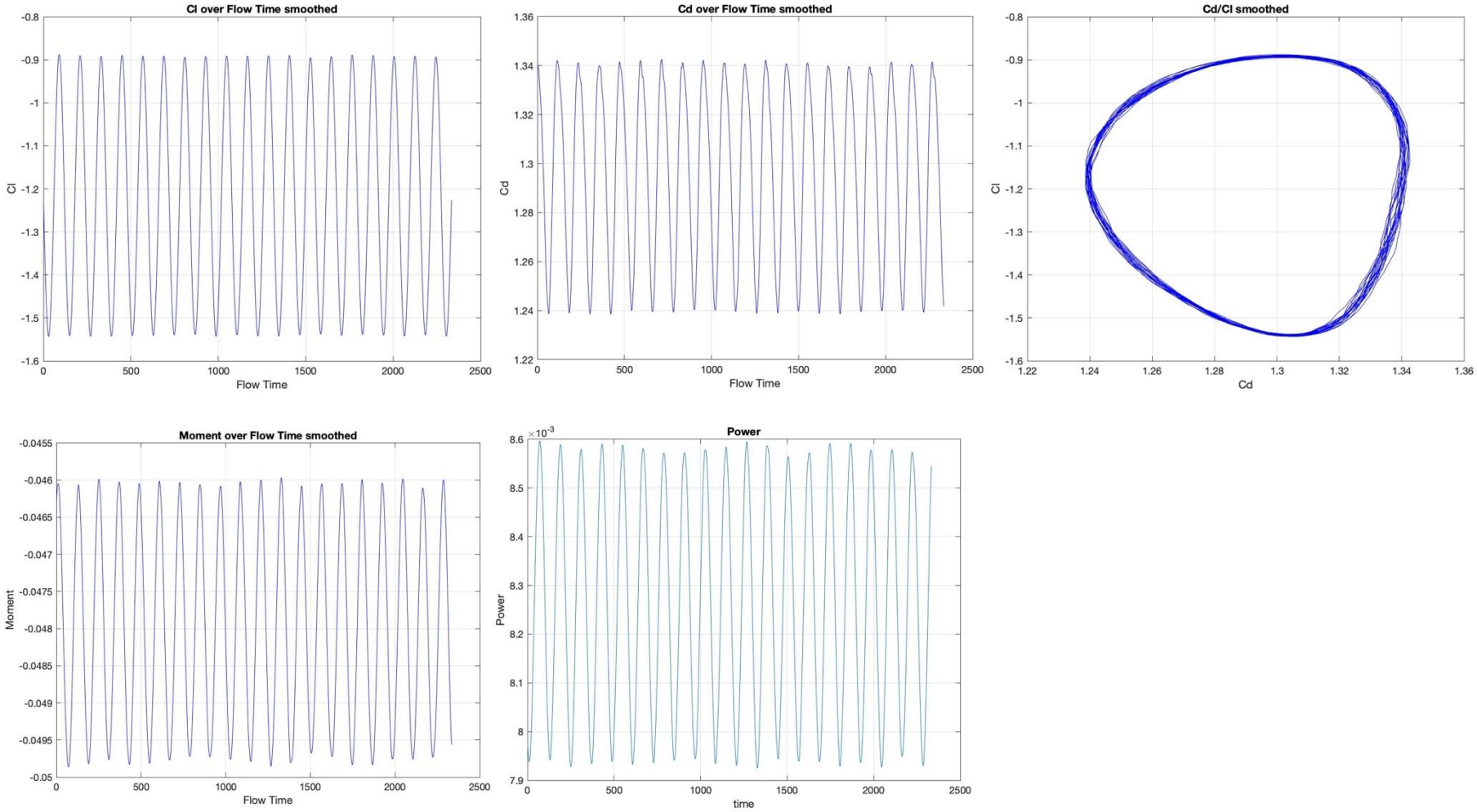

Figure 15 Results for case A1

Top Left: Lift Coefficient over flow time (smoothed), Upper Middle:Drag Coefficient over flow time (smoothed), Top Right: Drag Coefficient over Lift Coefficient, Bottom Left: Moment over flow time, Bottom Middle: Power over flow time, Bottom Right: Velocity Contour.

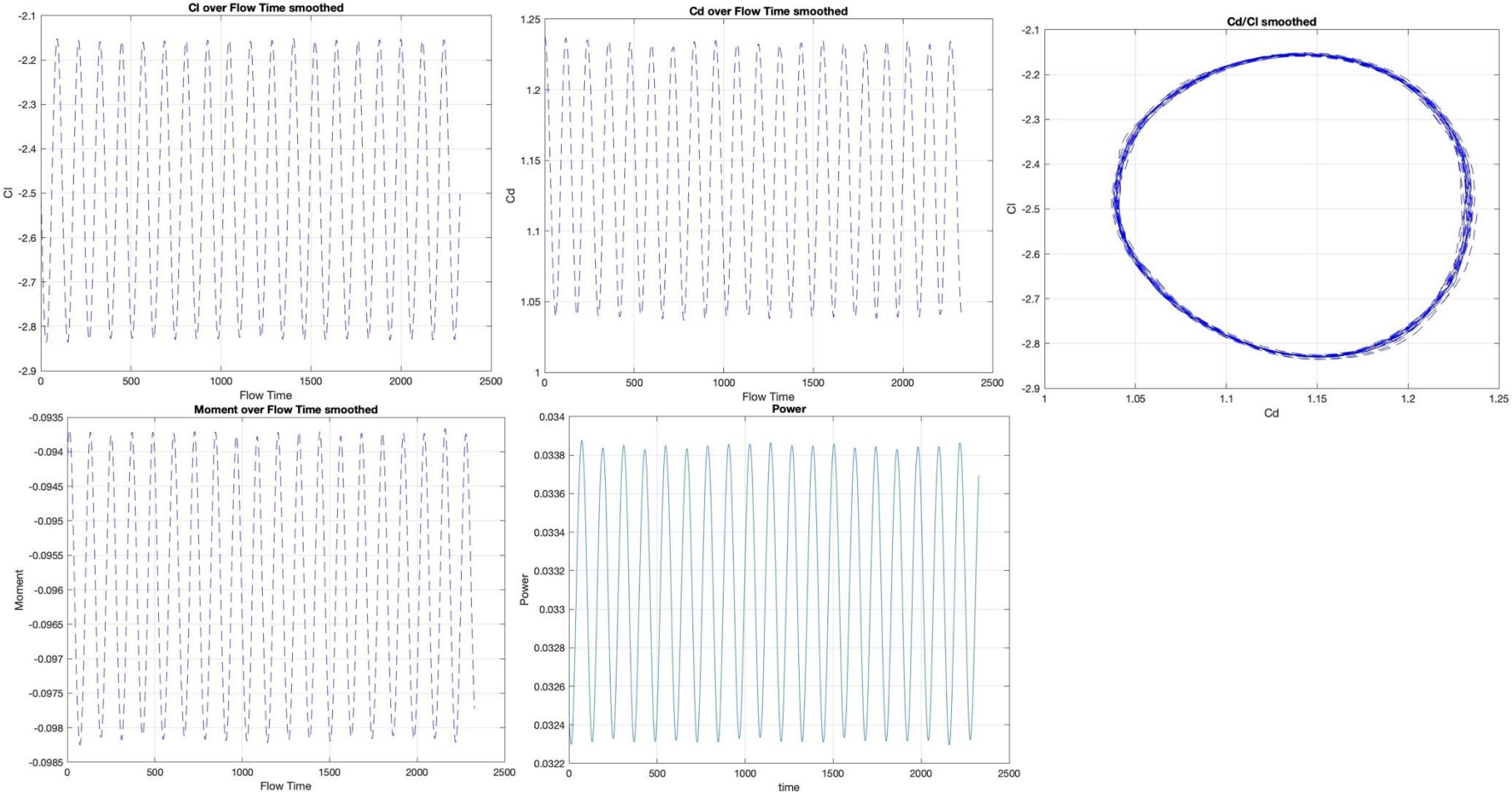

A2

Figure 16 Results for case A2

Top Left: Lift Coefficient over flow time (smoothed), Upper Middle:Drag Coefficient over flow time (smoothed), Top Right: Drag Coefficient over Lift Coefficient, Bottom Left: Moment over flow time, Bottom Middle: Power over flow time, Bottom Right: Velocity Contour.

A3

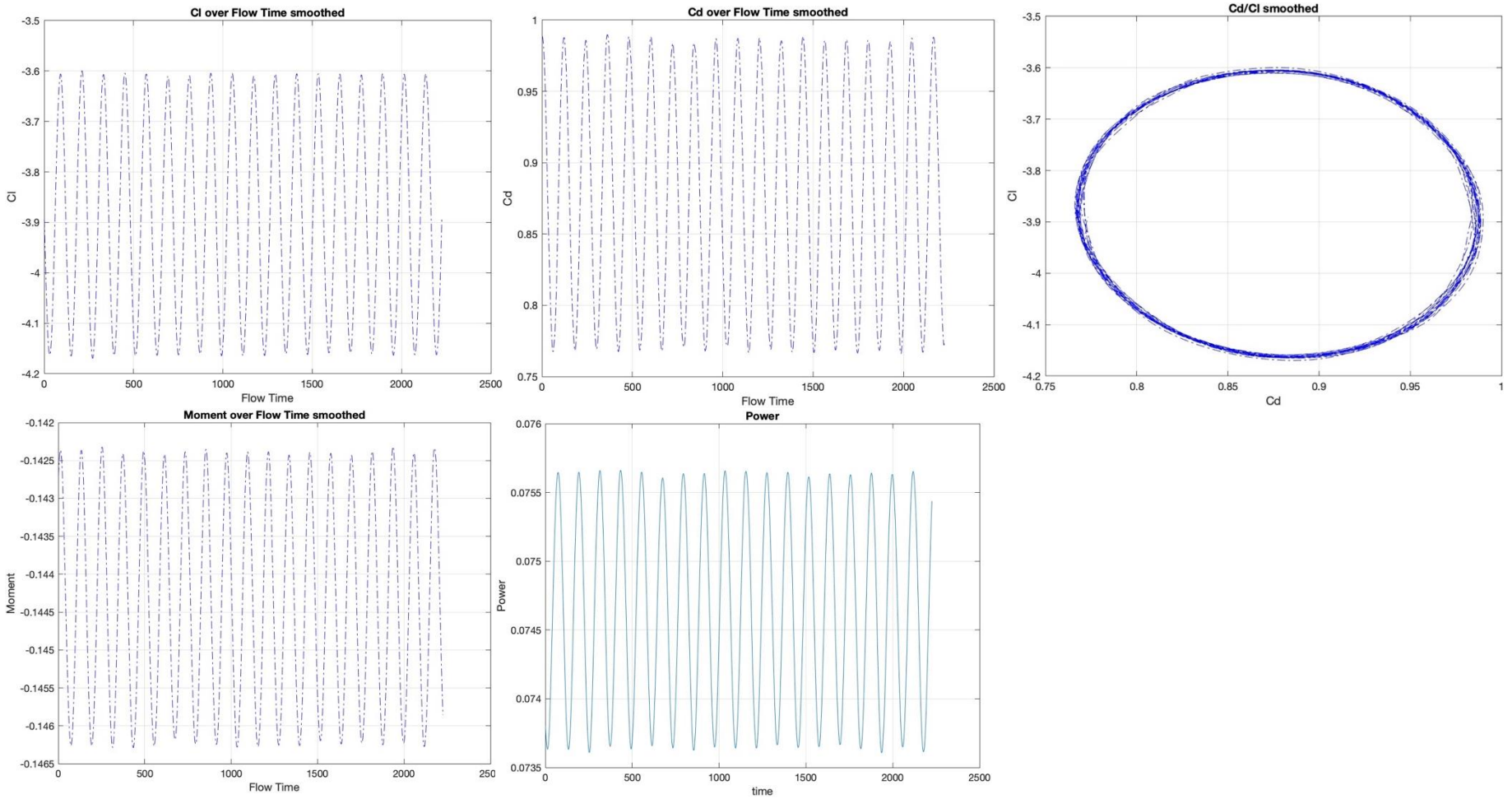

Figure 17 Results for case A3

Top Left: Lift Coefficient over flow time (smoothed), Upper Middle:Drag Coefficient over flow time (smoothed), Top Right: Drag Coefficient over Lift Coefficient, Bottom Left: Moment over flow time, Bottom Middle: Power over flow time, Bottom Right: Velocity Contour.

B1

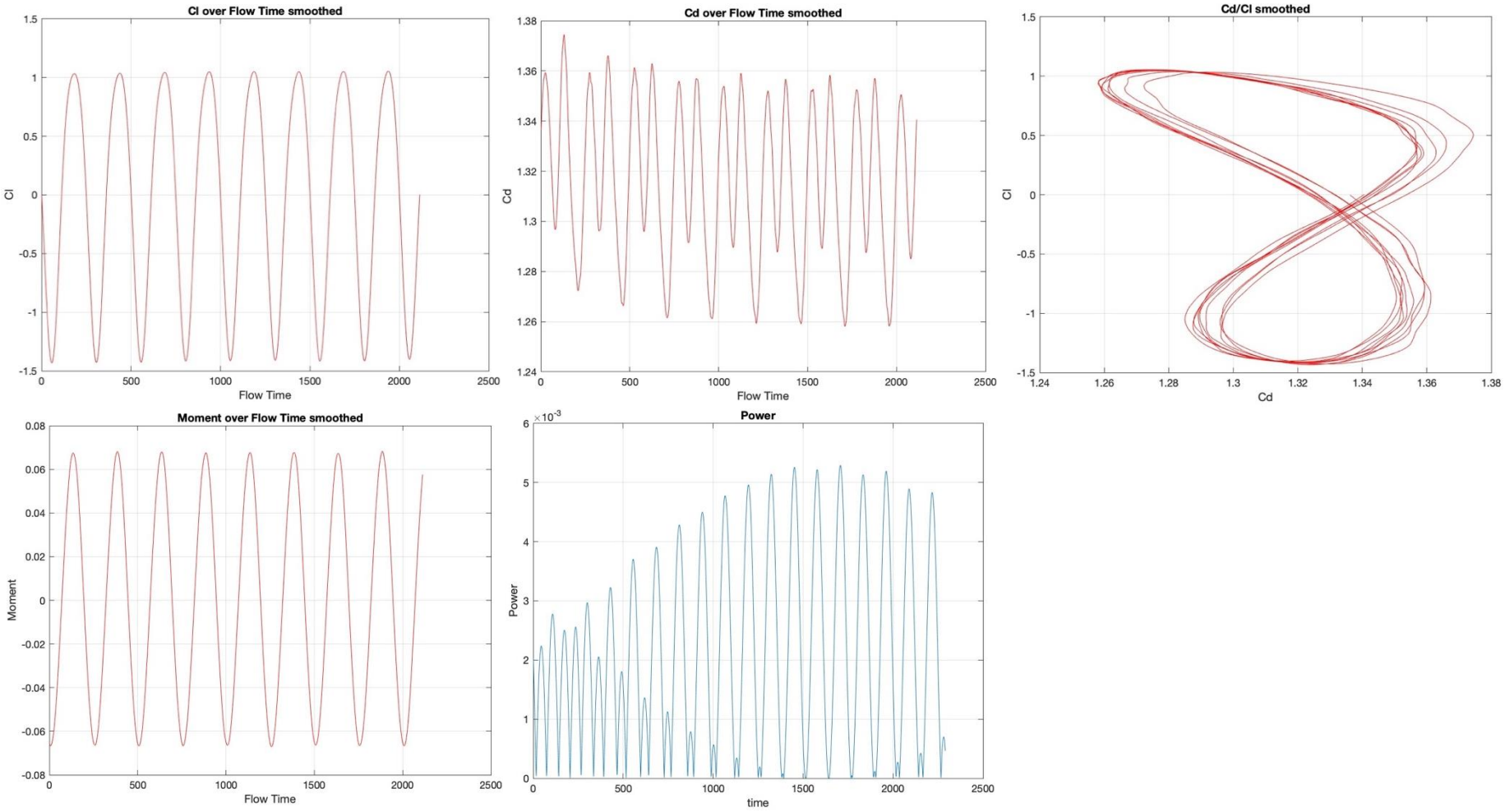

Figure 18 Results for case B1

Top Left: Lift Coefficient over flow time (smoothed), Upper Middle:Drag Coefficient over flow time (smoothed), Top Right: Drag Coefficient over Lift Coefficient, Bottom Left: Moment over flow time, Bottom Middle: Power over flow time, Bottom Right: Velocity Contour.

B2

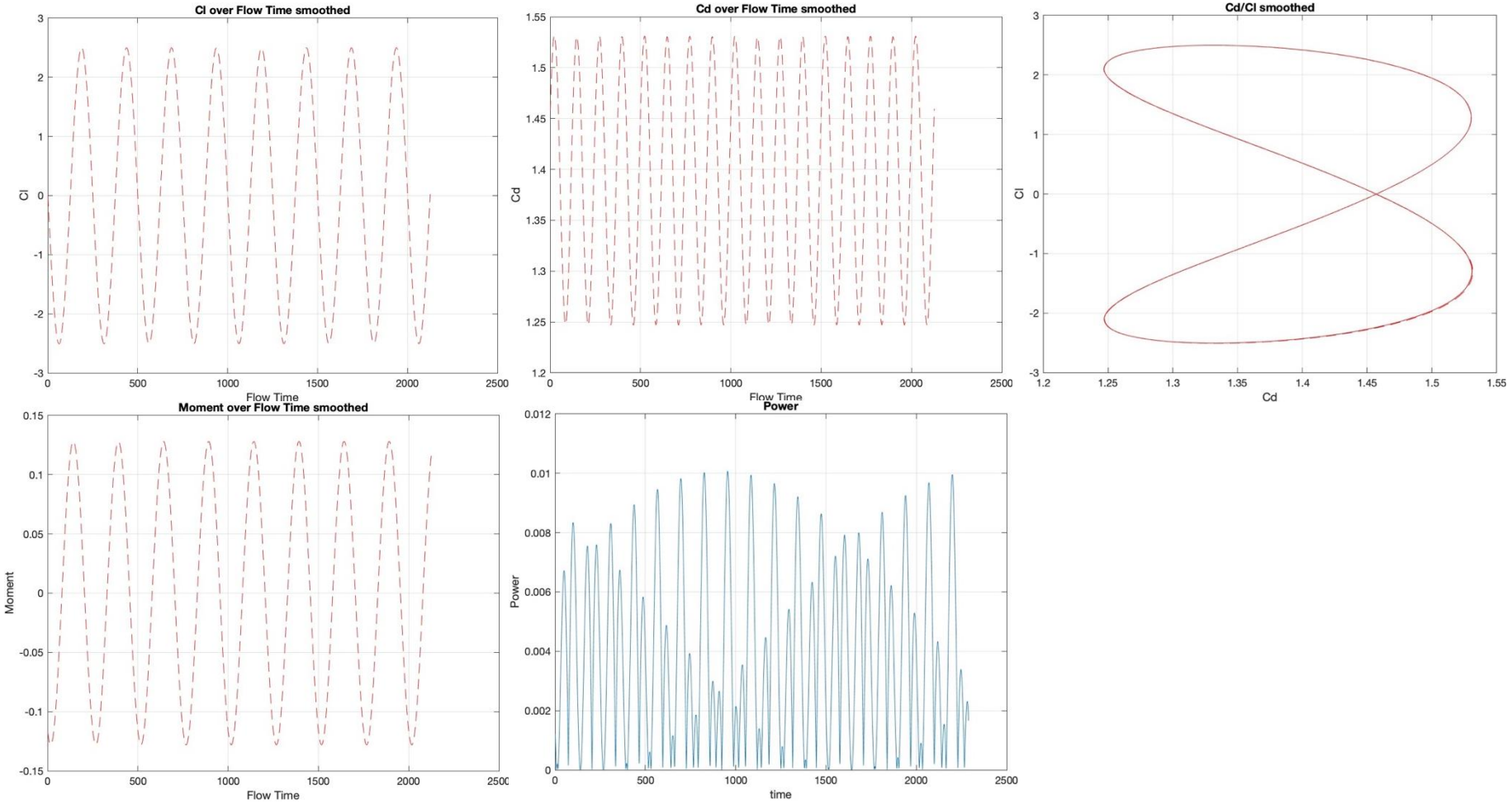

Figure 19 Results for case B2

Top Left: Lift Coefficient over flow time (smoothed), Upper Middle:Drag Coefficient over flow time (smoothed), Top Right: Drag Coefficient over Lift Coefficient, Bottom Left: Moment over flow time, Bottom Middle: Power over flow time, Bottom Right: Velocity Contour.

B3

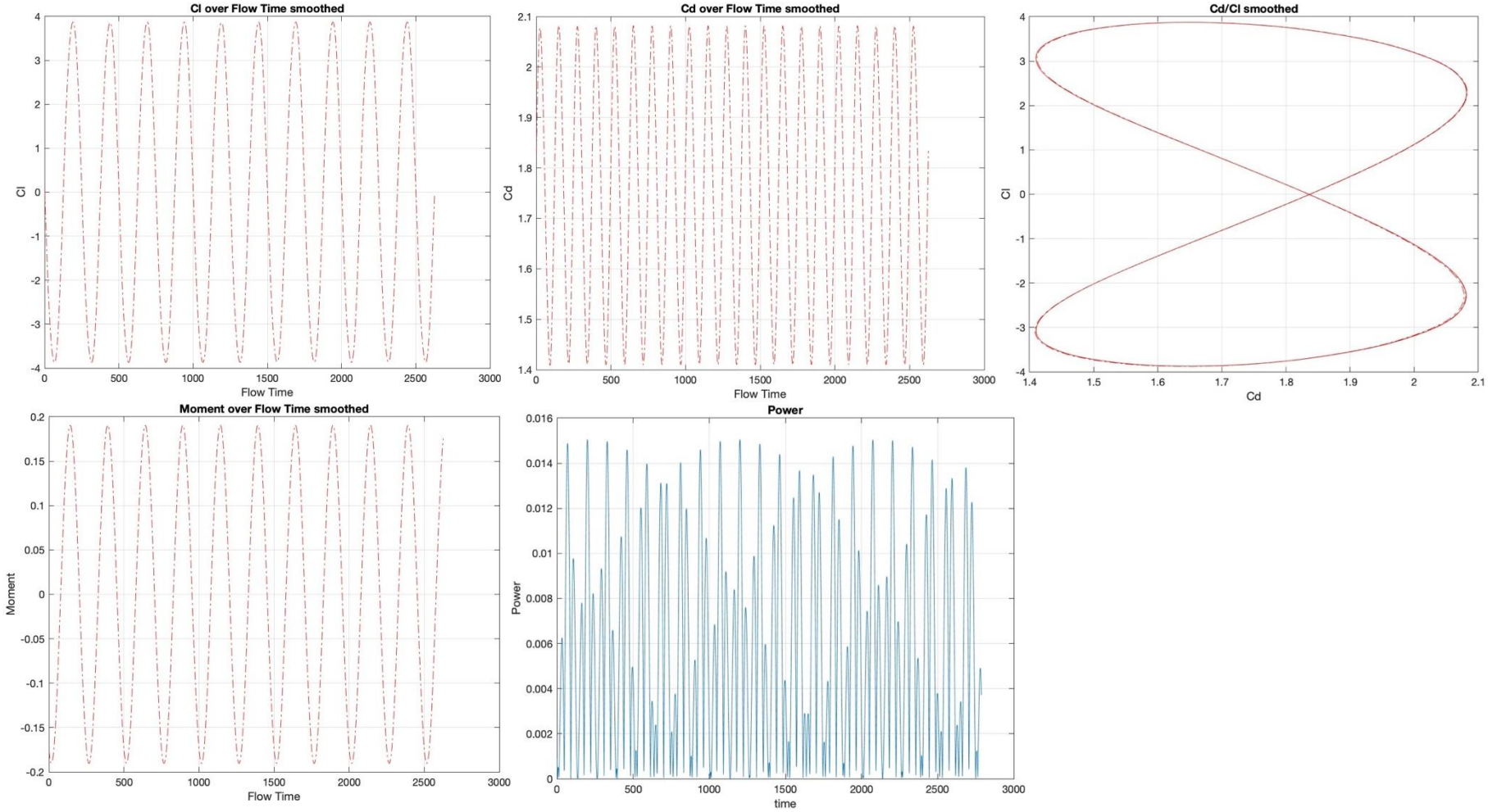

Figure 20 Results for case B3

Top Left: Lift Coefficient over flow time (smoothed), Upper Middle:Drag Coefficient over flow time (smoothed), Top Right: Drag Coefficient over Lift Coefficient, Bottom Left: Moment over flow time, Bottom Middle: Power over flow time, Bottom Right: Velocity Contour.

C1

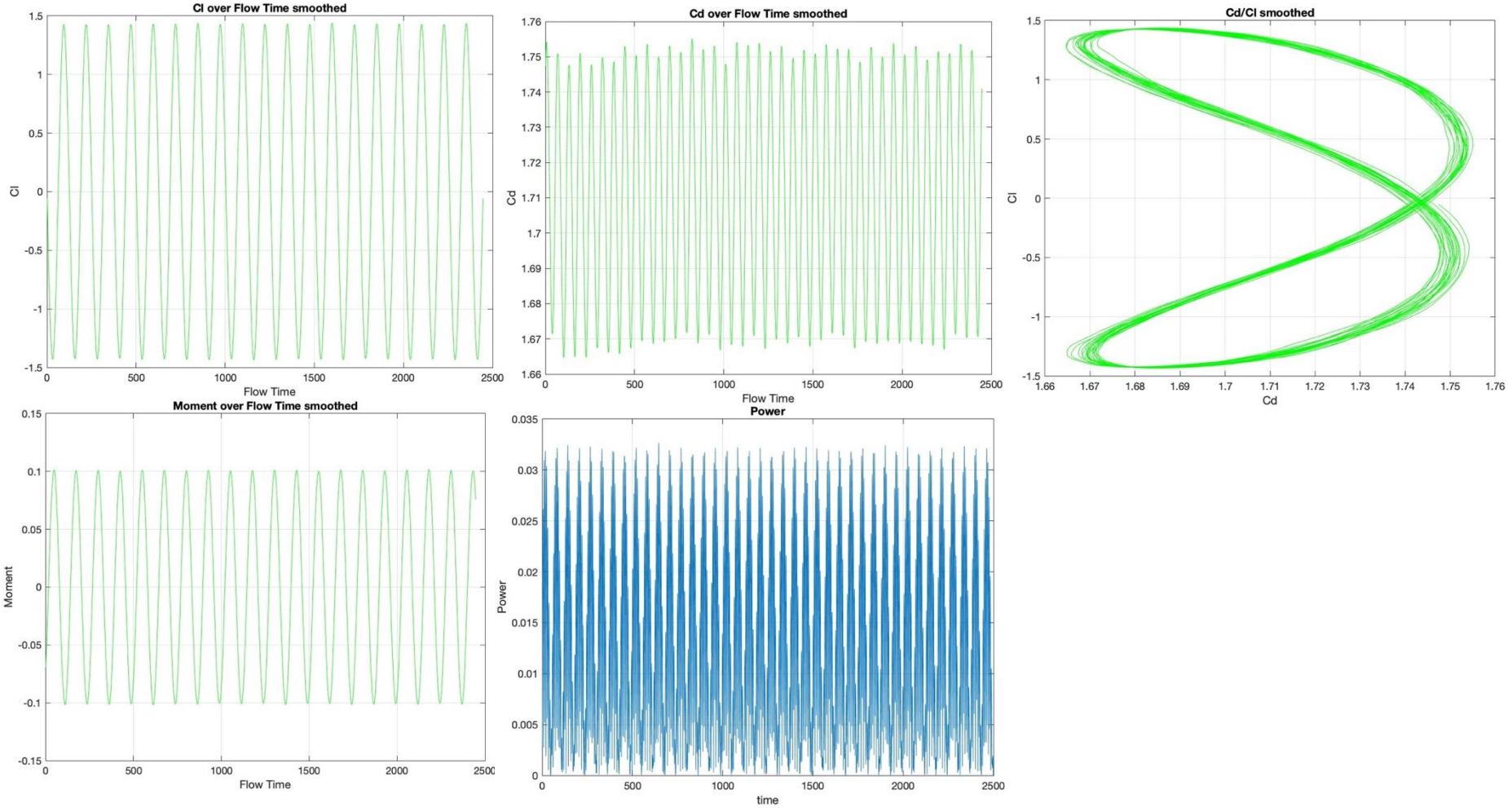

Figure 21 Results for case C1

Top Left: Lift Coefficient over flow time (smoothed), Upper Middle:Drag Coefficient over flow time (smoothed), Top Right: Drag Coefficient over Lift Coefficient, Bottom Left: Moment over flow time, Bottom Middle: Power over flow time, Bottom Right: Velocity Contour.

C2

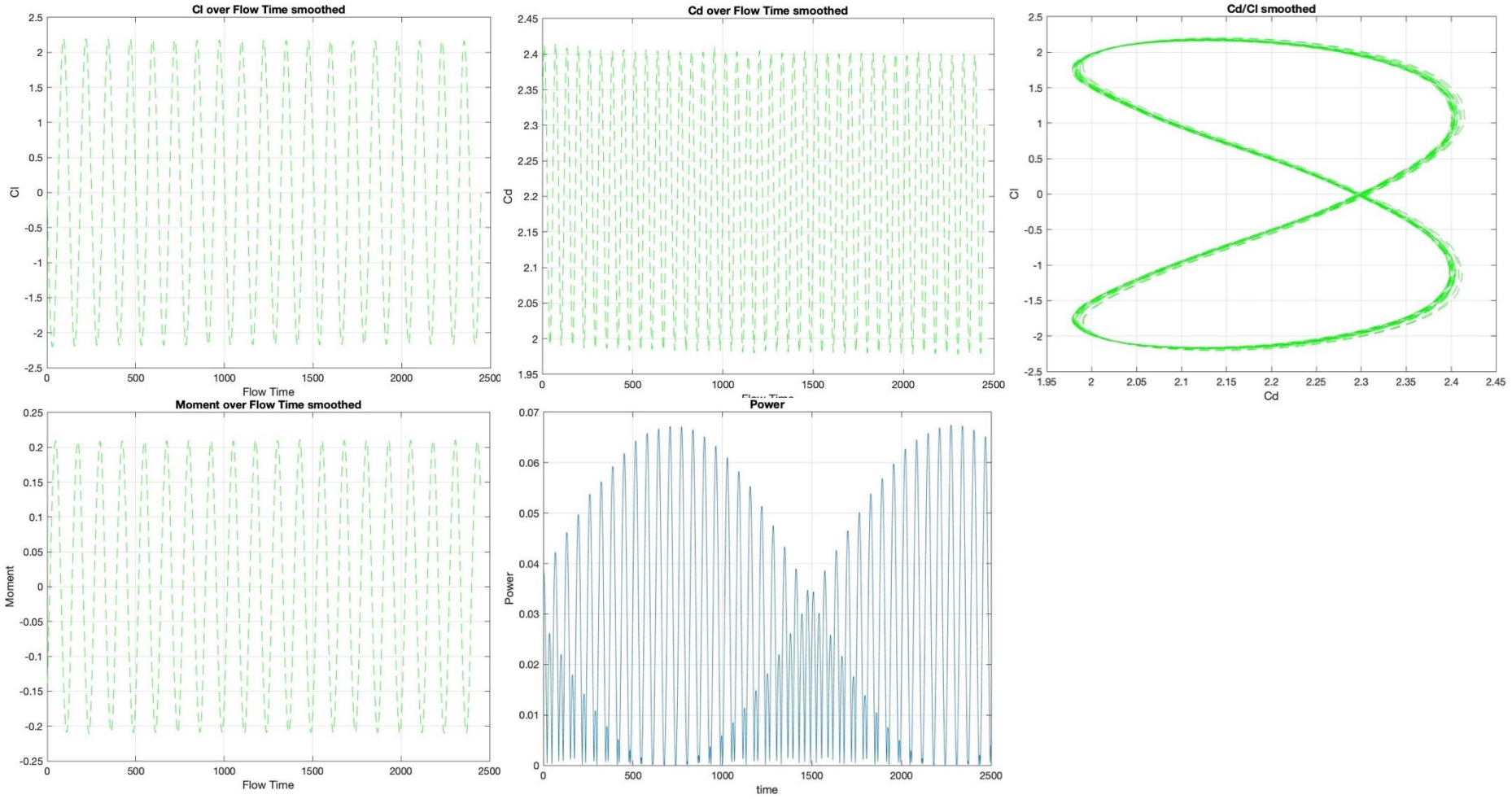

Figure 22 Results for case C2

Top Left: Lift Coefficient over flow time (smoothed), Upper Middle:Drag Coefficient over flow time (smoothed), Top Right: Drag Coefficient over Lift Coefficient, Bottom Left: Moment over flow time, Bottom Middle: Power over flow time, Bottom Right: Velocity Contour.

C3

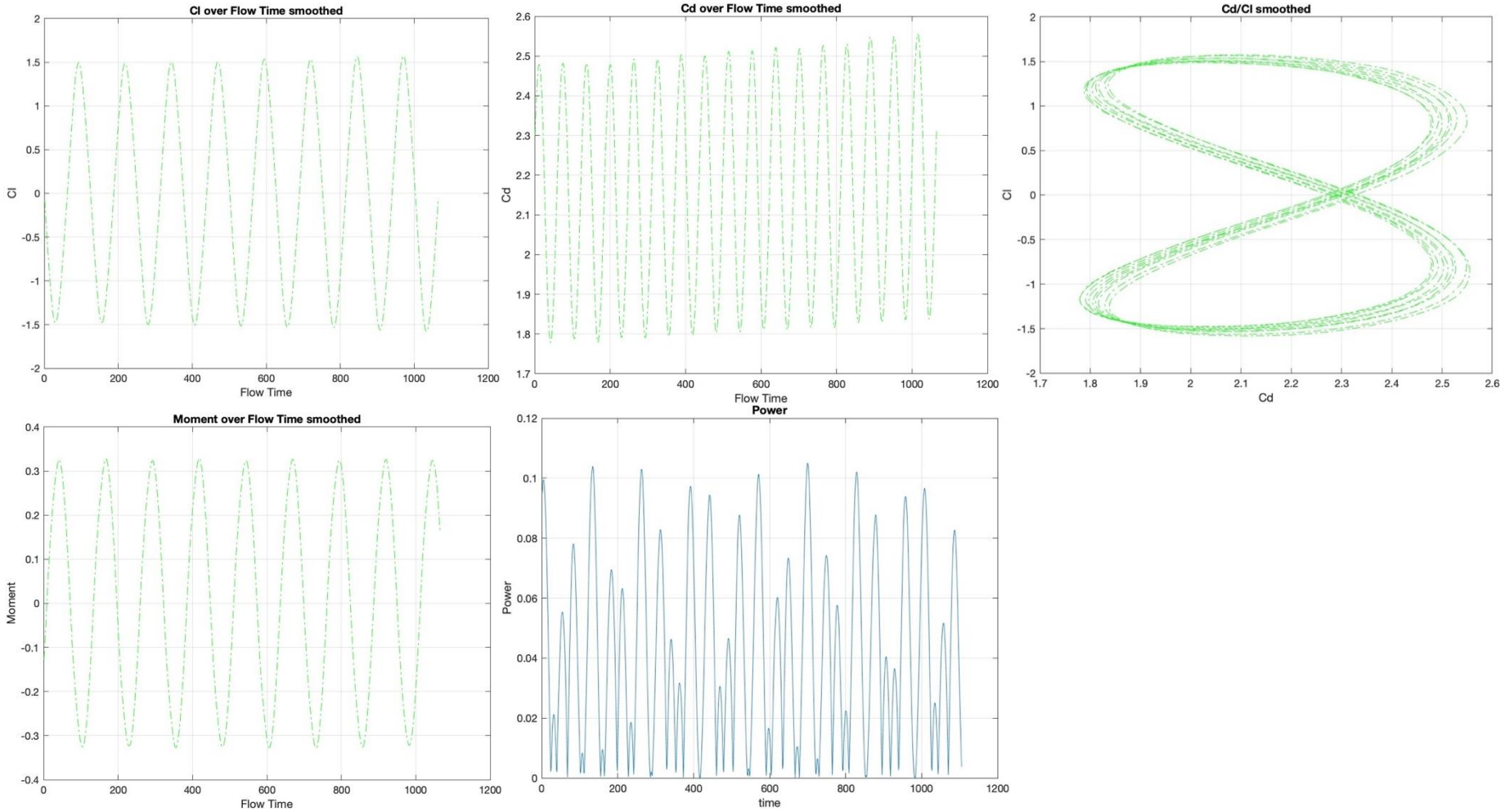

Figure 23 Results for case C3

Top Left: Lift Coefficient over flow time (smoothed), Upper Middle:Drag Coefficient over flow time (smoothed), Top Right: Drag Coefficient over Lift Coefficient, Bottom Left: Moment over flow time, Bottom Middle: Power over flow time, Bottom Right: Velocity Contour.

D1

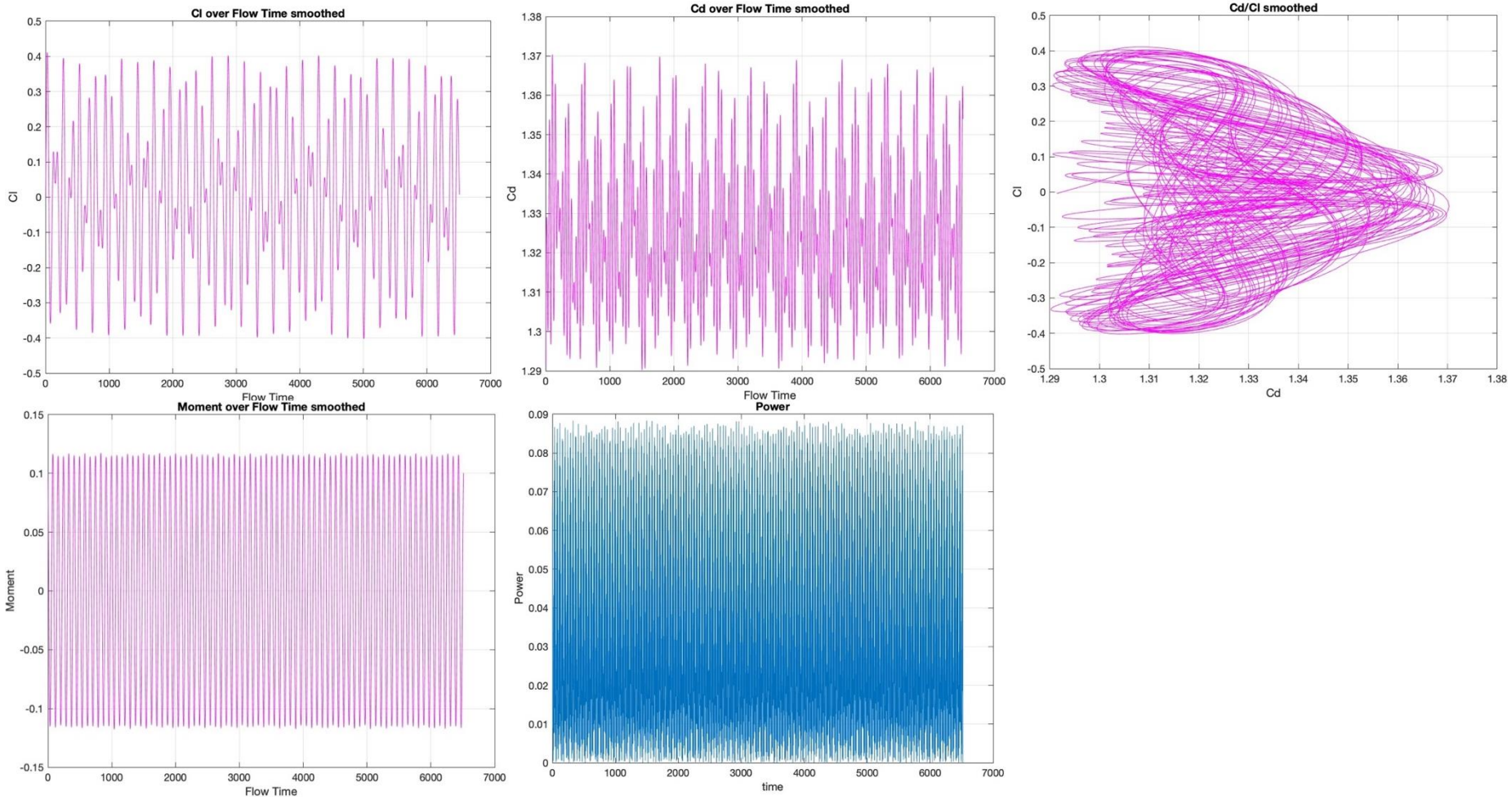

Figure 24 Results for case D1

Top Left: Lift Coefficient over flow time (smoothed), Upper Middle:Drag Coefficient over flow time (smoothed), Top Right: Drag Coefficient over Lift Coefficient, Bottom Left: Moment over flow time, Bottom Middle: Power over flow time, Bottom Right: Velocity Contour.

D2

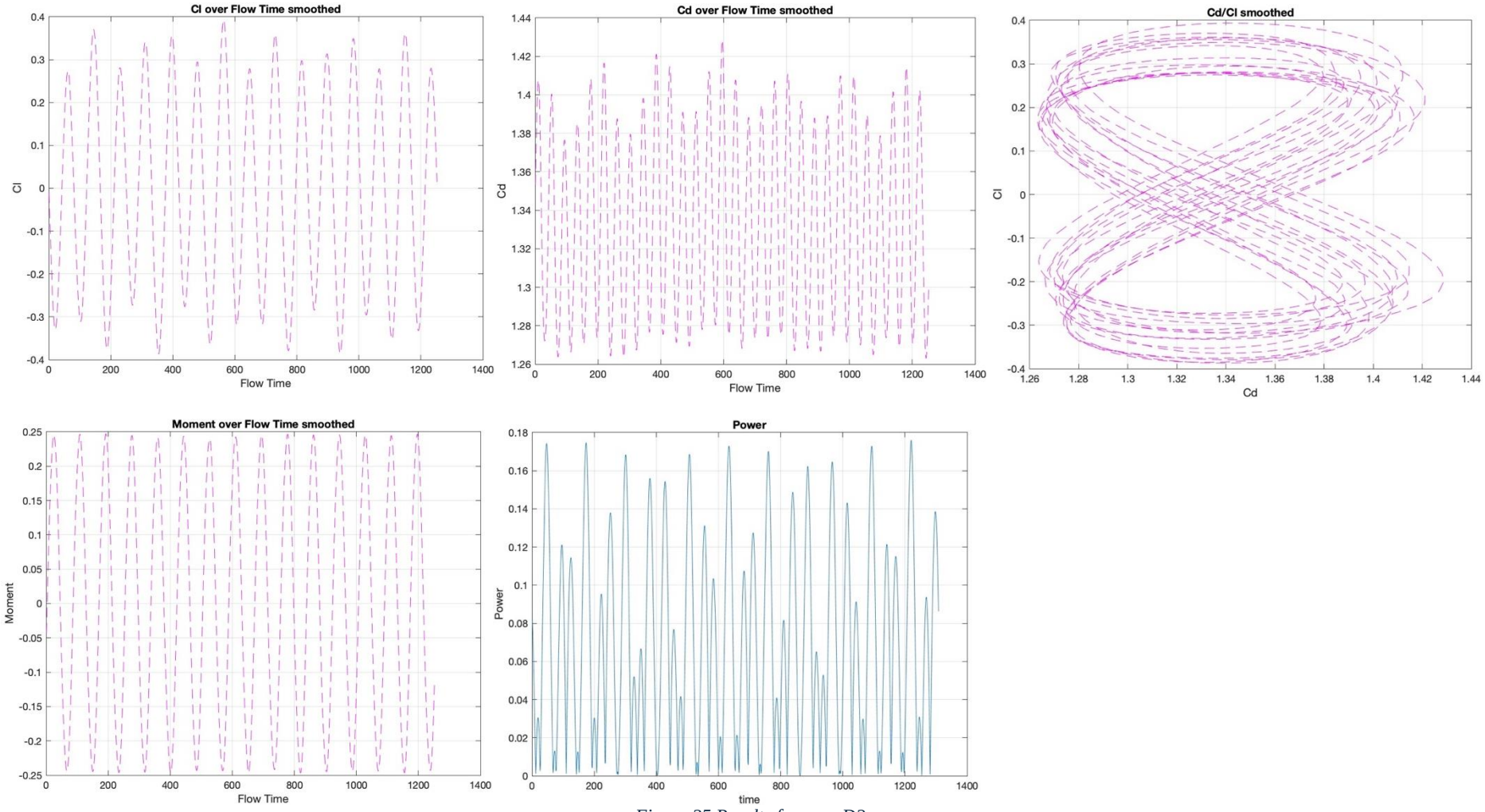

Figure 25 Results for case D2

Top Left: Lift Coefficient over flow time (smoothed), Upper Middle:Drag Coefficient over flow time (smoothed), Top Right: Drag Coefficient over Lift Coefficient, Bottom Left: Moment over flow time, Bottom Middle: Power over flow time, Bottom Right: Velocity Contour.

D3

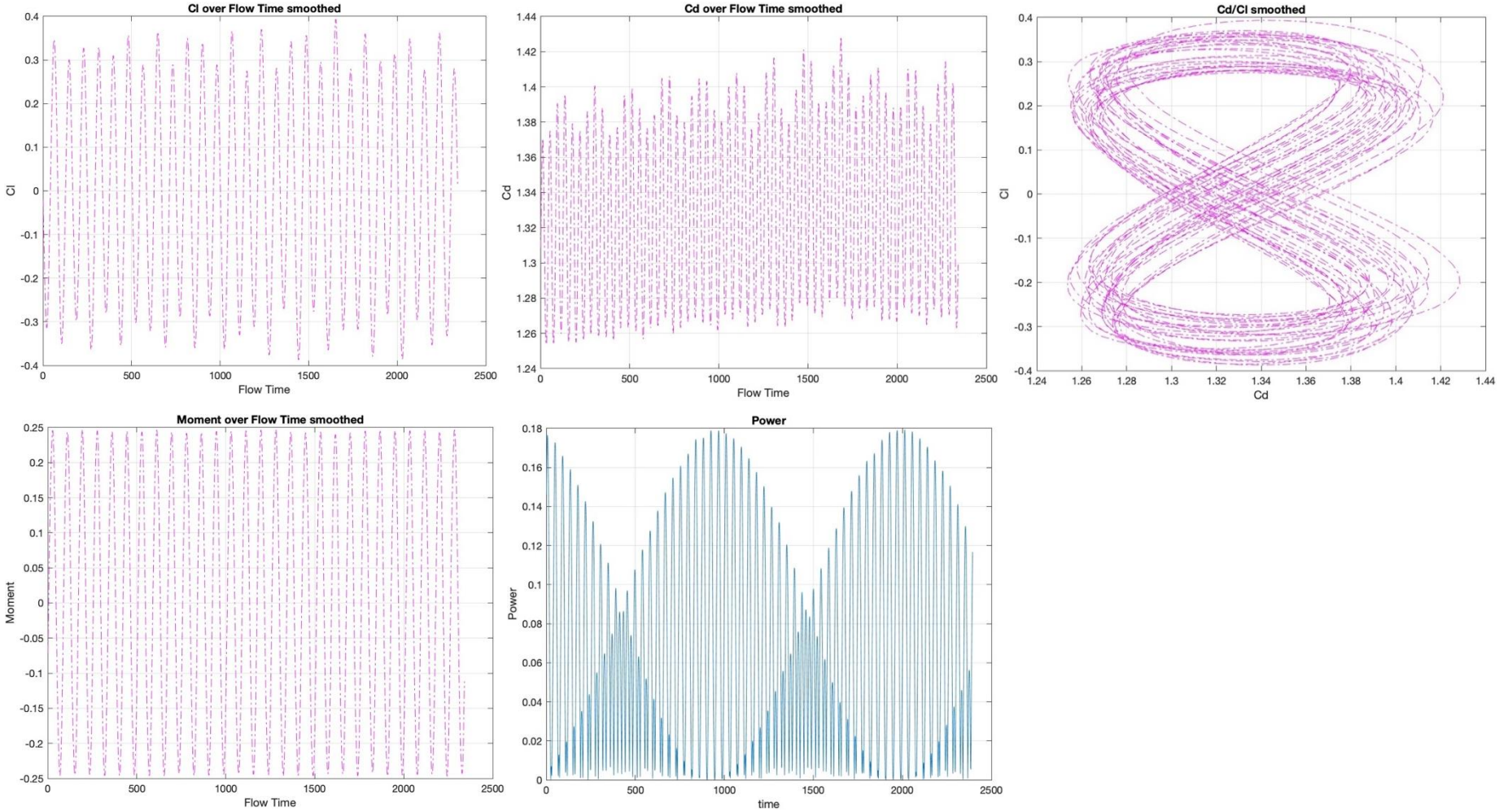

Figure 26 Results for case D3

Top Left: Lift Coefficient over flow time (smoothed), Upper Middle:Drag Coefficient over flow time (smoothed), Top Right: Drag Coefficient over Lift Coefficient, Bottom Left: Moment over flow time, Bottom Middle: Power over flow time, Bottom Right: Velocity Contour.

APPENDIX B

Bellow there is a table with all the outcomes from the simulations

	$C_{D_{MAX}}$	$C_{D_{MIN}}$	$\overline{C_D}$	$C_{L_{MAX}}$	$C_{L_{MIN}}$	$\overline{C_L}$	M_{MAX}	M_{MIN}	$\bar{M}$	P_{MAX}	P_{MIN}	$\bar{P}$	$\sum P$
AO	1.3567	1.3466	1.3367	0.3115	-0.3104	2.63E-04	0.0018	-2.71E-05	-0.0018				
A1	1.3426	1.2958	1.2386	-0.8878	-1.5432	-1.2223	-0.046	-0.0479	-0.0499	0.0086	0.0079	0.0083	0.0398
A2	1.238	1.1405	1.0369	-2.1516	-2.8355	-2.5002	-2.8355	-0.096	-0.0983	0.0339	0.0323	0.0331	0.1619
A3	0.9899	0.8781	0.7669	-3.5995	-4.1697	-3.8911	-0.1423	-0.1443	-0.1463	0.0757	0.0736	0.0746	0.3687
B1	1.3745	1.3159	1.2581	1.0544	-1.433	-0.0402	0.0682	-7.17E-04	-0.0671	0.0053	2.23E-07	0.0022	0.01
B2	1.5315	1.3927	1.2468	2.4996	-2.5086	-0.0929	0.1281	-0.0019	-0.1281	0.0101	4.72E-07	0.004	0.0036
B3	2.0824	1.7506	1.4086	3.8723	-3.877	-0.1196	0.1904	-0.0022	-0.1905	0.015	1.97E-06	0.0061	0.0021
C1	1.7551	1.7112	1.6647	1.4398	-1.4344	-0.0231	0.1015	0.0011	-0.1017	0.0327	3.33E-06	0.0131	0.106
C2	2.4149	2.2015	1.9782	2.1994	-2.2029	-0.0356	0.211	0.0025	-0.2108	0.0675	2.41E-07	0.0279	0.2259
C3	2.5551	2.164	1.778	1.5732	-1.5801	-0.0522	0.3282	0.0108	-0.3287	1.05E-01	4.13E-06	0.0423	0.5893
D1	1.3709	1.325	1.2896	0.4126	-0.4037	0.0012	0.1191	1.08E-04	-0.1182	0.0884	8.36E-16	0.0354	0.1965
D2	1.4285	1.3341	1.263	0.3937	-0.3873	-0.0048	0.2474	3.52E-04	-0.2468	0.1761	7.90E-05	0.0707	0.3841
D3	1.4285	1.3292	1.2537	0.3937	-0.3873	-0.0024	0.2474	1.39E-04	-0.2468	0.1794	1.41E-05	0.0725	0.998

Table 9 Summary table of results of simulations

Table of Figures

Table of Tables